

Beamforming for MC-CDMA

by

Ramasamy Venkatasubramanian

Thesis submitted to the faculty of

Virginia Polytechnic Institute and State University

in partial fulfillment of the requirements for the degree of

MASTER OF SCIENCE

in

Electrical Engineering

Approved

Dr. R. Michael Buehrer
Chairman

Dr. Brian D. Woerner

Dr. Jeffrey H. Reed

January 31 2003
Blacksburg, Virginia

Keywords: OFDM, MC-CDMA, Beamforming, MMSE detection
Copyright 2003, Ramasamy Venkatasubramanian

Beamforming for MC-CDMA systems

by

Ramasamy Venkatasubramanian

Committee Chairman: Dr. Michael Buehrer

Bradley Department of Electrical and Computer Engineering

(ABSTRACT)

Orthogonal Frequency Division Multiplexing (OFDM) has recently gained a lot of attention and is a potential candidate for Fourth Generation (4G) wireless systems because it promises data rates up to 10Mbps. A variation of OFDM is Multi-Carrier CDMA (MC-CDMA) which is an OFDM technique where the individual data symbols are spread using a spreading code in the frequency domain. The spreading code associated with MC-CDMA provides multiple access technique as well as interference suppression.

Often times in cellular and military environments the desired signal can be buried below interference. In such conditions, the processing gain associated with the spreading cannot provide the needed interference suppression. This research work investigates multi-antenna receivers for OFDM and MC-CDMA systems; specifically this work investigates adaptive antenna algorithms for MC-CDMA for very different channel conditions. Frequency domain beamforming is studied in this research predominantly through simulation. As an alternative a time domain beamforming is also studied.

Time variations in the channel can disrupt the orthogonality between subcarriers. Minimum Mean Square Error (MMSE) detection coupled with MMSE beamforming is proposed for time varying channels. Semi-analytic results are derived to study the Bit Error Rate (BER) performance. These results show significant performance improvement in the presence of interference. Joint MMSE weights in space and frequency is also investigated and semi-analytic results are derived to study their BER performance.

ACKNOWLEDGEMENTS

I would like to express my sincere appreciation and gratitude to my primary advisor Dr. Michael Buehrer. His vast experience and nice nature has given me a very great learning experience during the course of this research. While research contracts might be more alluring than the students' actual progress Dr. Buehrer gives more importance to the latter. I consider it a great honor to have Dr. Jeffrey Reed and Dr. Brian Woerner in my committee. I thank them for their review and comments on this work.

A lot of times discussions with the colleagues in MPRG has helped me gain a lot of insight into very difficult issues. I would like to thank Jay Tsai, a Bell-Labs veteran, for his time and the numerous fruitful discussions we have had. Thanks are also due to other colleagues, though not in any particular order, Fakhrul, James, Nory, Ramesh, Sarfraz, Nishant, Patrick, Mahesh and other MPRG colleagues. I would also like to thank the Raytheon Company and DARPA, the sponsors of this project, and the MPRG industrial affiliate program.

I thank my parents and my little sister who have been a great source of love and motivation always. Also I would like to thank my grand parents, other family members and friends whose blessings and wishes have made me reach where I am now.

TABLE OF CONTENTS

| | |
|--|-----------|
| 1 Introduction | 1 |
| 1.1 Contributions | 3 |
| 1.2 Thesis Outline | 3 |
| | |
| 2 Simulation Procedure | 5 |
| 2.1 System Model | 5 |
| 2.2 Generation of a Desired E_b / N_o | 10 |
| 2.3 Channel Model | 13 |
| 2.4 Simulation Flow | 17 |
| 2.5 Summary | 19 |
| | |
| 3 Introduction to OFDM and MC-CDMA | 20 |
| 3.1 Advantages of Multicarrier modulation | 20 |
| 3.2 Orthogonal Frequency Division Multiplexing | 22 |
| 3.2.1 Cyclic Prefix in OFDM | 25 |
| 3.2.2 Analysis of Cyclic Prefix in OFDM | 27 |
| 3.2.3 ICI Analysis for OFDM | 30 |
| 3.3 Multicarrier CDMA | 33 |
| 3.3.1 MC-DS CDMA | 36 |
| 3.3.2 MT-CDMA | 37 |
| 3.3.3 ICI Analysis for MC-CDMA | 38 |
| 3.3.4 Interference resistance in MC-CDMA | 39 |
| 3.3.5 Channel Estimation for MC-CDMA | 42 |
| 3.4 Summary | 46 |

| | |
|--|-----------|
| 4 Advanced detection techniques and robust channel estimation for MC-CDMA | 47 |
| 4.1 Improved detection techniques | 47 |
| 4.1.1. Conventional FFT detection for MC-CDMA | 47 |
| 4.1.2 LS Detection | 50 |
| 4.1.3 MMSE Detection | 51 |
| 4.1.4 MMSE with Successive Detection | 51 |
| 4.2 Robust Channel Estimation for MC-CDMA | 57 |
| 4.2.1 Literature Review | 57 |
| 4.2.3 Time Domain Estimator | 58 |
| 4.3 Summary | 68 |
| | |
| 5 Fundamentals of Adaptive arrays and Beamforming | 69 |
| 5.1 Introduction | 69 |
| 5.1.1 Diversity and Phased Array | 70 |
| 5.2 Uniform Linear Array | 71 |
| 5.3 Beamforming | 74 |
| 5.4 Analogy to FIR filter | 75 |
| 5.5 Adaptive antenna arrays | 77 |
| 5.6 Optimum Beamforming | 78 |
| 5.7 Adaptive Beamforming algorithm | 79 |
| 5.7.1 LMS | 79 |
| 5.7.2 RLS | 80 |
| 5.7.3 Direct Matrix Inversion | 81 |
| 5.7.4 Decision Directed algorithms | 82 |
| 5.8 Diversity Combining | 82 |
| 5.8.1 Selection Combining | 82 |
| 5.8.2 MRC | 83 |
| 5.8.3 Equal Gain Combining | 84 |
| 5.9 Summary | 85 |

| | |
|--|------------|
| 6 Beamforming for MC-CDMA systems | 86 |
| 6.1 Literature Review | 87 |
| 6.2 Frequency Domain beamforming | 87 |
| 6.2.1 Received signal model | 88 |
| 6.2.2 MMSE Beamforming | 90 |
| 6.3 Performance results in flat fading channel | 91 |
| 6.3.1 Effect of number of pilots | 92 |
| 6.3.2 Effect of desired user and interferer angle separation | 93 |
| 6.3.3 Effect of spreading factor | 95 |
| 6.4 Performance results in frequency selective fading | 98 |
| 6.5 Sub-band Beamforming | 101 |
| 6.6 Time domain beamforming | 103 |
| 6.7 MMSE in space and frequency | 108 |
| 6.8 Joint weights for MMSE in space and frequency | 111 |
| 6.8.1 Comparison of Joint MMSE weights with MMSE space & frequency | 116 |
| 6.9 Summary | 120 |
| | |
| 7 Conclusions and Future Work | 122 |
| 7.1 Conclusions | 122 |
| 7.2 Future Research Directions | 123 |
| References | 124 |
| Vita | 128 |

LIST OF FIGURES

| | |
|---|----|
| Figure 2.1 Spatio-Temporal fading using the vector channel model. ($f_d= 50\text{Hz}$ and angle-spread $\Delta = 8^\circ$) | 14 |
| Figure 2.2 Spatio-Temporal fading using the vector channel model. ($f_d= 200\text{Hz}$ and angle-spread $\Delta = 20^\circ$) | 15 |
| Figure 2.3 Flow diagram for the simulations performed in this research | 18 |
| Figure 3.1 Channel frequency responses for a single carrier and multicarrier system.... | 21 |
| Figure 3.2 A Basic OFDM system | 23 |
| Figure 3.3 Spectra of an OFDM signal | 24 |
| Figure 3.4 OFDM system Implemented using FFT | 25 |
| Figure 3.5 Effect of Cyclic Prefix on OFDM | 26 |
| Figure 3.6 OFDM Transceiver with Cyclic Prefix | 29 |
| Figure 3.7 Performance of OFDM in a Multipath channel | 30 |
| Figure 3.8 Error Floor due to ICI for various numbers of subcarriers (N) | 31 |
| Figure 3.9 Effect of ICI on the Signal to Interference Ratio | 32 |
| Figure 3.10 Block Diagram of a MC-CDMA system | 35 |
| Figure 3.11 (a) MC-DS CDMA Transmitter (b) MC-DS CDMA Receiver | 36 |
| Figure 3.12 (a) MT-CDMA Transmitter (b) MT-CDMA Receiver | 37 |
| Figure 3.13 Normalized ICI power for a MC-CDMA signal. $N = 1024$ | 39 |
| Figure 3.14 Normalized ICI power for the center subcarrier ($f_dT = 0.2$) | 39 |
| Figure 3.15 Performance of Multicarrier CDMA in presence of Interferers. SIR = 0dB and $f_dT = 0.01$ | 40 |
| Figure 3.16 Performance of MC-CDMA in presence of narrowband interferers for varying spreading code lengths. SIR = -20dB, $f_dT = 0.01$ | 41 |
| Figure 3.17 Frame format of MC-CDMA showing pilots multiplexed with data symbols..... | 42 |
| Figure 3.18 Effect of Time variations on Channel Compensation for MC-CDMA using the FFT method (64 Pilots per block, Spreading Factor = 4) | 44 |

| | |
|--|----|
| Figure 3.19 Effect of Delay spread on Channel Compensation for MC-CDMA using the FFT method (64 Pilots per block, Spreading Factor = 4, $f_d T = 0.01$)..... | 44 |
| Figure 3.20 Cubic Spline Channel Estimation performance for MC-CDMA for various channel delay spreads..... | 45 |
| Figure 4.1(a-c) Plot of the $\mathbf{H}^H \mathbf{H}$ matrix after FFT detection for MC-CDMA systems with 16 carriers, Spreading Factor = 1. The channel is frequency selective and time variant. (a) $f_d T = 0.1$ (b) $f_d T = 0.05$ (c) $f_d T = 0.01$ | 50 |
| Figure 4.2 Performance of different detection techniques for MC-CDMA using BPSK modulation. $f_d T = 0.1$, Spreading factor = 1, $N = 1024$ | 53 |
| Figure 4.3 Performance of different detection techniques for MC-CDMA using 16PSK modulation. $f_d T = 0.1$, Spreading factor = 1, $N = 1024$ | 54 |
| Figure 4.4 Performance of different detection techniques using 16PSK modulation. $f_d T = 1$, Spreading factor = 1, $N = 1024$ | 54 |
| Figure 4.5 Performance using 16PSK modulation for varying $f_d T$. SNR= 30dB | 55 |
| Figure 4.6 Performance using 16PSK modulation for varying $f_d T$. SNR= 30dB..... | 56 |
| Figure 4.7 Pilot pattern used for channel estimation..... | 59 |
| Figure 4.8 Performance of time domain Channel Estimator for FFT and MMSE detection with $f_d T = 0.1$, Spreading factor = 1, $N = 128$ | 62 |
| Figure 4.9 Normalized MSE for the channel estimator with $f_d T = 0.1$, 4 Data symbols for every Pilot symbol..... | 63 |
| Figure 4.10 Performance of time domain MMSE Channel Estimator for FFT and MMSE detection with $f_d T = 0.3$, Spreading factor = 1, $N = 128$, 10 Data symbols were inserted for every Pilot symbol..... | 63 |
| Figure 4.11 Normalized MSE for the channel estimator with $f_d T = 0.3$, SF = 1, $N = 128$, Data symbols for every Pilot symbol..... | 64 |
| Figure 4.12 Performance as a function of normalized Doppler for the channel estimator with $f_d T = 0.1$, 5 Data symbols for every Pilot symbol..... | 64 |
| Figure 4.13 Performance of the channel estimator using the mismatch channel statistic values for MMSE detection, Spreading factor = 1, $N = 128$ | 66 |
| Figure 4.14 Performance of the channel estimator using the mismatch channel statistic values for MMSE detection, Spreading factor = 1, $N = 128$ | 67 |

| | |
|---|----|
| Figure 4.15 Performance of the channel estimator using the mismatch channel statistic values for MMSE detection, Spreading factor = 1, $N = 128$. Delay spread varied from actual..... | 68 |
| Figure 5.1 A Uniform Linear Antenna Array showing the incident Plane wave | 71 |
| Figure 5.2 Narrowband beamformer | 75 |
| Figure 5.3 Beam pattern of a 4 element ULA with 3 interferers in AWGN channel..... | 81 |
| Figure 5.4 Selection Diversity | 83 |
| Figure 5.5 Maximal Ratio Combining | 83 |
| Figure 5.6 Equal Gain Combining | 84 |
| Figure 5.7 Performance of Maximal Ratio Combining in uncorrelated Rayleigh fading channels..... | 84 |
| Figure 6.1 Frequency Domain beamformer | 88 |
| Figure 6.2 Effect of Number of Pilots on the algorithm's performance | 92 |
| Figure 6.3 Effect of angle separation in degrees in an AWGN channel. SNR = 30dB, $N=1024$, SF = 1, Number of Pilots = 25, SIR = -10dB | 93 |
| Figure 6.4 Effect of angle separation in degrees in a Rayleigh fading channel. SNR = 8dB, $N=1024$, SF = 1, Number of Pilots = 128, $f_d T = 0.01$, SIR = -10dB..... | 94 |
| Figure 6.5 Effect of angle separation and number of pilots in an AWGN channel. SNR = 30dB, $N=1024$, SF = 1, SIR = -20dB | 94 |
| Figure 6.6 Effect of angle spread in degrees and varying spreading code length in a Rayleigh fading channel. $N=1024$, $f_d T = 0.01$, SIR = -20dB. User separation is 10 degrees..... | 95 |
| Figure 6.7 Performance comparison of MMSE beamforming with MRC. $N=1024$, $f_d T = 0.01$, SIR = -20dB. User separation is 40 degrees..... | 96 |
| Figure 6.8 Performance of MMSE beamforming with varying SIR. ($N=1024$, $f_d T = 0.01$, SF = 4. User separation is 10 degrees, Angle spread $\Delta = 0$) | 97 |
| Figure 6.9 Performance of MMSE beamforming with increase in normalized Doppler spread values. ($N = 1024$, User separation = 40 degrees and SF = 4, Angle spread $\Delta = 0$) | 98 |

| | |
|---|-----|
| Figure 6.10 Frequency Response of the channel (a) Delay spread = 200ns, (b) Delay spread = 400ns. N = 1024 | 99 |
| Figure 6.11 Performance of frequency domain beamforming with various values of delay spread (τ). N = 1024, SIR = -10 dB, SF = 4, $f_d T = 0.01$ | 100 |
| Figure 6.12 Performance of frequency domain beamforming with various values of Angle Spread (Δ) and Doppler spread. N= 1024, SF = 4, SIR = -10dB...101 | 101 |
| Figure 6.13 Sub-band beamforming for OFDM systems | 102 |
| Figure 6.14 Performance of Sub-band domain beamforming. (Angle Spread (Δ) = 0, $f_d T = 0.01$. N= 1024, SF = 4, SIR = -10dB, $\tau = 600$ ns)..... | 103 |
| Figure 6.15 Block diagram of Time domain Beamforming | 104 |
| Figure 6.16 Performance of Time domain Beamforming in flat fading channel. $f_d T = 0.01$, N=1024, SF = 4, SIR = -20dB | 105 |
| Figure 6.17 Performance of time domain beamforming in frequency selective channel with Channel Estimation. $f_d T = 0.01$, N = 1024, Angle spread (Δ) = 0° , delay spread (τ) = 200ns, SIR = -10dB | 106 |
| Figure 6.18 Performance Comparison of Time domain and Frequency domain beamforming in different angle spread environments. (N = 1024, Spreading factor = 4, $f_d T = 0.01$, SIR = -10dB) | 107 |
| Figure 6.19 Block Diagram of MMSE in Space and Time for OFDM systems | 108 |
| Figure 6.20 Performance comparison of MMSE in space and frequency with FFT in time and MMSE in space. SIR = -10dB, N = 128, Spreading Factor = 4. Channel assumed flat Rayleigh fading | 109 |
| Figure 6.21 Performance of MMSE in space and frequency in frequency selective channel, SIR = -20dB, N=1024, SF = 4, $f_d T = 0.01$ | 110 |
| Figure 6.22 Performance of MMSE in space and frequency in frequency selective channel. N = 1024, SIR = -20dB, SF = 4 | 110 |
| Figure 6.23 Joint weight formation for MMSE in Space and frequency | 111 |
| Figure 6.24 Performance of Joint MMSE weights in space and frequency through simulations and analysis for BPSK modulation. N = 16, Number of receive antennas = 4, SF = 1, Flat Rayleigh fading channel, SIR = ∞ | 115 |
| Figure 6.25 Performance comparison of Joint MMSE weights in space and frequency | |

with MMSE detection in time followed by space for BPSK modulation.
 N = 16, Number of receive antennas = 4, SF = 1, Flat Rayleigh fading,
 SIR = ∞ 118

Figure 6.26 Performance comparison of Joint MMSE weights in space and frequency
 with MMSE detection in time followed by space for BPSK modulation for
 varying angle spreads. N = 16, Number of receive antennas = 4, SF = 1, Flat
 Rayleigh fading channel, SIR = ∞ 119

Figure 6.27 Performance comparison of Joint MMSE weights in space and frequency
 with MMSE detection in time followed by space for BPSK modulation for
 varying SIR values.....120

LIST OF TABLES

| | | |
|------------------|---|----|
| Table 4.1 | Mismatch condition assumed in the channel estimator | 65 |
| Table 4.2 | Mismatch condition assumed in the channel estimator corresponding to Figure 4.14 | 66 |
| Table 4.3 | Mismatch condition assumed in the channel estimator corresponding to Figure 4.14 | 67 |

Chapter 1

Introduction

Third Generation (3G) mobile communication systems are already in deployment in several countries and this has enabled whole new ways to communicate, access information, conduct business and be entertained, liberating users from slow, cumbersome equipment and immovable points of access. In a way 3G has been the right bridge for mobile telephony and the internet. 3G services enable users to make video calls to the office and surf the internet simultaneously, or play interactive games wherever they may be. Second and third generation systems like EDGE, IS-95 and WCDMA can provide nominal data rates of about 50 – 384 Kbps. While 3G is just transforming itself into a reality from an engineer's dream, research efforts are already on to look into systems that can provide even higher data rates and seamless connectivity. Such systems are categorized under Fourth Generation (4G) and are predicted to provide packet data transmission rates of 5 Mbps in outdoor macro-cellular environments and up to 10 Mbps in indoor and microcellular environments. While wide-band systems could be a natural choice to provide high data rates, service providers have to pay dearly for the spectrum necessary. Hence, spectrum efficiency is always a factor on the choice of any wireless technology. Very wide-band systems usually require complex receivers as the channel is frequency selective due to the presence of large number of resolvable multipaths.

Orthogonal Frequency Division Multiplexing (OFDM) has recently gained a lot of attention and is a potential candidate for 4G systems. OFDM is very efficient in spectrum usage and is very effective in a frequency selective channel. By taking advantage of recent improvements in Digital Signal Processing (DSP) and RF technologies, OFDM can provide higher data rates and is a very good choice for service providers to compete with wire-line carriers. A variation of OFDM which allows multiple accesses is Multi-Carrier CDMA (MC-CDMA) which is essentially an OFDM technique where the individual data symbols are spread using a spreading code in the frequency domain. The

inherent processing gain due to the spreading helps in interference suppression in addition to providing high data rates. OFDM is already the technique used in Digital Audio and Video Broadcasting and Wireless LANs (802.11 family) and is believed to be the technique for future broadband wireless access.

Research into multiple antenna systems for wireless communications dates back to the 1960s. Multi-antenna receivers provide spatial diversity and are considered to be the last frontier to improve data rates without the necessity for additional spectrum. In addition to providing diversity they can provide interference suppression by exploiting the spatial signatures of the desired user and the interferers. In mobile cellular environments the use of such an antenna-array helps reduce co-channel interference which transforms itself into an improvement in system capacity. Such intelligent antenna arrays are becoming increasingly popular and are an option for future 4G systems.

The motivation behind this research effort is to study the use of antenna arrays for OFDM systems. Currently there is not a lot of research effort being concentrated on the use of adaptive antenna arrays for OFDM and MC-CDMA systems. As mentioned earlier MC-CDMA systems have the inherent ability to provide interference suppression but it is not sufficient when the interference is strong. This is the case in military applications where very high power jammers are present. During the course of this research we have found that the nature of the channel (flat or frequency selective) largely determines the performance of the MC-CDMA system. Thus the algorithms that we employ should be robust to the channel variations while providing interference suppression. This thesis investigates the use of adaptive antenna algorithms for OFDM and MC-CDMA systems in various channel conditions including narrow and wide angle spreads, slow and fast temporal fading, flat and frequency selective fading. Computer simulations are performed to evaluate the performance of these algorithms in different channel conditions as well as analysis for certain architectures.

1.1 Contributions

Some of the major contributions of the thesis are listed below.

- Studies the performance limitations of the OFDM and MC-CDMA systems in harsh channel conditions and the use of advanced detection techniques to improve performance in these channel conditions
- The trade-off between processing gain and adaptive antenna technology for MC-CDMA systems in various channel conditions is discussed. This has not been reported in literature previously.
- Presents a new beamforming technique for combining signals in time for OFDM and MC-CDMA systems. The simulation results for the same are presented for various channel conditions.
- Combining Minimum Mean Square Error (MMSE) detection for OFDM systems in time and MMSE beamforming for OFDM systems is an effective solution for time-varying channels that can provide interference suppression. This synergistic use of MMSE in space and frequency is a novel technique proposed in this work for time varying channels.
- The weights for joint MMSE in both space and frequency have been derived and semi-analytic results are also shown to match simulations. While joint MMSE combining in both space and frequency has been studied for CDMA systems, extending the analysis to OFDM which is presented here has not been reported in literature previously.

1.2 Thesis Outline

Chapter 2 discusses the simulation methodology used in this research work. All our simulations were performed in complex base-band and in the first part of the chapter we prove analytically that the complex base-band representation and the band pass representation are equivalent. A brief discussion of the vector channel model for receive antenna arrays are presented in the later part.

Chapter 3 discusses the fundamentals of Multicarrier modulation and the basic concepts behind OFDM and MC-CDMA systems. The effect of time variations and the delay spread of the channel and its effect on the performance of an OFDM system is presented with analytical results. Chapter 3 also discusses pilot based channel estimation for OFDM and simulation results are presented.

Chapter 4 discusses advanced detection techniques for OFDM systems. The limitations of simple FFT detection are first discussed and the usefulness of these detection techniques in harsh channel conditions is investigated in chapter 4. Another interesting problem for multicarrier systems is the channel estimation. Chapter 4 discusses an MMSE time domain channel estimation algorithm for OFDM and MC-CDMA systems.

The importance of multi-antenna systems and the performance improvement they provide is the focus in Chapter 5. Various beamforming algorithms are discussed and algorithms for combining signals for a diversity array are also presented.

Chapter 6 presents an investigation of the beam-forming algorithms for OFDM and MC-CDMA systems. Frequency domain beamforming is discussed first and performance results are presented for flat, frequency selective fading conditions. Time domain beamforming is discussed and the performance results are also shown. The usefulness of combining MMSE detection in frequency and MMSE beamforming in space is discussed in the final sections of the chapter. Joint MMSE detection in both space and frequency is also discussed. Simulations results are presented along with analytical results. Chapter 7 concludes the thesis and summarizes the important results. Potential and interesting problems that can be carried out in future research are also listed in Chapter 7.

Chapter 2

Simulation Procedure

In this chapter we discuss the basis behind the simulations performed for the adaptive antenna algorithms for MC-CDMA systems. In Section 2.1 we study the similarity between baseband and band pass simulation and show that they are equivalent. In Section 2.2 we discuss how the noise is generated for a specified Signal-to-Noise Ratio (SNR). Section 2.3 discusses the channel model that was used for simulation purposes. Finally section 2.4 discusses the general simulation that we followed for the purpose of this research.

2.1 System Model

We consider in all our simulations PSK modulation and for the sake of simplicity, a BPSK system is considered in our analysis here. We also consider a transmit signal of the multicarrier form

$$s(t) = \sum_{n=0}^{N-1} a_n \exp\{jw_c t + n w_s t\} \quad (2.1)$$

In the above expression w_c is the carrier frequency, w_s is the subcarrier spacing, N is the number of subcarriers, $\{a_n\}$ are the individual modulated symbols in each of the subcarriers and n is the subcarrier number. Practical implementations use FFT processors to create the user's data on parallel subcarriers. Here we adhere to the continuous time representation which is equivalent to its discrete time domain representation. We attempt to show that the performance of the band pass and the complex baseband representations are the same. This allows us to perform simulations in complex baseband. For this purpose we consider the continuous time output corresponding to the k th subcarrier of the transmitted signal. This is given by,

$$s_k(t) = \sqrt{2P_{bp}} b(t) \cos(w_c t + k w_s t + \theta) \quad (2.2)$$

where P_{bp} is the power of the transmitted band pass signal in subcarrier k , θ is a random phase and $b(t)$ is the data signal and is defined as $b(t) = \sum_{i=-\infty}^{\infty} b_i p_T(t)$ where

$$p_T(t) = \begin{cases} 1 & 0 \leq t \leq T \\ 0 & \text{else} \end{cases} \text{ and } b_i \text{ is a binary random variable which takes on } +1 \text{ and } -1 \text{ with}$$

equal probability during the symbol duration T . At the receiver, the received signal corresponding to the k th subcarrier is the transmitted signal plus a band pass Gaussian noise process. The multipath, time and frequency dispersive effects of the channel are not considered for the purpose of proving the equivalency between the complex baseband and band pass representations.

$$r_k(t) = s_k(t) + n_k(t) \quad (2.3)$$

where $n_k(t)$ is a band pass Gaussian random process. At the receiver the signal is mixed to baseband and integrated over the symbol duration to generate the decision statistic Z_k . The signal in the time domain is brought back to the frequency domain using the FFT engine in the case of digital implementation. The decision statistic is given as

$$Z_k = \int_0^T r_k(t) \cos(\omega_c t + k\omega_s t + \theta) dt \quad (2.4)$$

where we have assumed that a coherent phase reference is available. Now substituting for the expression of the received signal from (2.3) we obtain

$$\begin{aligned} Z_k &= \int_0^T (\sqrt{2P_{bp}} b(t) \cos^2(\omega_c t + k\omega_s t + \theta) + n_k(t) \cos(\omega_c t + k\omega_s t + \theta)) dt \\ &= \int_0^T \sqrt{2P_{bp}} b(t) \left[\frac{1 + \cos(2\omega_c t + 2k\omega_s t + 2\theta)}{2} \right] dt + \int_0^T n_k(t) \cos(\omega_c t + k\omega_s t + \theta) dt \\ &\approx \sqrt{\frac{E_{bp}}{2}} bT + w_k \end{aligned} \quad (2.5)$$

where we have assumed that the double frequency terms are negligible. Here Z_k is the decision statistic for the k th subcarrier signal, b is the current data bit on subcarrier k and

$$w_k = \int_0^T n_k(t) \cos(\omega_c t + k\omega_s t + \theta) dt \text{ is the resulting Gaussian Random variable.}$$

For a BPSK system, the Bit Error Rate (BER) in an AWGN channel is given as,

$$P_e = Q\left(\sqrt{\frac{E(Z_k)^2}{\text{var}(Z_k)}}\right) \quad (2.6)$$

Now using equation (2.5) the expected value of Z_k is given as,

$$\begin{aligned} E(Z_k) &= E\left(\sqrt{\frac{P_{bp}}{2}}bT + w_k\right) \\ &= \sqrt{\frac{P_{bp}}{2}}bT \end{aligned} \quad (2.7)$$

and the variance of Z_k is given as

$$\begin{aligned} \text{var}(Z_k) &= E\left[\left(\sqrt{\frac{P_{bp}}{2}}bT + w_k\right)^2\right] - \left(\sqrt{\frac{P_{bp}}{2}}bT\right)^2 \\ &= E\left[\frac{P_{bp}}{2}T^2 + w_k^2 + 2\sqrt{\frac{P_{bp}}{2}}bTw_k\right] - \frac{P_{bp}}{2}T^2 \\ &= E\left[w_k^2\right] \\ &= E\left[\left(\int_0^T n_k(t)\cos(w_c t + kw_s t + \theta)dt\right)^2\right] \\ &= E\left[\int_0^T \int_0^T n_k(t)n_k(m)\cos(w_c t + kw_s t + \theta)\cos(w_c m + kw_s m + \theta)dmdt\right] \\ &= \int_0^T \int_0^T E\left[n_k(t)n_k(m)\right]\cos(w_c t + kw_s t + \theta)\cos(w_c m + kw_s m + \theta)dmdt \end{aligned} \quad (2.8)$$

In the above we have used the facts that $E[b^2] = 1$ and $E[n_k(t)] = 0$ while computing the variance of the Z_k .

We know that the noise samples will be uncorrelated if the system uses a sampling rate which is an integer multiple of the noise bandwidth. Hence

$$E[w_k(t)w_k(m)] = \begin{cases} \sigma^2 \delta(t-m) & t = m \end{cases} \quad (2.9)$$

where σ^2 is the total noise power.

Thus,

$$\text{var}[Z_k] = \frac{\sigma^2 T}{2} \quad (2.10)$$

and the BER is thus given by,

$$P_e = Q\left(\sqrt{\frac{P_{bp} T}{\sigma^2}}\right) \quad (2.11)$$

We know that the energy per bit E_b and the power of the transmitted band pass signal are related as $E_b = P_{bp} T$ and the noise variance $\sigma^2 = \frac{N_o}{2}$ where N_o is the noise bandwidth assuming a matched filter detection at the receiver.

Thus equation (2.11) can be written as

$$P_e = Q\left(\sqrt{\frac{2E_b}{N_o}}\right) \quad (2.12)$$

This is the BER for the k th subcarrier in the multicarrier symbol. A similar analysis can be performed for the other subcarriers and by observation we can see that the BER for the entire multicarrier symbol would be the same as in equation (2.12).

Now we consider a complex base band system and analyze the performance of it in AWGN. The relation between the base band and band pass versions of any signal can be written as,

$$y(t) = \text{Re}\left[\tilde{y}(t)e^{jw_c t}\right] \quad (2.13)$$

where $\tilde{y}(t)$ is the base band equivalent of $y(t)$. The other way to express equation (2.13) is

$$y(t) = \tilde{y}_I(t) \cos(w_c t) - \tilde{y}_Q(t) \sin(w_c t) \quad (2.14)$$

The above has been written using the in-phase and quadrature phase parts of the signal $y(t)$. Using these expressions the baseband equivalent of the k th subcarrier information can be written as

$$\tilde{s}_k(t) = \sqrt{2P_{bp}} b(t) \cos(kw_s t + \theta) + j\sqrt{2P_{bp}} b(t) \sin(kw_s t + \theta) \quad (2.15)$$

The noise can be expressed as the sum of the in-phase component and the quadrature phase component.

$$\tilde{n}(t) = n_I(t) + jn_Q(t) \quad (2.16)$$

where $n_I(t)$ and $n_Q(t)$ are independent Gaussian processes each with power σ^2 . The decision statistic using this approach is given as

$$Z_k = \int_0^T \tilde{r}(t) (\cos(kw_s t + \theta) - j \sin(kw_s t + \theta)) dt \quad (2.17)$$

where $\tilde{r}(t)$ is the complex base band model of the received signal. Simplifying the above we get,

$$Z_k = \sqrt{2E_{bp}} bT + N_i + N_q \quad (2.18)$$

where $N_i = \int_0^T n_I(t) (\cos(kw_s t + \theta) - j \sin(kw_s t + \theta)) dt$

and $N_q = \int_0^T n_Q(t) (\cos(kw_s t + \theta) - j \sin(kw_s t + \theta)) dt$ (2.19)

The performance is determined by equation (2.12) where the mean and variance are given by

$$E[Z_k] = \sqrt{2E_{bp}} bT \quad \text{and} \quad \text{var}[Z_k] = E[N_i^2 + N_q^2] = 2\sigma^2 T \quad (2.20)$$

Hence the BER is given as

$$\begin{aligned} P_e &= Q\left(\sqrt{\frac{2E_{bp} T^2}{2T\sigma^2}}\right) \\ &= Q\left(\sqrt{\frac{E_{bp} T}{\sigma^2}}\right) \end{aligned} \quad (2.21)$$

Using a similar approach as was used for the complex baseband representation we can write equation (2.21) as

$$P_e = Q\left(\sqrt{\frac{2E_b}{N_o}}\right) \quad (2.22)$$

As was explained before, the analysis could be extended for all other subcarriers and the performance of the entire multicarrier system would be the same as that of equation

(2.22). From equation (2.22) and (2.12) it is evident that the band pass and the complex base band representations of the signal are equivalent.

2.2 Generation of a Desired E_b / N_o

In this section we describe how to create a desired E_b / N_o in our simulations. We assume that the data waveforms are square pulses (in absence of pulse shaping). In the simulations this would correspond to creating a desired number of symbols with amplitudes given as $A = \sqrt{2P_{bp}}$ where the actual chosen value of A or P_{bp} is arbitrary.

We require a value of σ^2 to generate a particular value of E_b / N_o or the SNR. The analysis can be performed using the sampled version of the complex base band envelope of the signals discussed above.

The complex envelope of any signal $s(t)$ can be expressed as the sum of the I and Q parts.

$$s(t) = s_I(t) + js_Q(t) \quad (2.23)$$

In simulations we use a sampled version of the complex envelope and this can be expressed as

$$\begin{aligned} s_k &= s(kt_s) \\ &= s_I(kt_s) + js_Q(kt_s) \\ &= s_{Ik} + js_{Qk} \end{aligned} \quad (2.24)$$

Now the power of the complex envelope signal and its sampled counterpart can be found from,

$$\begin{aligned} P_{ce} &= \lim_{\tau \rightarrow \infty} \frac{1}{\tau} \int_{-\tau/2}^{\tau/2} s_{ce}(t) s_{ce}^*(t) dt \\ &= \lim_{\tau \rightarrow \infty} \frac{1}{\tau} \int_{-\tau/2}^{\tau/2} A^2(t) e^{j\varphi(t)} e^{-j\varphi(t)} dt \\ &= A^2 \end{aligned} \quad (2.25)$$

$$\begin{aligned}
P_{sim} &= \lim_{L \rightarrow \infty} \frac{1}{L+1} \sum_{-L/2}^{L/2} s_k s_k^* \\
&= \lim_{L \rightarrow \infty} \frac{1}{L+1} \sum_{-L/2}^{L/2} A_k^2 e^{j\phi_k} e^{-j\phi_k} \\
&= A^2
\end{aligned} \tag{2.26}$$

The symbol energies are thus given as

$$\begin{aligned}
E_s^{ce} &= P_{ce} T = A^2 T \\
E_s^{sim} &= P_{sim} T = A^2 m t_s
\end{aligned}$$

where T is the symbol duration, m is the number of samples per symbol and t_s is the time duration between the samples.

The base band noise is given by the following expression,

$$n_{ce}(t) = n_I(t) + j n_Q(t) \tag{2.27}$$

and the sampled version of it can be expressed as

$$n_k = n_I(k t_o) + j n_Q(k t_o) \tag{2.28}$$

Hence the PSD of the noise can be written as

$$N_I(f) = N_Q(f) = \begin{cases} N_o & |f| \leq \frac{B}{2} \\ 0 & \text{else} \end{cases} \tag{2.29}$$

Using the autocorrelation function of the noise can be found out to be $N_o B$ and thus the noise variances are found to be

$$\sigma_{ce}^2 = \sigma_{sim}^2 = 2 N_o B \tag{2.30}$$

Thus the SNR of the complex envelope system and the sampled version used in our simulations can be expressed as

$$\begin{aligned}
\left(\frac{S}{N} \right)_{ce} &= \frac{A^2}{\sigma_{ce}^2} = \frac{A^2}{2 N_o B} \\
\left(\frac{S}{N} \right)_{sim} &= \frac{A^2}{\sigma_{sim}^2} = \frac{A^2}{2 N_o B}
\end{aligned} \tag{2.31}$$

The noise power spectral density is defined as N_{sim}^o and this can be written as

$$N_{sim}^o = \frac{\sigma_{sim}^2}{B} = \frac{\sigma_{sim}^2}{1/t_s} \quad (2.32)$$

The E_s/N_o of the complex envelope and the simulated system can thus be written as

$$\begin{aligned} \left(\frac{E_s}{N_o}\right)_{ce} &= \frac{A^2 T}{\frac{\sigma_{ce}^2}{B}} = \frac{A^2 T B}{\sigma_{ce}^2} = T B \left(\frac{S}{N}\right)_{ce} \\ \left(\frac{E_s}{N_o}\right)_{sim} &= \frac{A^2 m t_s}{\frac{\sigma_{sim}^2}{B}} = \frac{A^2 m t_s}{\sigma_{sim}^2 t_s} = m \left(\frac{S}{N}\right)_{sim} \end{aligned} \quad (2.33)$$

In simulations we often wish to find the σ_{sim}^2 for a specified value of $\frac{E_s}{N_o}$. This value of

σ_{sim}^2 can thus be found from equation (2.32) and is given as

$$\sigma_{sim}^2 = 2\sigma_I^2 = 2\sigma_Q^2 = \frac{A^2 m}{\left(\frac{E_s}{N_o}\right)} \quad (2.34)$$

where the variables σ_I^2 and σ_Q^2 are the variance of the in-phase and quadrature components of the noise signal and are given,

$$\sigma_I^2 = \sigma_Q^2 = \frac{A^2 m}{2 \left(\frac{E_s}{N_o}\right)} \quad (2.35)$$

In simulations we specify the $\frac{E_b}{N_o}$ instead of $\frac{E_s}{N_o}$. In this case equation (2.35) can be

modified as

$$\sigma_I^2 = \sigma_Q^2 = \frac{A^2 m}{2n \left(\frac{E_b}{N_o}\right)} \quad (2.36)$$

where n is the number of bits per symbol.

Convolutional coding of a particular rate r might be used sometimes to improve performance and in such cases the noise variances have to be changed to take into

account the coding gain provided by the use of convolutional codes. Thus noise variance is given as

$$\sigma_I^2 = \sigma_Q^2 = \frac{A^2 m}{2rn \left(\frac{E_b}{N_o} \right)} \quad (2.37)$$

In simulations that involve interferers we usually specify the Signal-to-Interference Ratio (SIR) and thus the interferer's power level above or below the desired signal level can be found using this value of SIR. This value is used while scaling the interferer signal amplitude to maintain the specified SIR in our simulations. In simulations involving beamforming using multiple antennas, the SNR value specified is the SNR at each of the antenna elements.

2.3 Channel Model

In order to consider realistic radio propagation channels, studying the performance of the algorithms in AWGN alone is not sufficient. We must also include the effects of multipath propagation. To do so we must understand the effect of multipath on the received signal and how to emulate these effects in base band.

The received signal is composed of several time delayed versions of the transmitted signal. These signals add at the receiver with different phases as a result of different propagation delays. It has been shown that the envelope of this follows a Rayleigh distribution [Jak74]. Additionally the rate at which the signal varies is inversely proportional to the Doppler spread of the channel. A simple way to model the Rayleigh fading effect is the quasi-static assumption wherein the channel is assumed to be constant over a block period of time. In this model we generate a Rayleigh random variable and a complex exponential with a uniform phase and multiply it with the transmitted signal and then compensate for this distortion in the receiver. However, a more accurate method which can incorporate the effects of the Doppler spread due to the channel will be to use the Clark and Gans model for simulation of the Rayleigh fading coefficients [Rap95].

Now in simulations that involve beamforming and studying the effects of beamforming in performance improvement we use a vector channel model which is a widely accepted channel model for modeling the propagation effects on uniform linear array [Bue99]. The model assumes that the propagation between the mobile and a base station antenna array occurs via many paths resulting from scatterers in the vicinity of the mobile. Also the scatterers are assumed to be distributed in a circular region around the mobile. The received signal at the base station array is thus the sum of many versions of the transmitted signal, with each version weighted with an independent complex weight due to the different time delays and scatterers associated with each path. When the distance between the mobile and the base station is large with respect to the scattering radius the angular extent of the received signal will appear small at the antenna array. The received signal at each element of the array will appear as phase shifted versions of the same signal where the phase shift is related to the angle of arrival of the plane wave relative to the array. However as the angle spread grows, the signals become decorrelated and spatial fading will result. Spatial fading is due to the constructive and destructive addition of the signals from various paths in different ways along the extent of the array. Some examples of spatial and temporal fading are shown in Figure 2.1 and Figure 2.2.

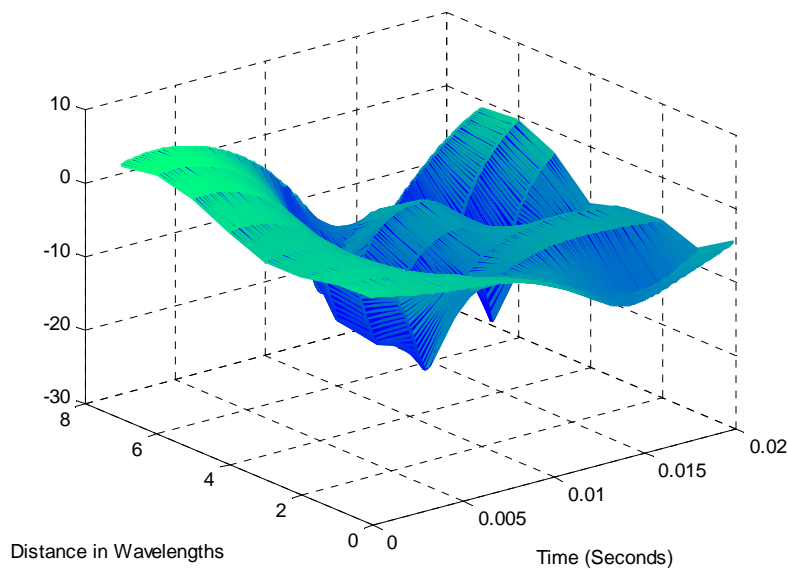


Figure 2.1 Spatio-Temporal fading using the vector channel model. ($f_d= 50\text{Hz}$ and angle spread $\Delta = 8^\circ$)

We see from Figure 2.1 that the temporal fading is not very significant as the Doppler spread assumed was very small and thus the channel changes slowly. The effect of the angle spread is evident as the signals at each antenna element are not equal and show slight decorrelation.

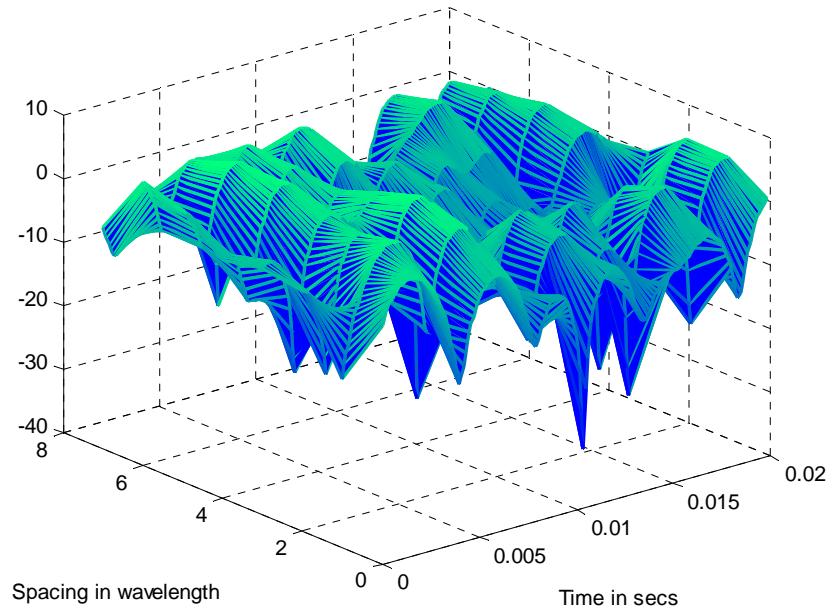


Figure 2.2 Spatio-Temporal fading using the vector channel model. ($f_d= 200\text{Hz}$ and angle spread $\Delta = 20^\circ$)

In Figure 2.2 we see that the effect of the Doppler spread and the angle spread in a more severe case. Here the Doppler and angle spreads are larger resulting in faster temporal variations and more spatially selective fading.

For the purpose of this research, a uniform linear array was considered for the base station with a fixed number of elements M . Also it was assumed that the multipath components can be lumped into a number of groups that correspond to the resolvable paths, which the receiver can distinguish. The base band equivalent of the multiplicative distortion is an $M \times 1$ vector, which is actually modeled using the extended Jakes model [Bue99]. The resolvable path can be thought of as a sum of J scatterers that extends into a vector of antennas. On the k th antenna the multiplicative distortion of the l th resolvable multipath can be written as

$$u_{l,k}(t) = \sqrt{P_l} \frac{1}{\sqrt{J}} \sum_{i=0}^{J-1} e^{j[2\pi f_d \cos(\Phi_{l,i})t + \phi_{l,i}]} e^{j[2\pi d_k \sin(\theta_{l,i})/\lambda]} \quad (2.38)$$

In the above expression,

P_l – Average power received for the l th path

J – Number of scatterers composing of each resolvable path

f_d – Maximum Doppler spread frequency = v/λ where v is the velocity of the vehicle

$\phi_{l,i}$ - Uniformly distributed random phase

$\Phi_{l,i}$ - Random angle of departure or arrival relative to the motion of the mobile of each multipath

d_k – Distance between the antenna k and antenna 0

Also we assume that $\theta_{l,i}$ is distributed as

$$p_{\theta_{l,i}}(x) = \begin{cases} \frac{1}{\Delta_l} & \Theta_l - \frac{\Delta_l}{2} \leq x \leq \Theta_l + \frac{\Delta_l}{2} \end{cases} \quad (2.39)$$

where Θ_l is the central angle of arrival and Δ_l is the angle spread of the l th resolvable multipath.

In general there are the three main parameters that affect the performance of the system.

The angle spread will determine the amount of spatial fading that will be seen at the array. The maximum Doppler spread determines the rate of change of the channel and when the fading seen at the array is not correlated, it determines the update rate necessary for the weights. Finally there is the delay spread, which is a relative term with respect to the symbol duration, and it determines if temporal processing (i.e. equalization) should accompany spatial processing.

Frequency selective fading occurs when the delay spread is commensurate with the symbol duration. In our simulations we generate frequency selective fading effects by using the vector channel model described above for each dominant multipath with independent delays and energies. Then we sum the signals due to all these multipaths and this is effective way to simulate a frequency selective channel. Thus the received signal in a frequency selective channel can be expressed as

$$r_k(t) = \sum_{l=1}^L u_{l,k}(t - \tau_l) s(t - \tau_l) \quad (2.40)$$

where L is the number of dominant multipaths and $u_{l,k}$ is the channel corresponding to each of those paths.

2.4 Simulation Flow

In the previous sections we discussed the procedure for generating the channel model (i.e. AWGN level, fading coefficient generation using the vector channel model) used for simulations in this work. We discuss in this section the flow of the overall simulation procedure. All simulations were carried out using MATLAB student version software. The flow diagram of the entire simulation procedure is shown in Figure 2.3. The first section of each simulation program is dedicated to defining the overall channel and system parameters, as well as the parameter that is to be varied. This variable can be the desired E_b/N_o , the interference power level, the normalized Doppler spread etc. and will be denoted by v .

After initialization, we first determine a particular value of v and then run a fixed number of blocks for that value. That is, for a fixed value of v we desire to run a fixed number of bits. Usually we run simulations using OFDM symbols with 1024 subcarriers and each block having up to 200 such OFDM symbols. Also when MC-CDMA is used, spreading codes are generated at the transmit side and care must be taken to run sufficient number of blocks in order to obtain consistent results. Fading envelopes are created once for each value of v and these are then segmented and used for each individual block of symbols. For the simulation of frequency selective channels we used a 2-tap channel model. The path delays can be expressed in terms of chips or symbols and then we shift and add the individual paths to simulate frequency selective fading channels. Once the total number of bits necessary for each value of v is generated we calculate the overall probability of error for the current value of v and then increment v . When v reaches the limit we stop our simulations.

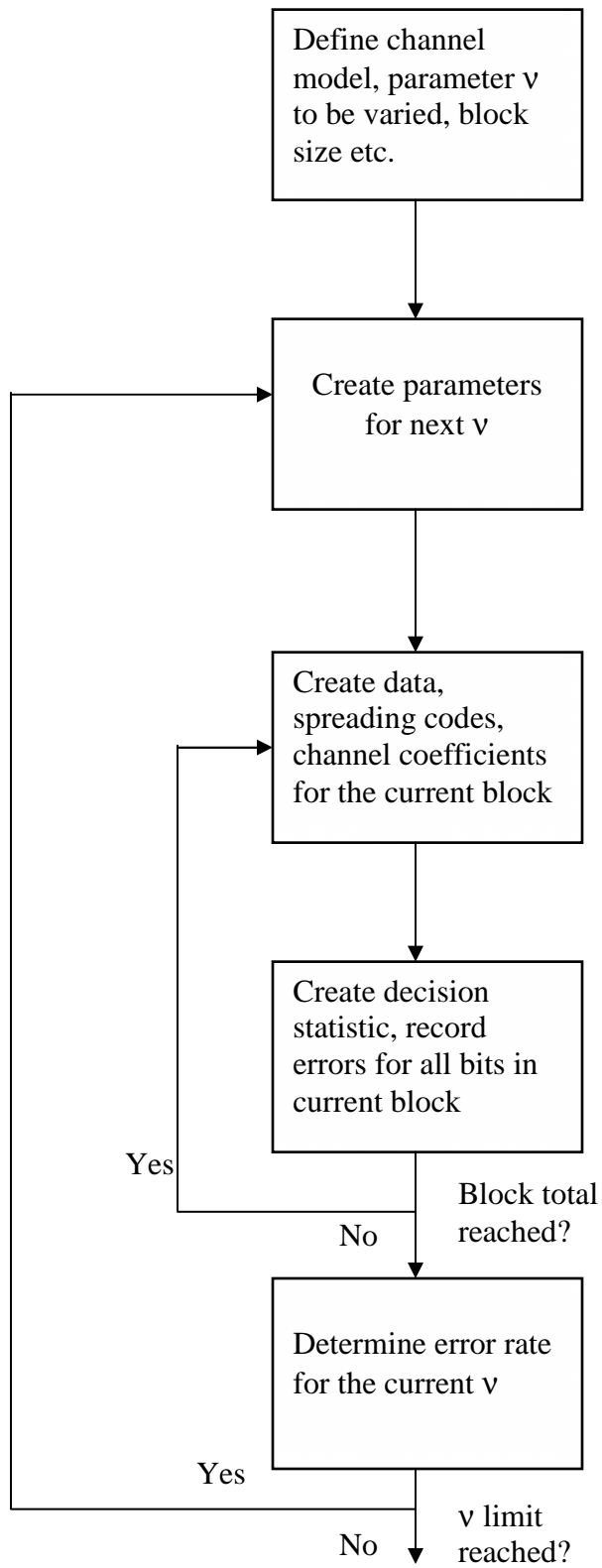


Figure 2.3 Flow diagram for the simulations performed in this research

2.5 Summary

In this chapter we presented an outline of all simulations that were carried out in this research. We have shown that the base band and band pass simulations were the same and hence all simulations were carried in base band. Also we discussed how to generate noise for a given SNR. The final sections of the chapter also discussed the vector channel model used for simulations and the spatio-temporal fading effects that were studied using the model. Finally the general simulation flow was discussed and this will be used in subsequent chapters.

Chapter 3

Introduction to OFDM and MC-CDMA

Recent advances in multimedia mobile communications have sparked much research in techniques that can deliver very high data rates. Data rate is really what broadband is all about. Traditional single carrier modulation techniques can achieve only limited data rates due to the restrictions imposed by the multipath channel and the receiver complexity. Multi-carrier techniques can provide high data rates at reasonable receiver complexities and are increasingly becoming popular in audio/video broadcasting, mobile local area networks and future generation wideband cellular systems.

This chapter gives an introduction to Orthogonal Frequency Division Multiplexing (OFDM) and the CDMA version of it called the Multicarrier CDMA (MC-CDMA). Sections 3.1 and 3.2 discuss the advantages of using multicarrier techniques and OFDM and Section 3.3 elaborates on the fundamentals of MC-CDMA. Finally section 3.4 concludes the chapter with a brief summary.

3.1 Advantages of Multicarrier modulation

Mobile radio channels introduce severe multipath propagation due to multiple scattering from objects in the vicinity of the mobile. This scattering introduces rapid fluctuation of the received signal envelope as well as phase variations. Measurements and theoretical analysis have shown that the envelope of the signal received is typically Rayleigh distributed. Also the motion of the mobile unit introduces a Doppler shift which causes a broadening of the signal spectrum [Jak74].

The multipath channel can also be frequency selective in which case the fading envelope of the received signal at one frequency might not be correlated with the envelope at another frequency. This is due to the fact that the symbol duration might be less than (or on the order of) the maximum delay spread. As a result, the received signal consists of overlapping versions of the transmitted symbols or Inter Symbol Interference (ISI). Also, if we consider a cellular environment or military applications, there is the effect of

cochannel interference due to the frequency reuse of the available spectrum. In addition to this, the received signal is subjected to large scale fading also called shadow fading due to the propagation effects [Rap95]. Given these adverse mobile environments it is necessary to look for intelligent transmission and reception techniques. In a conventional serial data transmission, the symbols are transmitted sequentially with the frequency spectrum of the each transmitted symbol occupying the entire bandwidth available. The delay spread due to the channel dictates the symbol duration or alternatively the data rate that can be achieved to prevent the effects of the ISI.

The idea behind multicarrier modulation is that it is a technique where multiple low data rate carriers are combined by a transmitter to form a composite high data rate transmission. In a parallel transmission system several sequential streams of data are transmitted simultaneously. In a classical parallel transmission system, the available spectrum is split into several non-overlapping frequency sub channels. The individual data elements are modulated into these sub channels and are thus frequency multiplexed. The main advantage is that the parallel transmission increases the symbol time by modulating the symbols into narrow sub channels. This increase in symbol time makes it more robust to the channel delay spread effects. The Figure 3.1 below shows the channel frequency response for a single carrier and multi carrier system.

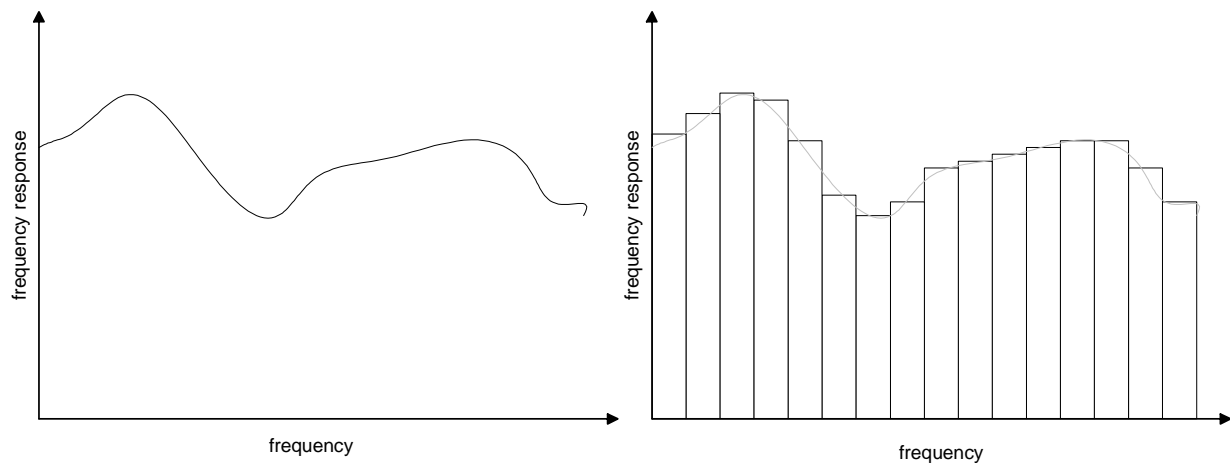


Figure 3.1 Channel frequency responses for a single carrier and multicarrier system. In multicarrier system each sub channel only undergoes slight distortion.

Such parallel data transmission techniques were in vogue even during the early 1960's. They were used for high frequency military communication systems like the KINEPLEX, ANDEFT [Van00]. . To implement the multiple carrier scheme using a bank of parallel modulators would not be very efficient in analog hardware. However, in the digital domain, multi-carrier modulation can be done efficiently with currently available DSP hardware and software. Hence multicarrier modulation is a very attractive technique for commercial applications as high power Digital Signal Processors are available for affordable prices in recent times.

3.2 Orthogonal Frequency Division Multiplexing (OFDM)

When there is sufficient bandwidth available for data transmission, a classical parallel system can be used where the entire bandwidth available is split into narrow sub channels and data can be modulated into each of these sub channels. In such a system there is usually sufficient guard space in between the adjacent sub channels to effectively isolate them at the receiver using filters of appropriate cut-off frequencies. A better and more efficient use of the bandwidth is possible if the spectra of individual sub-channels are allowed to overlap. By allowing the subcarrier tones to be separated by the inverse of the signaling symbol duration, independent separation of the frequency multiplexed tones is possible. This ensures that the spectra of individual sub channels are zeros at other subcarrier frequencies. This is the fundamental concept of OFDM. The Figure 3.2 explains the basic OFDM system [Cim85]. There are N serial data elements and spaced

by $\Delta t = \frac{1}{f_s}$ where f_s is the desired symbol rate. N serial elements modulate N subcarrier

frequencies which are then frequency division multiplexed. The symbol interval T has now been increased to $N\Delta t$ which provides robustness to the delay spread due to the channel. The subcarrier frequencies are spaced as

$$f_n = f_0 + n\Delta f, \Delta f = \frac{1}{N\Delta t} \quad (3.1)$$

This ensures that the subcarriers are separated by multiples of $1/T$ so that the sub-channels are orthogonal over a symbol duration (in the absence of channel distortion). If

the channel is slowly time-varying the capacity can be enhanced significantly by adapting the data rate per subcarrier according to the signal to noise ratio of that subcarrier. Also, OFDM is very robust to narrow band interference because such interference can only affect a small percentage of the subcarriers [Van00].

OFDM is widely used in many wireless communication systems. IEEE 802.11a uses OFDM to provide up to 54Mbps data rates. Recent WAN technologies like 802.16 and BRAN (proposed by ETSI) also utilize OFDM as their key physical layer technology. In addition to this, Digital Audio Broadcasting (DAB) and Digital Video Broadcasting (DVB) utilize OFDM to provide up to 10Mbps data rates.

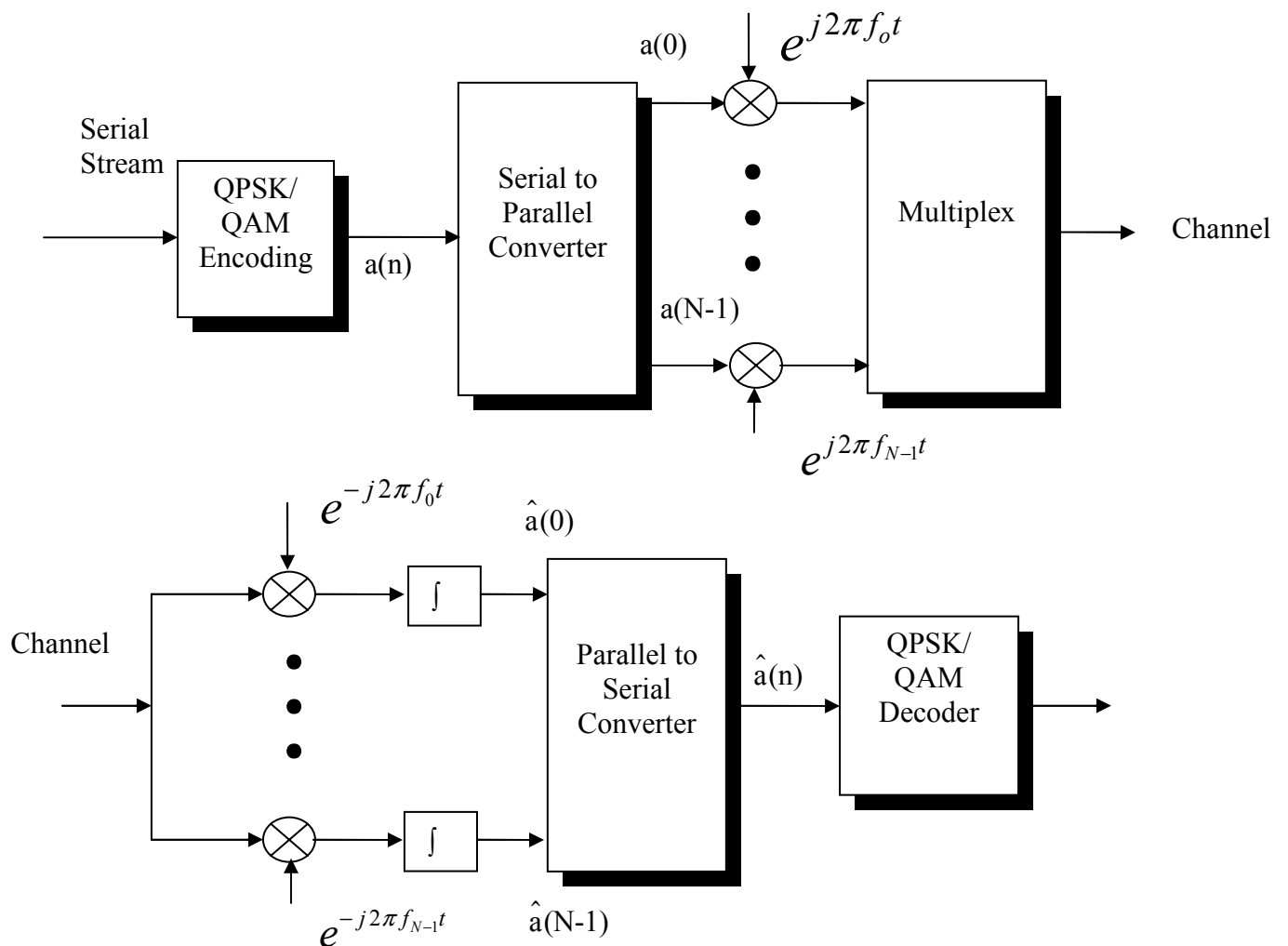


Figure 3.2 A Basic OFDM system

Figure 3.3 shows the spectra of an OFDM signal. We see that there is no cross talk between the subcarriers.

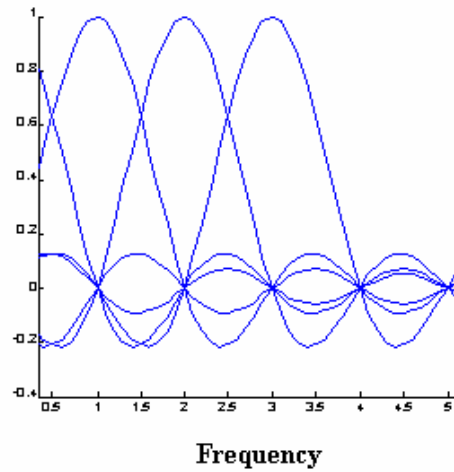


Figure 3.3 Spectra of an OFDM signal

The main difficulty in using the parallel data system as shown in Figure 3.2 is the complexity of the equipment needed for the implementation of the system. Severe mutual interference between the subcarriers is possible and filters of accurate cut-off frequencies will be needed. The complexity can be greatly reduced by using the Discrete Fourier Transform to implement the modulation process. It has been shown in the literature [Sal69] that a multitone modulation is essentially a Fourier Transform of the original stream and the bank of coherent demodulators at the receiver is an Inverse Fourier Transform operation. The Discrete Fourier Transform can in turn be implemented using a Fast Fourier Transform (FFT) algorithm particularly when the N is large. Figure 3.4 shows a simplified implementation of OFDM using FFT engines.

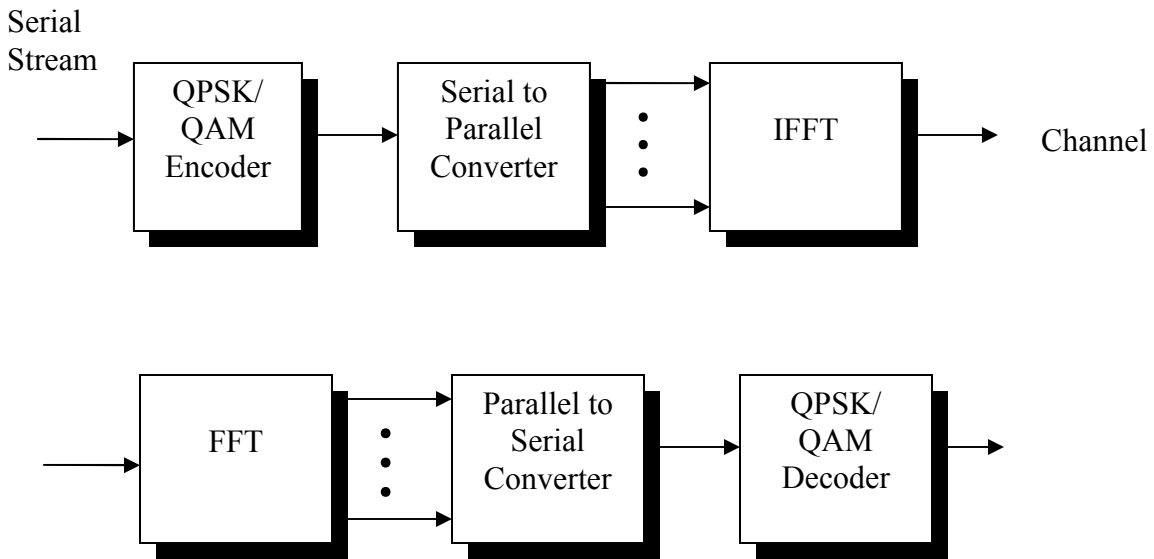


Figure 3.4 OFDM system Implemented using FFT

3.2.1 Cyclic Prefix in OFDM systems

A very important reason to use OFDM modulation is its resistance to multipath delay spread. By dividing the input data stream into N subcarriers, the symbol duration is made N times larger, which reduces the multipath delay spread relative to the symbol time, by the same factor. To eliminate the Inter Symbol Interference (ISI) completely a guard time is inserted in each OFDM symbol. This guard time is always chosen to be larger than the maximum delay spread due to the channel. This guard time could consist of no symbol at all but this would result in InterCarrier Interference (ICI). The multipath channel introduces delayed versions of the same transmitted signal and hence during the FFT interval, there is no longer an integer number of cycles. The subcarriers are thus not orthogonal for the multipath replicas and there is interference between the subcarriers. To eliminate the ICI completely, the OFDM symbol is cyclically extended in the guard time. This ensures that the delayed replicas always have an integer number of cycles during the FFT interval. [Mor01] has shown the effects of zero padding and the use of cyclic prefix for OFDM in a multipath channel. The guard time T_g should be always greater than the worst case delay spread τ_{\max} of the channel.

Figure 3.5 shows the effect of the cyclic prefix for OFDM.

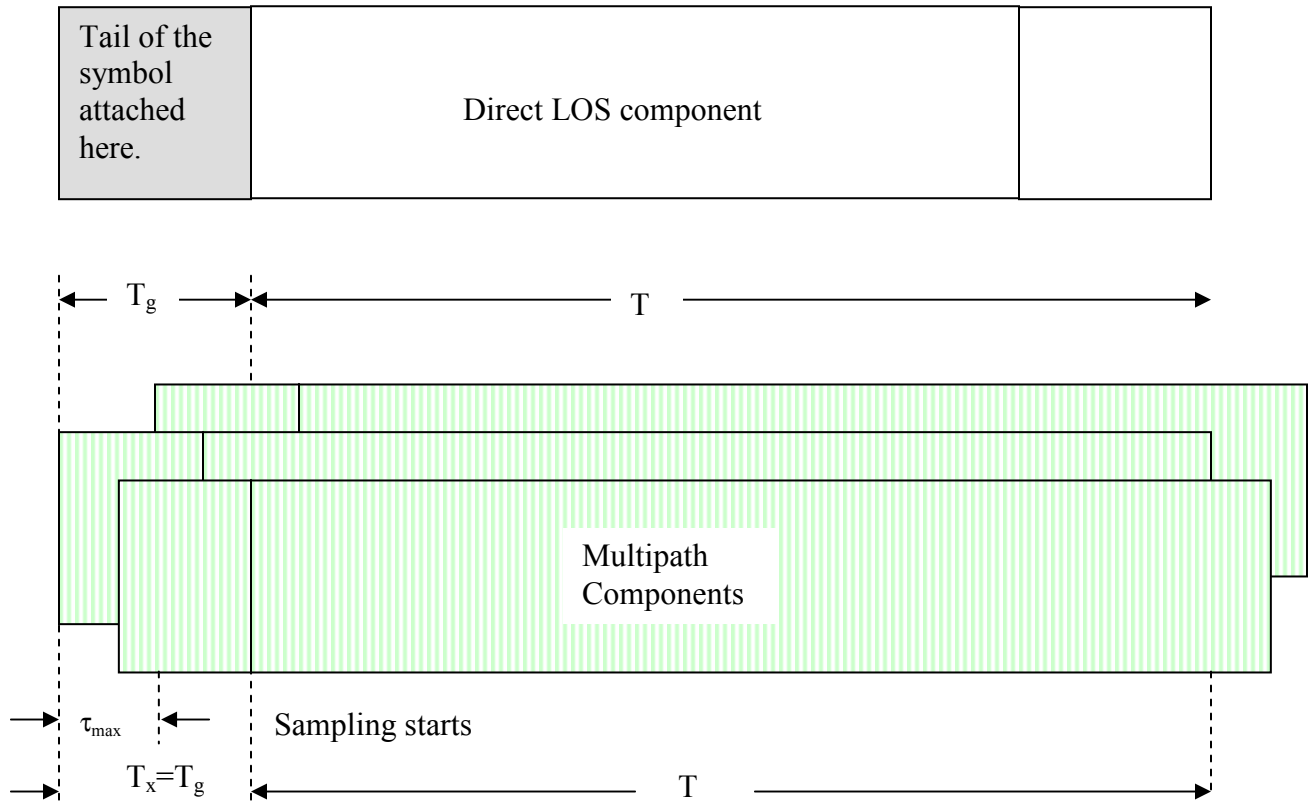


Figure 3.5 Effect of Cyclic Prefix on OFDM

Here a certain point within the cyclic prefix is chosen as the sampling starting instant which satisfies the criteria $\tau_{\max} < T_x < T_g$ where τ_{\max} is the worst case delay spread of the channel. As shown in Figure 3.5 if this condition is met then there is no ISI because the previous symbol will only have effect on the next symbol during the interval $[0 \tau_{\max}]$. Since sampling starts after τ_{\max} there is no ISI. Also it is clear that sampling after T_x , encompasses the contribution from all multipath components for a particular symbol only, and hence there is no ICI. During the FFT interval, the OFDM receiver sees a sum of pure sine waves which does not destroy the orthogonality between the subcarriers.

3.2.2 Analysis of Cyclic prefix in OFDM

A multipath channel can be modeled as a Finite Impulse Response (FIR) filter with a fixed number of taps L . If $L > 1$, then there is Inter Symbol Interference (ISI) due to the addition of the delayed replicas with the direct Line of Sight component. The received signal can always be expressed as a linear convolution of the transmitted signal with the channel coefficients. Thus, if the channel is not an impulse then there is ISI and equalizers are necessary at the receiver to remove the ISI. In case of OFDM systems the effects of the channel introduced ISI can be removed by making the physical channel look like circular convolution instead of linear convolution [Wan00].

Let us consider the transmitted sequence at the output of the IFFT block as $\mathbf{x}_{N \times 1}$ and a channel Impulse response defined as $\mathbf{h}_{L \times 1}$. The received sequence after circular convolution of \mathbf{x} and the channel \mathbf{h} is given as

$$y = h \otimes x \quad \Leftrightarrow \quad Y[k]=H[k]X[k] \quad (k=0,1,2,\dots,N-1) \quad (3.2)$$

where $Y[k]$, $H[k]$ and $X[k]$ are the Fourier transforms of the received signal, channel vector and the transmitted signal respectively.

From matrix theory we have that every circulant matrix can be diagonalized by the FFT basis (i.e.) where \mathbf{F}^H is the Hermitian transform of the FFT matrix \mathbf{F}

$$\mathbf{H}_c = \mathbf{F}^H \Delta \mathbf{F} \quad (3.3)$$

Another important property is that the circular convolution $y = h \otimes x$ is equivalent to the linear convolution of \mathbf{h} with \mathbf{x}' where \mathbf{x}' is the cyclically extended transmitted signal \mathbf{x} . This property can be explained using a simple example. Let us consider a sequence $[x_0 \ x_1 \ x_2]$ and the channel coefficients be defined as $[h_0 \ h_1 \ 0]$. The received sequence after circular convolution can be defined as [Pro89]

$$\mathbf{y} = [h_0 \ h_1 \ 0] \otimes [x_0 \ x_1 \ x_2] \quad (3.4)$$

$$\begin{bmatrix} y_0 \\ y_1 \\ y_2 \end{bmatrix} = \begin{bmatrix} h_0 & 0 & h_1 \\ h_1 & h_0 & 0 \\ 0 & h_1 & h_0 \end{bmatrix} \begin{bmatrix} x_0 \\ x_1 \\ x_2 \end{bmatrix} = \begin{bmatrix} h_0 x_0 + h_1 x_2 \\ h_1 x_0 + h_0 x_1 \\ h_1 x_1 + h_0 x_2 \end{bmatrix} \quad (3.5)$$

Now linear convolution of the transmitted sequence with cyclic prefix and the channel can be expressed as

$$\mathbf{y} = [h_0 \ h_1 \ 0] * [x_2 \ | \ x_0 \ x_1 \ x_2] \quad (3.6)$$

The above can be written in matrix format as the following,

$$\begin{bmatrix} * \\ y_0 \\ y_1 \\ y_2 \end{bmatrix} = \begin{bmatrix} h_0 & 0 & 0 & 0 \\ h_1 & h_0 & 0 & 0 \\ 0 & h_1 & h_0 & 0 \\ 0 & 0 & h_1 & h_0 \end{bmatrix} \begin{bmatrix} x_2 \\ x_0 \\ x_1 \\ x_2 \end{bmatrix} = \begin{bmatrix} h_0 x_2 \\ h_0 x_0 + h_1 x_2 \\ h_1 x_0 + h_0 x_1 \\ h_1 x_1 + h_0 x_2 \end{bmatrix} \quad (3.7)$$

Equation (3.7) can be modified and considering the data symbols only we get, (asterisk mark denotes the cyclic prefix symbols)

$$\begin{bmatrix} * \\ y_0 \\ y_1 \\ y_2 \end{bmatrix} = \begin{bmatrix} * & * & * \\ h_0 & 0 & h_1 \\ h_1 & h_0 & 0 \\ 0 & h_1 & h_0 \end{bmatrix} \begin{bmatrix} x_0 \\ x_1 \\ x_2 \end{bmatrix} = \begin{bmatrix} * \\ h_0 x_0 + h_1 x_2 \\ h_1 x_0 + h_0 x_1 \\ h_1 x_1 + h_0 x_2 \end{bmatrix} \quad (3.8)$$

From equations (3.8) and (3.5) we see that the expressions are the same if we exclude the cyclic prefix symbol. The important thing to be noted here is that the \mathbf{H} matrix in equation (3.8) and (3.5) are the same for the data symbols. Thus the received vector can be written as

$$\mathbf{y} = \mathbf{H}\mathbf{x}' = \mathbf{H}_c \mathbf{x} \quad (3.9)$$

$$\text{where } \mathbf{H}_c = \begin{bmatrix} h_0 & 0 & h_1 \\ h_1 & h_0 & 0 \\ 0 & h_1 & h_0 \end{bmatrix} \quad (3.10)$$

The effect of the cyclic prefix is to make the channel matrix circulant¹. Hence we conclude that the cyclic prefix makes the channel look like circular convolution instead of linear convolution and thereby eliminates the ISI completely. The estimate of the transmitted signal is obtained in the receiver after the FFT operation. Thus the vector received after the FFT operation can be written as

$$\hat{\mathbf{s}} = \mathbf{F}\mathbf{y} = \mathbf{F}\mathbf{H}_c \mathbf{x} = \mathbf{F}\mathbf{H}_c \mathbf{F}^H \mathbf{s} \quad (3.11)$$

$$= \Delta \mathbf{s} \quad (\text{From Equation 3.3}) \quad (3.12)$$

¹ An $N \times N$ matrix whose rows are composed of cyclically shifted versions of length N

where \mathbf{s} is the vector of data symbols transmitted, and $\Delta = N \begin{bmatrix} H(0) & & 0 \\ & \ddots & \\ 0 & & H(N-1) \end{bmatrix}$ is the

Fourier transform of the channel coefficients. A general OFDM transceiver with Cyclic Prefix is as shown in Figure 3.6.

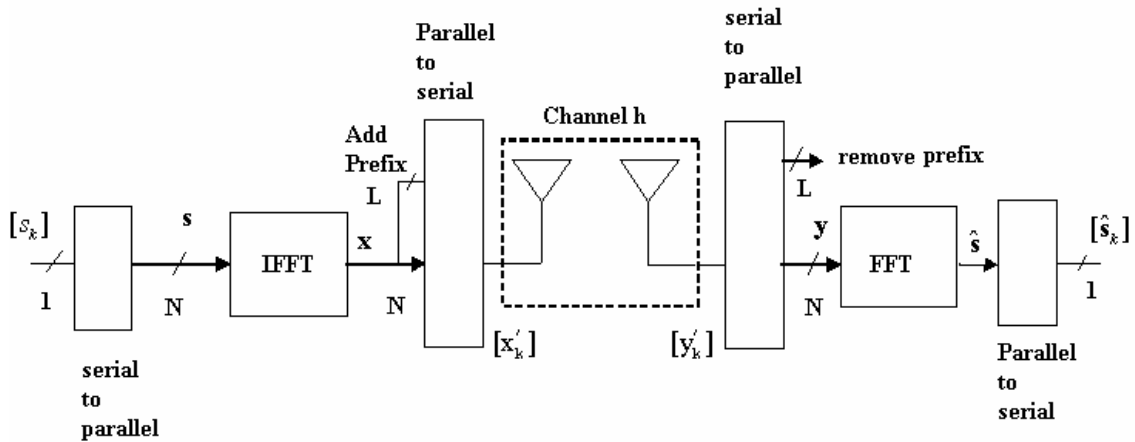


Figure 3.6 OFDM Transceiver with Cyclic Prefix

Figure 3.7 shows the performance of OFDM in a multipath channel. The effect of cyclic prefix is also shown in comparison with the zero padding. The cyclic prefix restores the orthogonality between the subcarriers and the performance with cyclic prefix is same as the performance of OFDM in flat fading. The Doppler is assumed low and the channel was modeled as a two-ray channel with equal powers in both the paths. Zero padding doesn't help remove the ICI introduced due to the multipath and hence the performance decreases as the delay spread increases.

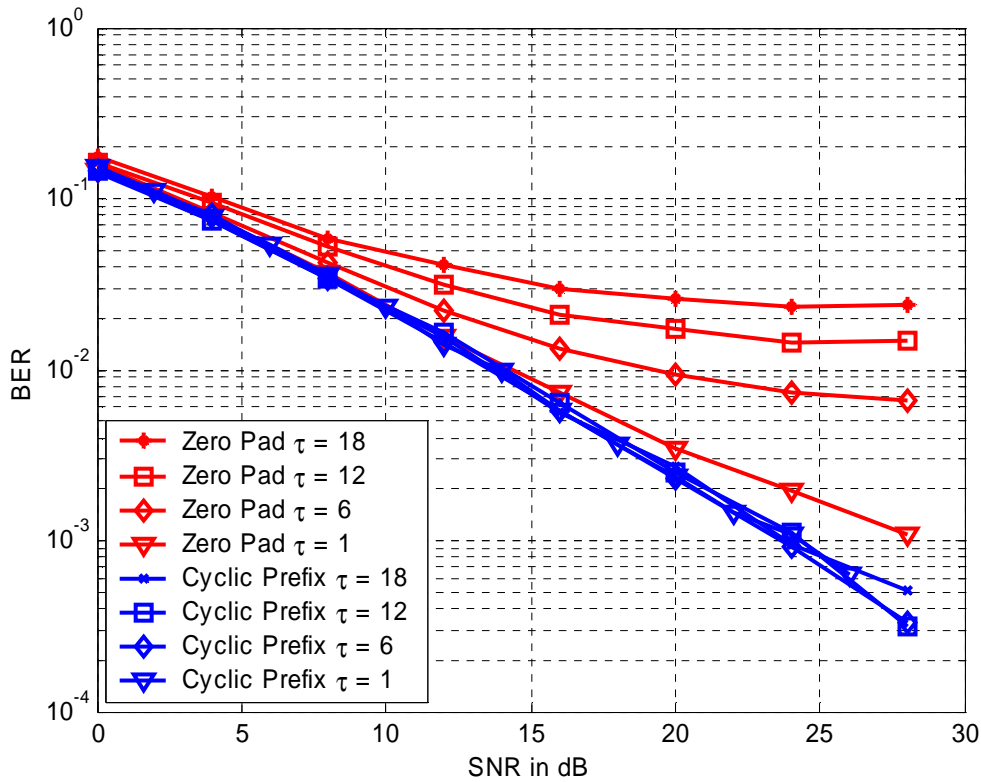


Figure 3.7 Performance of OFDM in a Multipath channel. Delays are expressed in samples.

3.2.3 ICI Analysis for OFDM systems

The insertion of guard time is an effective means of eliminating the Inter Symbol Interference in a dispersive fading channel. However, the time variations of the channel also disrupt the orthogonality between the subcarriers and results in InterCarrier Interference. The extent to which the channel can vary within an OFDM block period decreases with increasing symbol rate. Hence for some high data rate applications the literature often assumes that the channel doesn't change significantly within the OFDM block period. The effect of ICI is very prominent for mobile reception in vehicles such as trains or buses. If not compensated, ICI would result in an error floor. If the channel impulse response can be estimated by using some pilot tones it is possible to reduce the ICI through proper equalization. In [Cim85], some pilot tone assisted estimation and equalization is performed to compensate for the ICI. In [Rus95] theoretical expressions are derived for ICI variance by modeling the ICI as additive Gaussian random processes.

This approximation is due to the Central limit theorem and is valid when the number of carriers is large. The ICI variance is given as [Rus95]

$$E[|c_l|^2] = E_s - \frac{E_s}{N^2} \left\{ N + 2 \sum_{i=1}^{N-1} (N-i) J_0(2\pi f_D T_s i) \right\} \quad (3.13)$$

where c_l is the ICI, E_s is the Energy per symbol, N is the number of subcarriers, f_D is the Doppler frequency, T_s is the symbol duration and J_0 is the zero-order Bessel function of the first kind. It is interesting to note that the ICI variance is independent of the signal constellation. The bit error rate for coherent PSK in a Rayleigh fading channel is given as [Pro95]

$$P_e = 1/4\bar{\gamma}_b \quad (3.14)$$

Now knowing the ICI power from Equation 3.13, we can calculate the Signal to Interference Ratio (SIR). This SIR value is substituted for $\bar{\gamma}_b$ in the above expression to calculate the bit error rate. Figure 3.8 shows the error floor due to the ICI for QPSK modulation with increasing values of the Doppler frequency. Theoretical results were found to match with the simulation results.

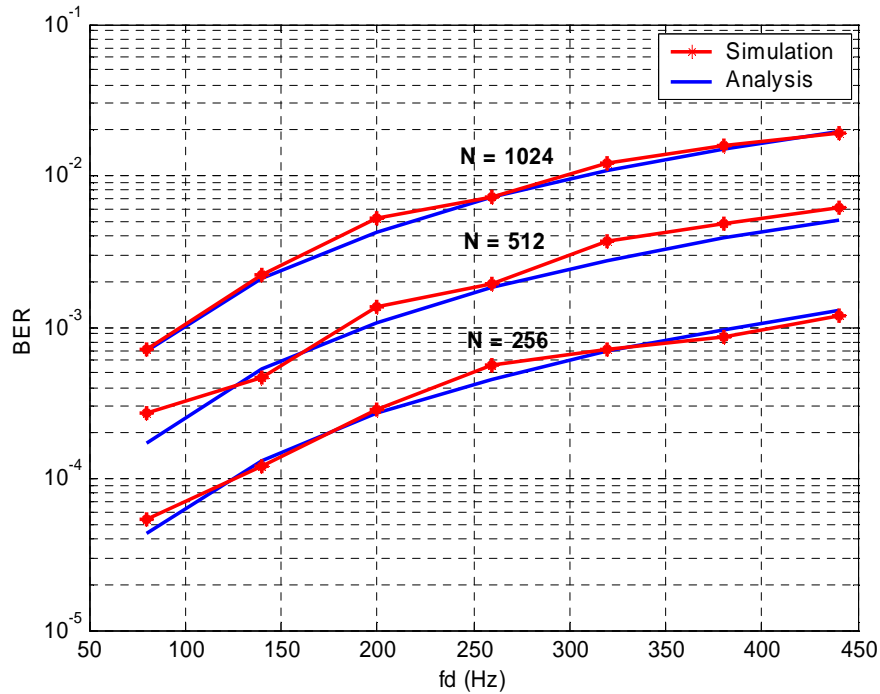


Figure 3.8 Error Floor due to ICI for various numbers of subcarriers (N)

The effect of ICI and the decrease in SIR for increasing values of the Doppler frequency is shown in Figure 3.9

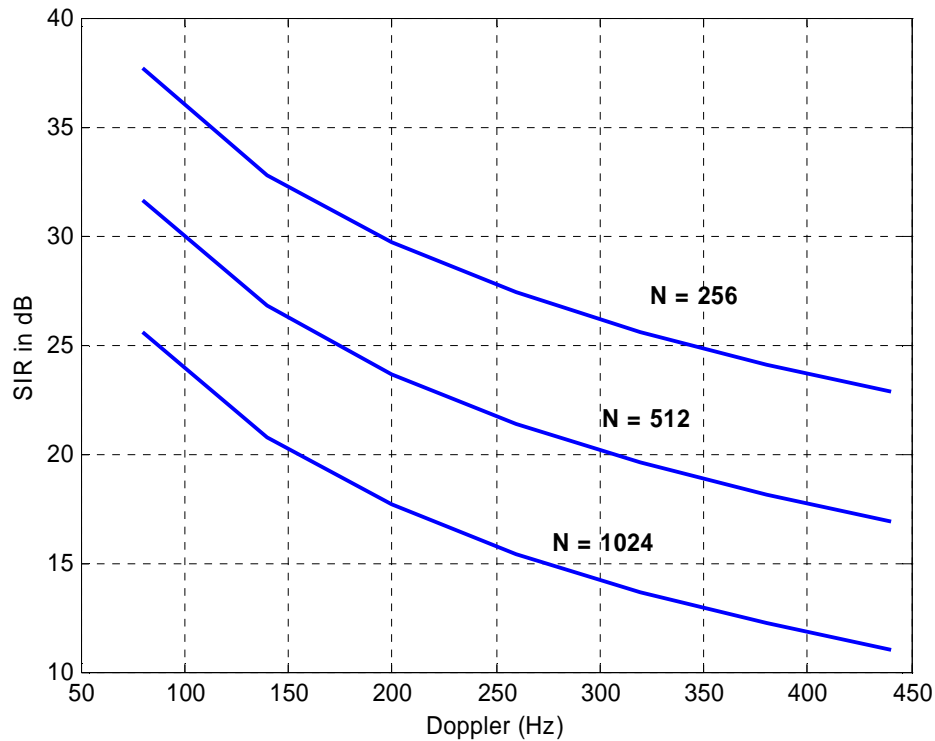


Figure 3.9 Effect of ICI on the Signal to Interference Ratio

We see from Figures 3.8 and 3.9 that the ICI power is dependent on the number of subcarriers. The larger the number of subcarriers, more the ICI variance and lower the SIR.

The above sections gave a brief introduction to OFDM and the importance of Multicarrier techniques. Also the performance of OFDM under different Doppler conditions was studied and analytic results matched with simulations. The importance of the cyclic prefix was analyzed from a matrix theory point of view and simulations results were shown to improve performance in a multipath channel using the cyclic prefix. In the coming sections we will study the CDMA version of OFDM namely MC-CDMA and discuss its advantages.

3.3 MultiCarrier CDMA

The previous sections presented an overview of OFDM systems, the importance of cyclic prefix and the analysis of Inter Carrier Interference in OFDM. OFDM is an effective technique to combat the frequency selectivity of the channel. Code Division Multiple Access (CDMA) has been a strong candidate to support multimedia mobile services because it has the ability to cope up with the asynchronous nature of the multimedia traffic and can provide higher capacity as opposed to the conventional access schemes such as TDMA or FDMA. By employing Rake receivers CDMA systems can coherently combine the multipath components due to the hostile frequency selective channel. The processing gain due to spreading provides robustness to the multi-user interference. The use of conventional CDMA does not seem to be realistic when the data rates go up to a hundred megabits per second due to severe ISI and the difficulty in synchronizing a fast sequence. Techniques for reducing the symbol and chip rate are essential in this case.

Recent studies by researchers have combined the principle of CDMA with OFDM which allows one to use the available spectrum in an efficient way and retain the many advantages of a CDMA system. If the number and spacing between the subcarriers are chosen appropriately, it is unlikely that all the subcarriers will be in deep fade and thus provides frequency diversity. This combination of OFDM-CDMA is a useful technique for 4G systems where we need variable data rates as well as provide reliable communication systems. In [Yee93] this form of OFDM-CDMA or MultiCarrier CDMA (MC-CDMA) was first proposed and the performance of MMSE detection was studied for MC-CDMA. [Cho93] also proposed the same idea at the same time and analyzed the performance of Maximum Likelihood Detection (MLD) for MC-CDMA systems. A MC-CDMA system basically applies the OFDM type of transmission to a Direct Sequence (DS) - CDMA signal. In conventional DS-CDMA each user symbol is transmitted in the form of sequential chips, each of which is narrow in time and hence wide in bandwidth. In contrast to this, in MC-CDMA due to the FFT transform along with OFDM the chips are longer in time duration and hence narrow in bandwidth. The multiple chips for a data symbol are not sequential but instead transmitted in parallel over many subcarriers. An

interesting feature of MC-CDMA is that the modulation and demodulation can be easily implemented using simple FFT and IFFT operators.

Although OFDM is robust to frequency selective fading, it has severe disadvantages in subcarrier synchronization and sensitivity to frequency offset estimation. The other main issue with respect to OFDM is the presence of a large number of subcarriers which exhibits a non-constant nature in its envelope. The combining of OFDM and CDMA has one major advantage though. It can lower the symbol rate in each subcarrier compared to OFDM so that longer symbol duration makes it easier to synchronize [Che95].

The MC-CDMA not only mitigates the ISI but also exploits the multipath. [Kai95] has shown that MC-CDMA suffers only slightly in presence of interference as opposed to DS-CDMA whose performance decreases significantly in presence of interference.

Multicarrier CDMA schemes can be broadly categorized into two groups [Pra96]. The first type spreads the original data stream using a spreading code and then modulates different carriers with each chip, i.e., spreading the chips in the frequency domain. This is usually referred to as MC-CDMA and is the technique of interest to us. The second type spreads the serial to parallel converted streams using a spreading code and then modulates different carriers with each data stream, i.e., spreading in the time domain. Again two schemes are reported in this spreading in time domain approach based on the subcarrier frequency separation. If we denote the bit duration as T_b and the chip duration as T_c , then the subcarrier spacing in one system is $1/T_c$ and the other is $1/T_b$. The former is called the Multicarrier DS-CDMA (MC-DS-CDMA) and the latter is called the Multi-tone CDMA (MT-CDMA). The performance of these two schemes has been studied for an uplink channel in [Sou96]. [Har97] has shown that MC-CDMA outperforms MC-DS-CDMA and MT-CDMA in terms of downlink BER performance. MC-CDMA is thus an attractive technique for the downlink. The authors cite the reason as MC-CDMA scheme can always utilize all the received signal scattered in frequency domain compared to MT-CDMA and MC-DS-CDMA scheme.

A simple block diagram of a MC-CDMA system is as shown below in Figure 3.10

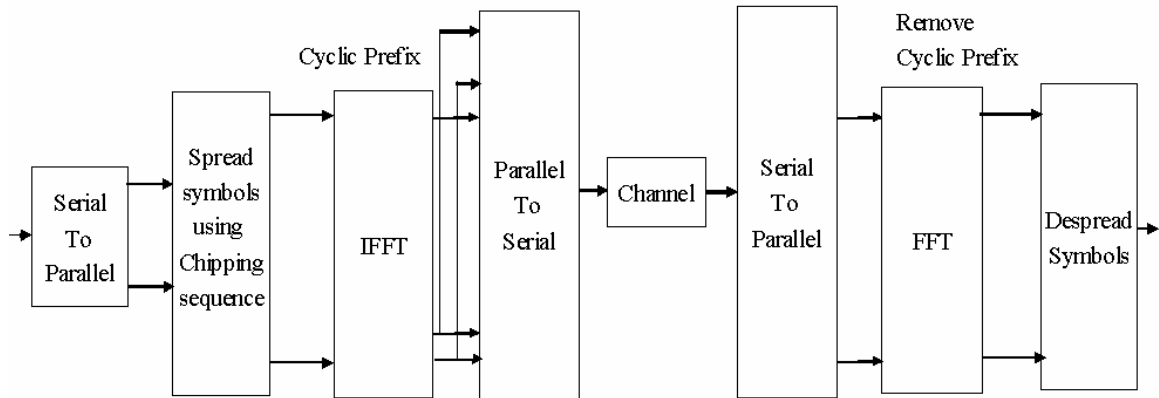


Figure 3.10 Block Diagram of a MC-CDMA system

The input data stream is spread using the spreading sequence which could be a Walsh-Hadamard code or a PN sequence. The resultant chips after spreading the symbols are modulated into different subcarriers using the IFFT operator. The end few symbols are appended at the beginning of the frame to act as the cyclic prefix. The cyclic prefix maintains orthogonality between the subcarriers in a multipath channel. The receiver first removes the cyclic prefix and then performs an FFT operation of the received symbols and brings them back to the frequency domain. Then despreading and decoding of the chips in frequency domain are performed.

In the sections that follow we will discuss MC-DS CDMA and Multi-Tone CDMA. We focus more on MC-CDMA as that is the area of our interest. The performance analysis of MC-CDMA in the presence of interferers, the effect of ICI and the subcarrier position on the ICI and some pilot assisted channel estimation techniques for MC-CDMA will be discussed.

3.3.1 MC-DS CDMA

The block diagram of a MC-DS CDMA transmitter is shown in Figure 3.11(a). The incoming data stream is first converted to a parallel stream and then spread in time using spreading codes. This ensures that the resulting spectrum has orthogonal subcarriers. The spreading code is represented as $C(t)$ and the processing gain is N . The receiver block is shown in Figure 3.10(b). The despreading is done in time after the FFT followed by a low pass filter and demodulation. The figures are adapted from [Har97].

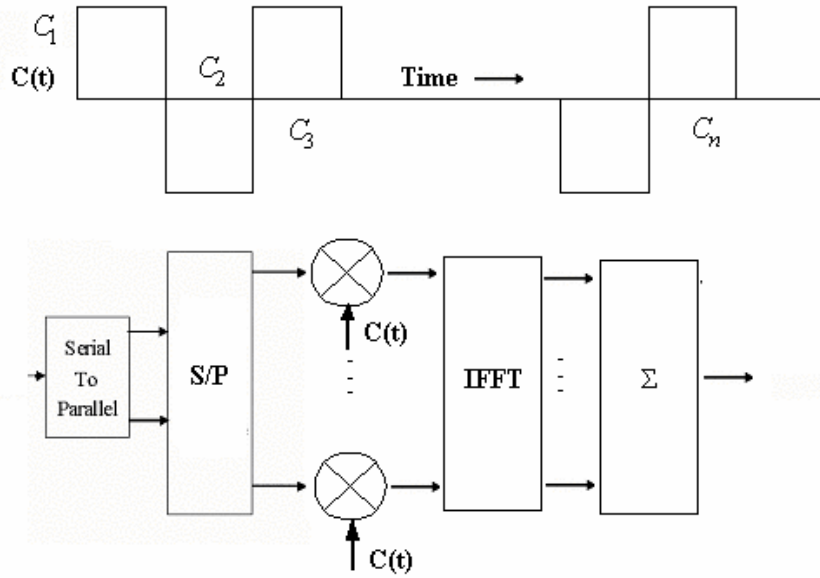


Figure 3.11(a)

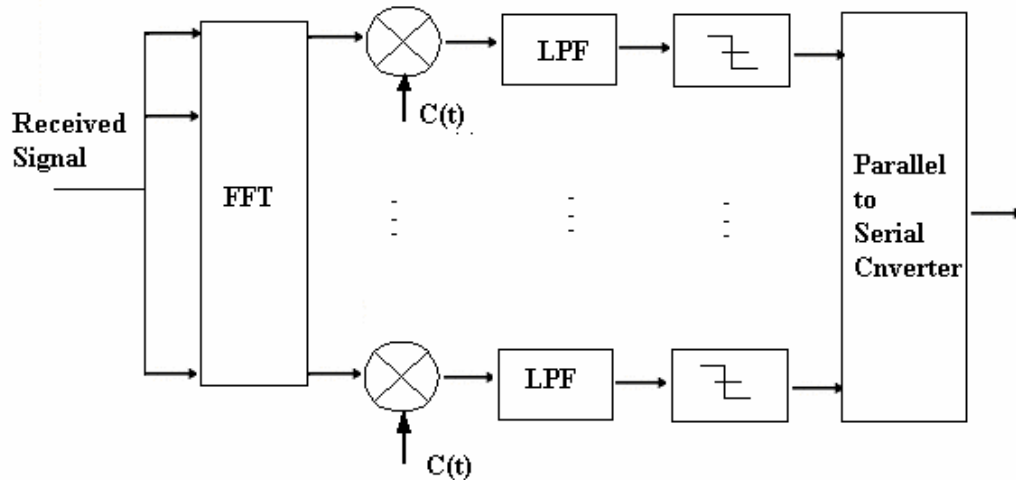


Figure 3.11(b)

Figure 3.11 (a) MC-DS CDMA Transmitter (b) MC-DS CDMA Receiver.

3.3.2 Multi-Tone CDMA (MT-CDMA)

Multi-Tone CDMA transmitter spreads the serial parallel converted data streams using a spreading code in time domain so that the spreading operation can satisfy the orthogonality condition. The MT-CDMA uses spreading codes in multiples of the number of subcarriers as compared to MC-DS CDMA. The transmitter block is shown in Figure 3.12(a). The receiver employs Rake combining to effectively utilize the diversity due to multipath. The figures are adapted from [Har97].

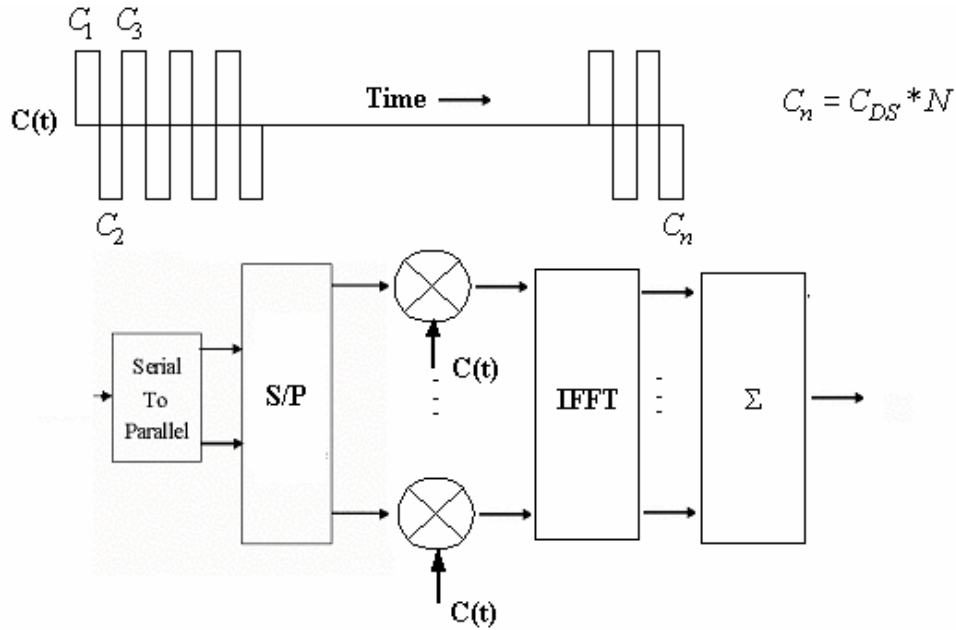


Figure 3.12(a)

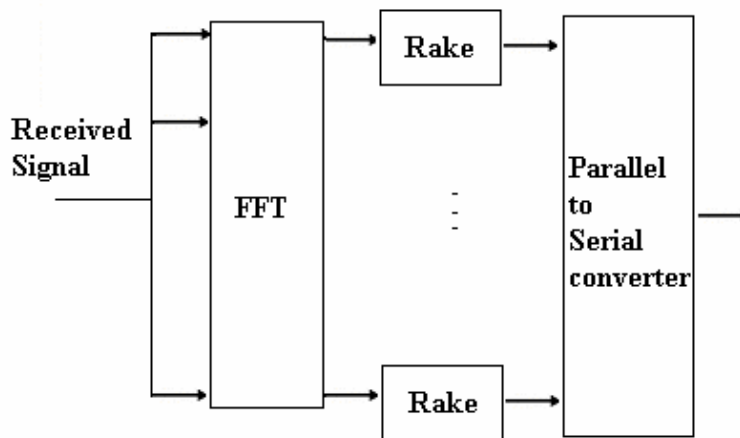


Figure 3.12 (b)

Figure 3.12(a) MT-CDMA Transmitter (b) MT-CDMA Receiver

3.3.3 ICI Analysis for MC-CDMA

MC-CDMA being an OFDM technique suffers from Inter Carrier Interference due to the loss of subcarrier orthogonality when the channel changes significantly in time. Like OFDM, there is an irreducible error floor in MC-CDMA due to the ICI. The performance results vary for OFDM and MC-CDMA and are discussed extensively in [Lin94]. In [Cho01] the ICI power has been evaluated and is shown to be a function of the subcarrier index k . This is due to the fact that at the output of the FFT block, the k th subcarrier output can be written as [Cho01],

$$Y_k = \frac{1}{\sqrt{N}} \sum_{n=0}^{N-1} y(n) e^{-j2\pi nk/N} = d_k H_k + \alpha_k + n_k \quad (3.15)$$

where $y(n)$ is the received signal, N is the IFFT size, d_k are the original transmitted symbols, H_k is the Fourier transform of the channel at the subcarrier index k , α_k is the ICI term due to the time varying nature of the channel and n_k is the noise term at the k th subcarrier. In a time invariant channel due to the orthogonality of subcarrier waveforms the α_k is zero and $E\{|H_k|^2\} = 1$. When the normalized Doppler frequency (fdT) is high the ICI term is non-zero. The ICI power has been evaluated and is shown to be a function of the subcarrier index k as follows [Cho01].

$$E\{|\alpha_k|^2\} = \frac{1}{N^2} \sum_{m=0, m \neq k}^{N-1} \left(N + 2 \sum_{n=1}^{N-1} (N-n) J_0(2\pi f_d T n / N) \cos(2\pi n(m-k)/N) \right) \quad (3.16)$$

Here N is the number of subcarriers and the normalized ICI power is described as $E\{|\alpha_k|^2\} / E\{|H_k|^2\}$ where the $E\{|H_k|^2\}$ is defined as

$$E\{|H_k|^2\} = \frac{1}{N^2} \left(N + 2 \sum_{n=1}^{N-1} (N-n) J_0(2\pi f_d T n / N) \right) \quad (3.17)$$

Figure 3.13 shows the effect of the Normalized ICI power and how the subcarrier location affects the ICI power. The center subcarrier experiences more ICI power than the edge subcarrier. Figure 3.14 shows the effect of ICI with respect to the number of subcarriers. It is seen that the ICI power difference is negligible when the number of subcarriers is large. The ICI contribution due to the edge subcarriers on the central is not much significant and hence we see that the curve flattens with increase in FFT size.

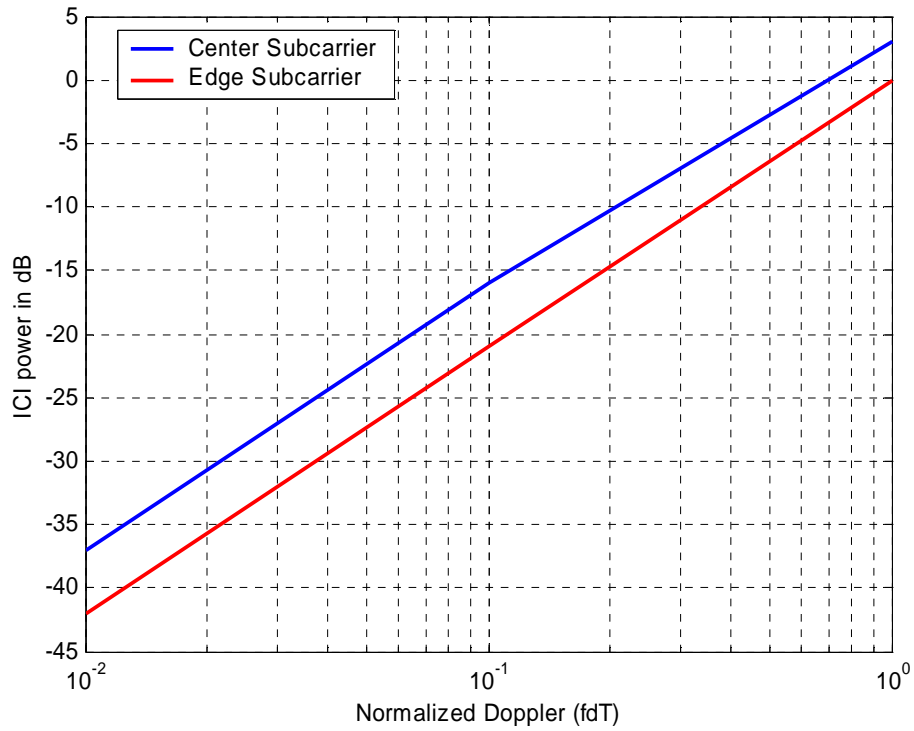


Figure 3.13 Normalized ICI power for a MC-CDMA signal. $N = 1024$.

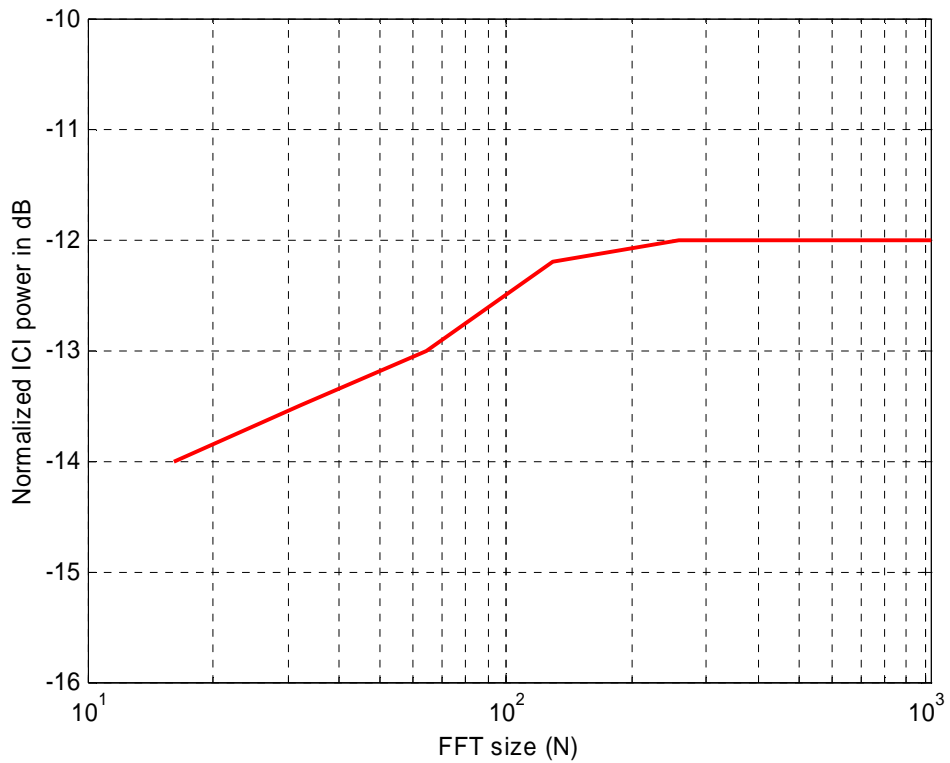


Figure 3.14 Normalized ICI power for the center subcarrier ($f_d T = 0.2$)

3.3.4 Interference resistance in MC-CDMA

MC-CDMA provides an access technique for different users by its inherent processing gain. The users are distinguished using different spreading codes and this enables efficient use of the radio resources. The spreading code provides the interference rejection capability. Use of Walsh-Hadamard codes or PN sequences with good autocorrelation properties can reduce the impact of interference. The performance of MC-CDMA with various spreading factors was studied and the results are shown in Figure 3.15. The simulations were performed using a wide-band Jammer type of interference. We see that higher spreading factor gives better interference rejection. Though higher spreading gives better performance, it reduces the actual throughput and hence we need to employ some other interference rejection technique if high data rates are desired. The use of smart antennas is one possible solution which will be discussed in detail in Chapter 5.

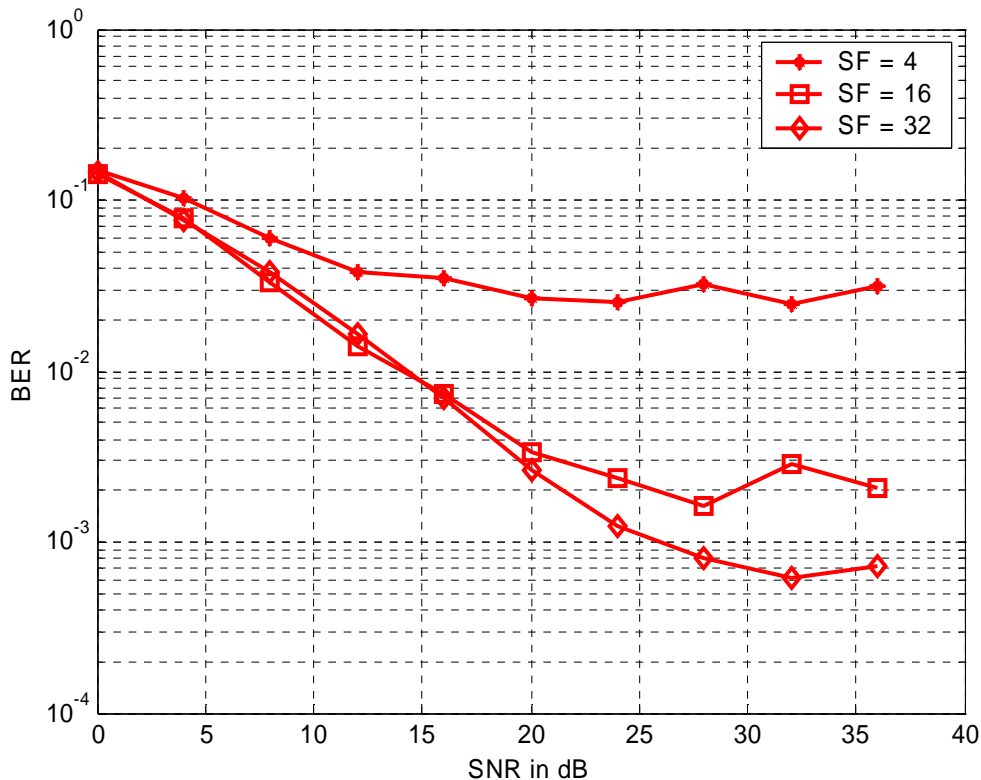


Figure 3.15 Performance of Multicarrier CDMA in presence of Interferers. SIR = 0dB and $f_d T = 0.01$ Increasing spreading factor reduces the error floor.

The effect of narrow-band interference is shown in Figure 3.16. We see that as the spreading factor is increased the BER performance worsens. This can be attributed to the following reason. As we increase the spreading factor (SF) the number of data symbols is reduced in an MC-CDMA symbol, assuming that the number of subcarriers (N_c) is fixed. The probability of bit error P_e is inversely proportional to the number of data symbols (N).

$$P_e \propto \frac{1}{N} = \frac{SF}{N_c}$$

Thus we see from the above equation that as we increase the spreading factor the probability of bit error is increased.

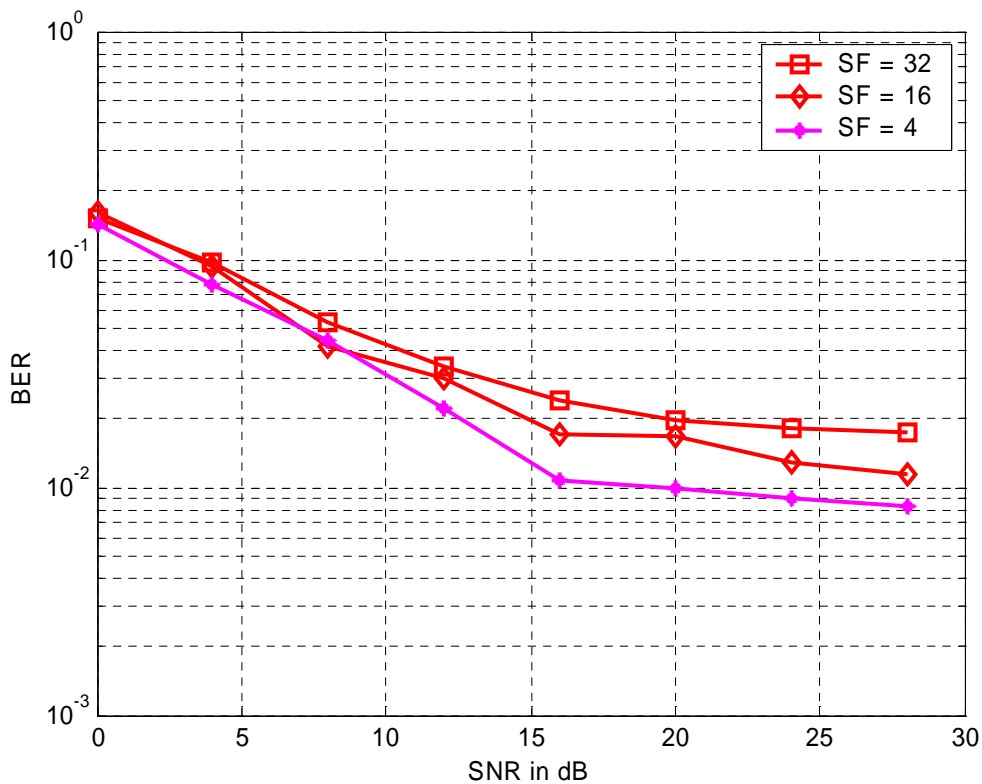


Figure 3.16 Performance of MC-CDMA in presence of narrowband interferers for varying spreading code lengths. SIR = -20dB, $f_d T = 0.01$

3.3.5 Channel Estimation for MC-CDMA

Despite the several advantages for MC-CDMA the increased symbol duration in MC-CDMA makes channel estimation difficult. This is because the changes in the channel from symbol to symbol are more significant than in a single carrier modulation. Also the time variations of the channel introduce ICI which results in an irreducible error floor in conventional receivers. In this section, some simple pilot based channel estimation techniques will be considered while more robust channel estimation techniques will be dealt with in chapter 4. The two important parameters that affect the channel estimation algorithm are the Doppler spread and the delay spread. The performance of different channel estimation algorithms were tested under various conditions.

Channel Estimation using the FFT method

A Rayleigh fading compensation technique using the FFT method was originally proposed by [Oka95] for QAM signals. We apply the same technique for a MC-CDMA signal. Pilot chips are inserted before the IFFT block at the transmitter or can be said to be in the frequency domain. The least squares estimate of the pilots is obtained in the receiver by dividing those corrupted pilots with the known pilot symbols. To obtain the channel coefficients for the data symbols interpolation is performed in the frequency domain.

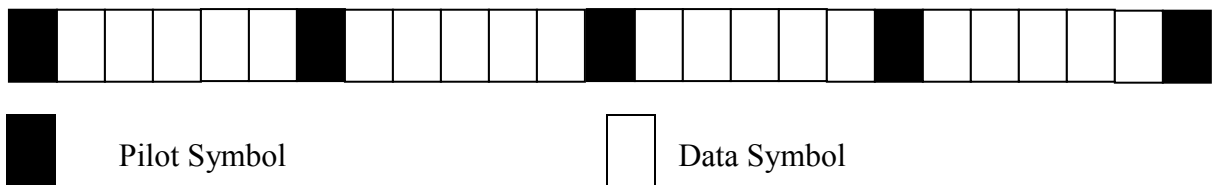


Figure 3.17 Frame format of MC-CDMA showing pilots multiplexed with data symbols

Let us assume that there are N_p pilot symbols in a frame. Also let N be the number of data symbols inserted between the pilot symbols. The pilot chips are recovered after the FFT operation in the receiver. If we say that these pilot chips are represented as $g(l)$, then we have a Fourier transform pair as follows,

$$G(n) = \sum_{l=0}^{N_p-1} g(l) \exp(-j2\pi nl / N_p) \quad (n = 0, 1, \dots, N_p - 1) \quad (3.18)$$

$$g(l) = \frac{1}{N_p} \sum_{n=0}^{N_p-1} G(n) \exp(j2\pi nl / N_p) \quad (l = 0, 1, \dots, N_p - 1) \quad (3.19)$$

We interpolate this sequence $G(n)$ and form another sequence of length NN_p , $G'(n)$ which is given as

$$\begin{aligned} G'(n) &= NG(n) & [0 \leq n \leq (N_p / 2 - 1)] \\ G'(n) &= 0 & [N_p / 2 \leq n \leq N_p / 2(2N - 1) - 1] \\ G'(n) &= NG(n - N_p(N - 1)) & [N_p / 2(2N - 1) \leq n \leq N_p N - 1] \end{aligned} \quad (3.20)$$

Now this $G'(n)$ denotes the frequency domain version of the original fading series $c(k)$ and is given by the NN_p point Inverse Fourier Transform of $G'(n)$ and is given as follows,

$$c(k) = \frac{1}{NN_p} \sum_{n=0}^{NN_p-1} G'(n) \exp(j2\pi nk / NN_p) \quad (k = 0, 1, \dots, NN_p - 1) \quad (3.21)$$

The $c(k)$'s are the Fourier transform of the original fading coefficients. The received sequence after the FFT operation are then multiplied by the conjugate of $c(k)$ to compensate for the channel. The performance of this channel compensation technique was studied in various Doppler conditions and the BER curves are presented in Figure 3.14. We see that the Doppler introduces InterCarrier interference and hence the performance decreases as expected. The number of pilots can be increased to improve performance at the expense of throughput. The Figure 3.14 below shows the performance for a fixed number of pilots per MC-CDMA symbol. For low Doppler spreads the performance of the estimation is only worse by about 3-4 dB from the perfect channel estimation. The effect of Doppler on the performance is two fold. First the pilot symbols are corrupted due to the rapid amplitude fluctuations and the high Doppler also introduces Inter-Carrier Interference (ICI). Thus we see in Figure 3.18 the error floor as a result of increase in ICI. Figure 3.19 shows the effect of the time dispersiveness on the channel estimation performance. The delay spread causes rapid changes in the frequency response of the channel. The channel estimation is poor with increasing delay spread as the FFT method attempts to estimate the frequency response of the channel.

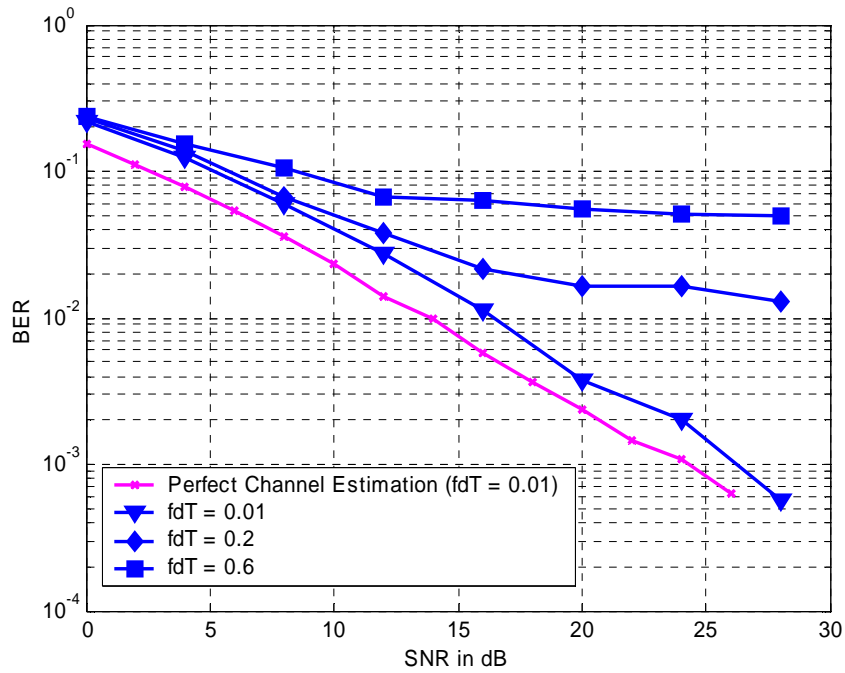


Figure 3.18 Effect of Time variations on Channel Compensation for MC-CDMA using the FFT method (64 Pilots per block, Spreading Factor = 4)

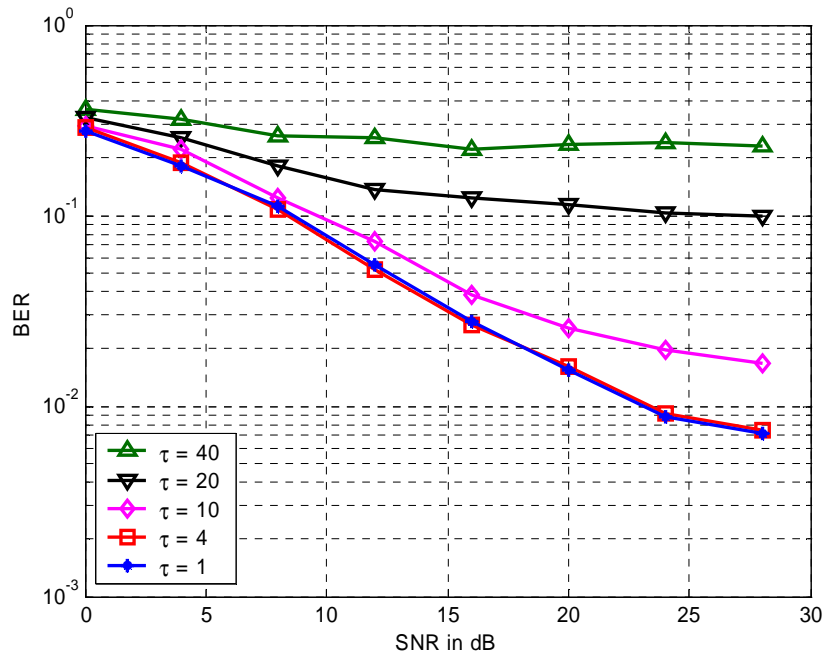


Figure 3.19 Effect of Delay spread on Channel Compensation for MC-CDMA using the FFT method (64 Pilots per block, Spreading Factor = 4, $f_d T = 0.01$). Delays (τ) expressed as number of samples.

Channel Estimation by Cubic Spline Interpolation

The FFT method discussed above can be computationally complex although its performance is good for low Doppler spreads. The estimator involves FFT and IFFT computations of long sequences which can consume more DSP cycles. A simple technique is to perform straight-forward interpolation between the pilot symbols to obtain channel coefficients for the data symbols. Like the FFT method, we multiplex the pilot symbols between the data symbols and a least squares estimate of the pilot symbols are obtained at the receiver using knowledge of the transmitted pilot symbols. A cubic spline interpolation is then performed between the pilot positions to obtain channel coefficients for the data symbols. The cubic spline interpolator tries to approximate the given pilot position values with a third degree polynomial. Using this polynomial the channel coefficients for the data symbols can be estimated. The performance of the cubic spline interpolator for various channel delay spreads are shown in Figure 3.20.

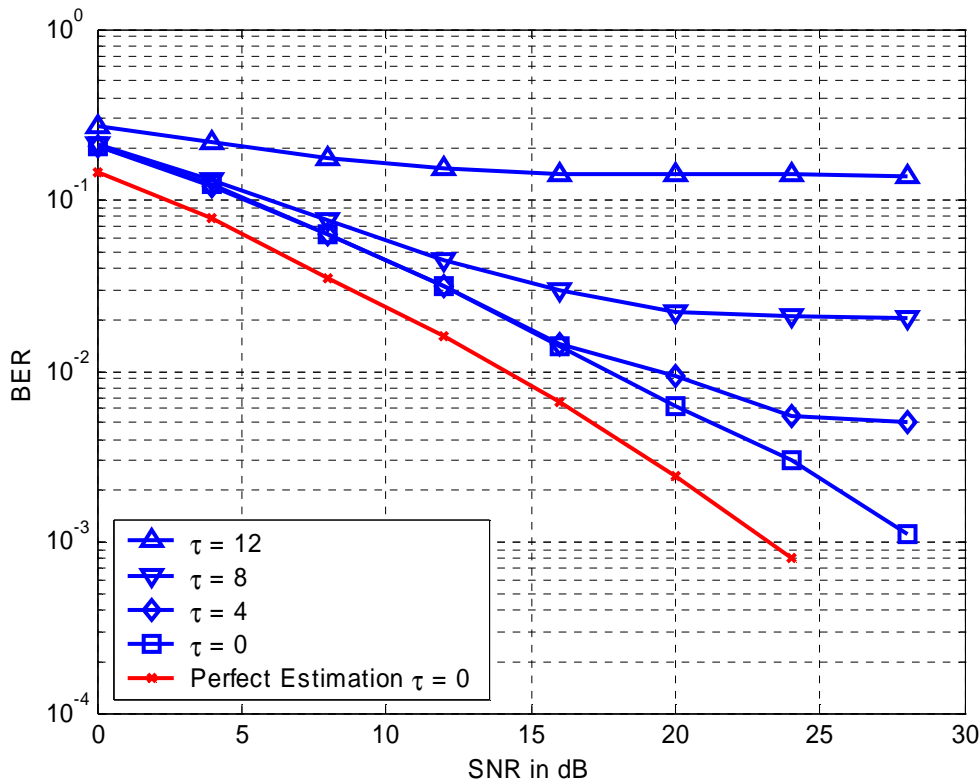


Figure 3.20 Cubic Spline Channel Estimation performance for MC-CDMA for various channel delay spreads. Delay spread expressed in units of samples.

We see that the channel delay spread worsens the performance of the channel estimation algorithm. Even though we insert cyclic prefix which can bring back the orthogonality between the subcarriers the interpolation between the pilot chips results in an error floor. This can be attributed to the fact that the channel variations in frequency are more significant as the delay spread is increased and this corrupts the pilot symbols. Increase in the channel delay spread only helps to worsen the performance further as can be seen in the figure above. For low delay spreads the channel estimator works fine and we see some 3-4 dB performance loss from Ideal channel estimation.

3.4 Summary

This chapter has dealt with the basic concepts of multicarrier modulation. The importance of OFDM and its ability to provide high data rates in adverse channel conditions were explained. The performance of OFDM in high Doppler environments was studied and analytical expressions were used to match the simulation results. The usefulness of the cyclic prefix for multipath channels and its ability to restore the orthogonality between the subcarriers was also analyzed. Some basic concepts and the advantages of MC-CDMA were also discussed. The interference rejection capability of MC-CDMA was studied and simulation results were shown. Finally channel estimation techniques were discussed for MC-CDMA. More robust channel estimation techniques will be discussed in Chapter 4.

Chapter 4

Advanced detection techniques and robust channel estimation for MC-CDMA

The previous chapter gave an introduction to MC-CDMA and dealt with its performance in channels with rapid time variations. Some simple straightforward channel estimation techniques were also discussed. The time varying channel disrupts the orthogonality between the subcarriers and induces what is called Inter Carrier Interference (ICI). Recent literature has proposed some advanced detection techniques for MC-CDMA, which provide improved performance in such harsh channel conditions. These detection schemes will be discussed in this chapter. The increased symbol duration in multicarrier modulation techniques results in the channel changing significantly from symbol to symbol, necessitating the need for more robust channel estimators. A robust channel estimator which estimates the channel parameters in the time domain will be discussed in this chapter and the performance results will be presented.

4.1 Improved detection techniques

[Faz93] and [Kai95] were among the earliest to study the performance of different detection techniques for MC-CDMA systems. In this section we will investigate the performance improvement achieved using LS and MMSE detection techniques as compared to conventional FFT detectors.

4.1.1 Conventional FFT detection for MC-CDMA systems

A detailed analysis of the conventional detection scheme is provided in [Cho01]. The received MC-CDMA signal can be written as

$$y(n) = \sum_{l=0}^L h(n,l)s(n-l) + w(n) \quad (4.1)$$

Here L is the number of multipaths, $h(n,l)$ represents the time varying nature of the channel coefficients for each path, l , $w(n)$ is the additive white gaussian noise and $s(n)$ represents the output of the IFFT at the transmitter.

The received signal can be rewritten as [Cho01],

$$y(n) = \frac{1}{\sqrt{N}} \sum_{k=0}^{N-1} d_k H_k(n) \exp(j2\pi nk / N) + w(n) \quad 0 \leq n \leq (N-1) \quad (4.2)$$

Here d_k are the individual modulated symbols and $H_k(n)$ is the Fourier transform of the channel impulse response at time 'n'. From the equation (4.2) we see that the multipath channel introduces a time varying complex multiplier $H_k(n)$ at each of the subcarriers. At the receiver, the output of the FFT block for the k th subcarrier can be written as

$$Y_k = \frac{1}{\sqrt{N}} \sum_{n=0}^{N-1} y(n) \exp(-j2\pi nk / N) = d_k H_k + \alpha_k + W_k \quad (4.3)$$

In the above equation α_k represents the Inter Carrier Interference term while W_k represents the noise term. In a time invariant channel α_k for each subcarrier is zero, and for channels with high Doppler spreads the power of ICI cannot be ignored since it can cause severe performance degradation.

In vector form the expression for the received signal after the removal of the guard time can be written as [Cho01]

$$\mathbf{y} = \mathbf{H}\mathbf{d} + \mathbf{w} \quad (4.4)$$

where \mathbf{d} is the vector containing the individual modulated symbols and \mathbf{H} is the matrix containing the channel coefficients. The \mathbf{H} matrix is given by,

$$\mathbf{H} = \frac{1}{\sqrt{N}} \begin{bmatrix} H_0(0) & H_1(0) & \cdots & H_{N-1}(0) \\ H_0(1) & H_1(1)e^{j2\pi/N} & \cdots & H_{N-1}(1)e^{j2\pi(N-1)/N} \\ \vdots & \vdots & \ddots & \vdots \\ H_0(N-1) & H_1(N-1)e^{j2\pi(N-1)/N} & \cdots & H_{N-1}(N-1)e^{j2\pi(N-1)(N-1)/N} \end{bmatrix} \quad (4.5)$$

The FFT detection can be thought of as a matched filter for the channel matrix. The decision statistic is thus given as

$$\mathbf{z} = \mathbf{H}^H \mathbf{y} = \mathbf{H}^H \mathbf{H}\mathbf{d} + \mathbf{H}^H \mathbf{w} \quad (4.6)$$

For a time invariant channel the $\mathbf{H}^H \mathbf{H}$ matrix becomes an identity matrix. This is not valid for a time-varying channel. Hence the FFT detection suffers from ICI for time-varying channels.

Figure 4.1 below shows the $\mathbf{H}^H\mathbf{H}$ matrix results for high and low Doppler spreads. For high Doppler spreads the $\mathbf{H}^H\mathbf{H}$ is not an identity matrix and we see some non-zero entries along the non-diagonal elements. This is not true for low Doppler spreads where the $\mathbf{H}^H\mathbf{H}$ matrix is an identity matrix.

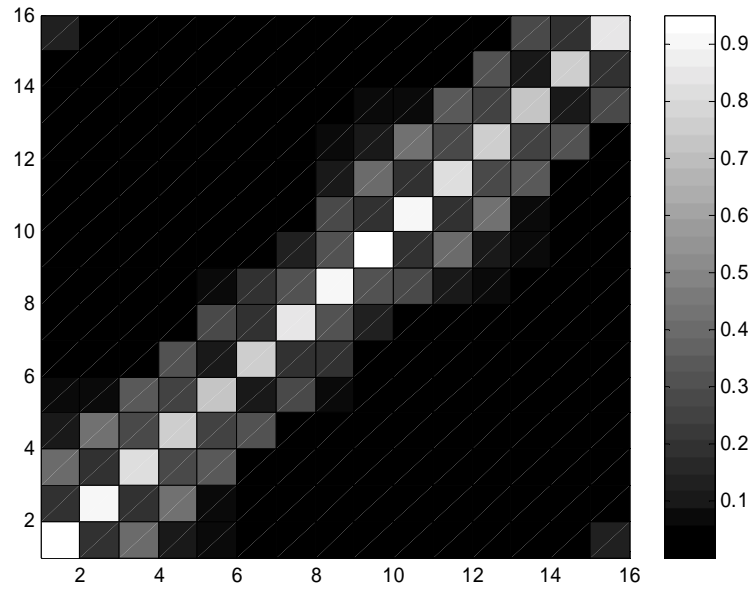


Figure 4.1(a)

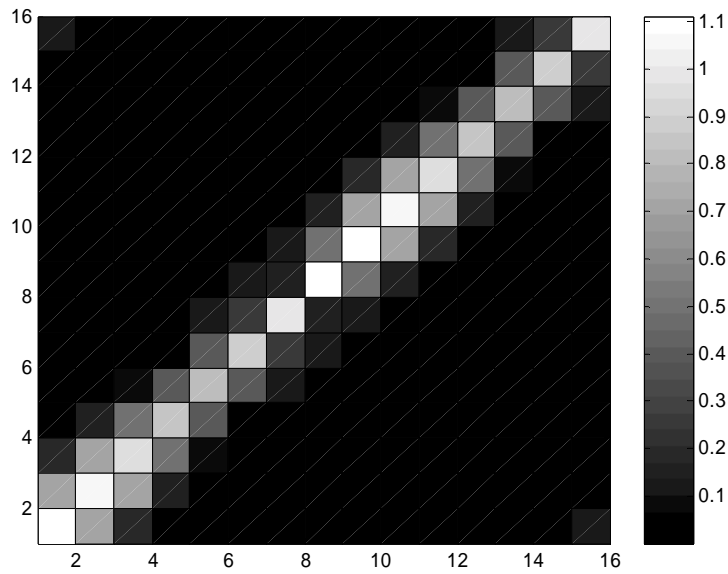


Figure 4.1(b)

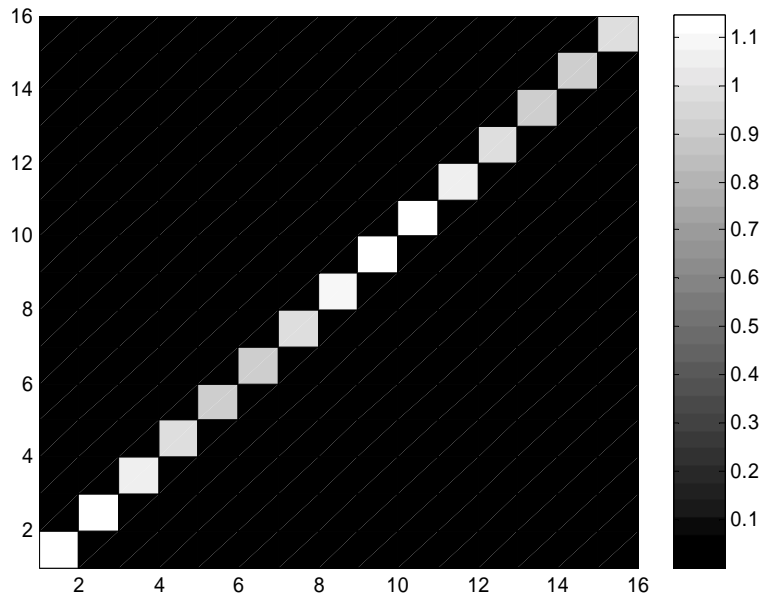


Figure 4.1 (c)

Figure 4.1(a-c) Plot of the $\mathbf{H}^H \mathbf{H}$ matrix after FFT detection for MC-CDMA systems with 16 carriers, Spreading Factor = 1. The channel is frequency selective and time variant. **(a)** $f_d T = 0.1$ **(b)** $f_d T = 0.05$ **(c)** $f_d T = 0.01$ The plots are obtained by averaging over 20 simulation runs.

4.1.2 LS Detection

The least squares detection statistic is given by,

$$\mathbf{z} = \mathbf{G} \mathbf{y} \quad (4.7)$$

where the equalizer matrix \mathbf{G} can be expressed as

$$\mathbf{G} = (\mathbf{H}^H \mathbf{H})^{-1} \mathbf{H}^H \quad (4.8)$$

The \mathbf{G} matrix can be thought of as the Moore Penrose pseudo inverse of the \mathbf{H} matrix. A potential problem with the LS detection is that the equalizer matrix tends to enhance the noise and hence the LS detection might not be a good choice when the SNR is low. Nevertheless, the LS detection performs better than simple FFT detection in channels with high Doppler as we will see.

4.1.3 MMSE detection

The MMSE detector's decision statistic is given by

$$\mathbf{z} = \mathbf{G}^H \mathbf{y} \quad (4.9)$$

where the equalizer matrix can be expressed as

$$\mathbf{G}^H = \mathbf{H}^H (\mathbf{H}\mathbf{H}^H + \sigma^2 I_N)^{-1} \quad (4.10)$$

It can be shown that this choice minimizes the cost function, $E\{|\mathbf{d} - \mathbf{z}|^2\}$. The MMSE detector is similar to the LS detector except that the identity matrix accounts for the noise power. This also helps reduce the noise enhancement.

4.1.4 MMSE with Successive Detection

The decision statistic at the output of the MMSE or LS detector has two terms as can be seen from equations (4.9) and (4.4),

$$z = \mathbf{G}^H \mathbf{H} \mathbf{d} + \mathbf{G}^H \mathbf{w} \quad (4.11)$$

For LS detection the $\mathbf{G}^H \mathbf{H}$ term becomes an identity matrix and hence the ICI is completely removed after equalization. However, performing such an inversion will result in noise enhancement. This noise enhancement is more prominent when the normalized Doppler frequency is higher. The MMSE detector is capable of providing a better performance because it balances noise power and residual ICI.

If the Doppler frequency is increased the channel becomes more time selective. The time varying channel destroys the orthogonality but also provides time diversity. The FFT method generates ICI while the LS detection enhances the noise. On the other hand the MMSE method reduces the ICI and noise. Hence the diversity advantage from the channel can be properly utilized through the MMSE detector by some improvements to MMSE. The performance of such a detector would improve as the channel time selectivity increases due to increased diversity. To fully utilize the diversity in time, [Cho01] has proposed detecting the data successively rather than in one shot as in the previous methods. This type of detection is common in Multi-user detection problems for DS-CDMA and has also been used in MIMO systems to provide high data rates [Wol98].

For successive detection, we first detect the data that has the highest post-detection SINR, assuming MMSE detection. This is done by choosing the $(k+1)$ th column of the equalizer matrix that satisfies the condition,

$$\arg \max \text{SINR}_k = \frac{|\langle \mathbf{g}_k, \mathbf{h}_k \rangle|^2}{\sum_{m, m \neq k} |\langle \mathbf{g}_k, \mathbf{h}_m \rangle|^2 + \sigma^2 \|\mathbf{g}_k\|^2} \quad (4.12)$$

where \mathbf{g}_k is the $(k+1)$ th column of the equalizer matrix \mathbf{G} . The column with the highest post detection SINR is chosen. The received vector \mathbf{y} is then modified after making a hard decision on the received data,

$$z_k = \mathbf{g}_k^H \mathbf{y} \quad (4.13)$$

$$\mathbf{y}_{new} = \mathbf{y} - \mathbf{h}_k \hat{d}_k \quad (4.14)$$

where \hat{d}_k is the hard decision data of the decision statistic z_k . The k th column vector \mathbf{h}_k of the channel matrix \mathbf{H} is then replaced by zeros and the corresponding equalizer matrix is computed again. This procedure is continued till all data symbols are detected. The ordering influences the performance and is chosen by the SINR criteria given above.

In the following we show via simulations the performance of the various detection techniques under various Doppler conditions. For the purpose of simulation an OFDM symbol with 32 subcarriers was chosen. The delay spread was assumed to be 2 samples and a guard time of 4 samples was used. The performance was studied for BPSK and 16PSK and the corresponding symbol error rates were plotted.

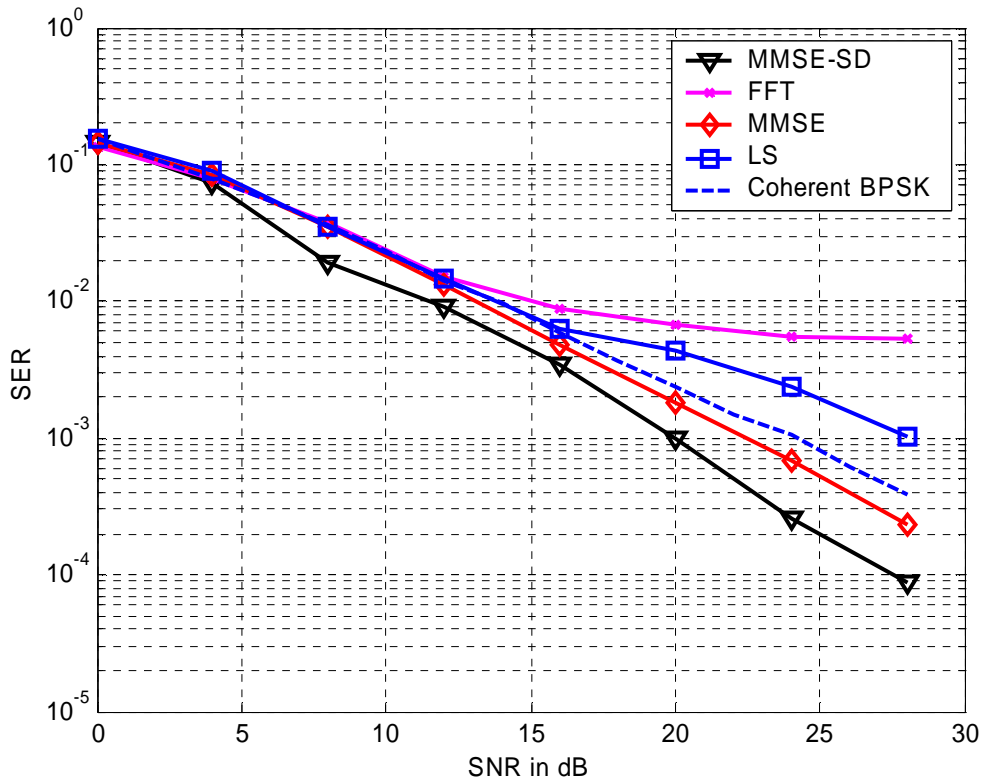


Figure 4.2 Performance of different detection techniques for MC-CDMA using BPSK modulation. $f_d T = 0.1$, Spreading factor = 1, $N = 1024$

Our simulations for the results in Figure 4.2 assumed a moderate normalized Doppler spread of $f_d T = 0.1$. From figure 4.4 we see that FFT detection suffers from ICI and hence we observe an error floor for high SNR values. Least Squares detection suffers less degradation than the FFT method, while MMSE and MMSE with successive detection are found to perform better. It is also seen that MMSE and MMSE with Successive Detection are found to perform better than single carrier Coherent BPSK system in a flat fading channel assuming perfect channel estimation due to the diversity enhancement.

Figures 4.3 and 4.4 show the performance of 16PSK modulation. Here we see that the performance difference is even more dramatic. FFT detection cannot achieve better than 20% SER. MMSE with Successive Detection was found to perform the best compared to other detection techniques. When the normalized Doppler is high ($f_d T = 1$) the MMSE with SD performs best due to time diversity while other detectors suffer due to ICI.

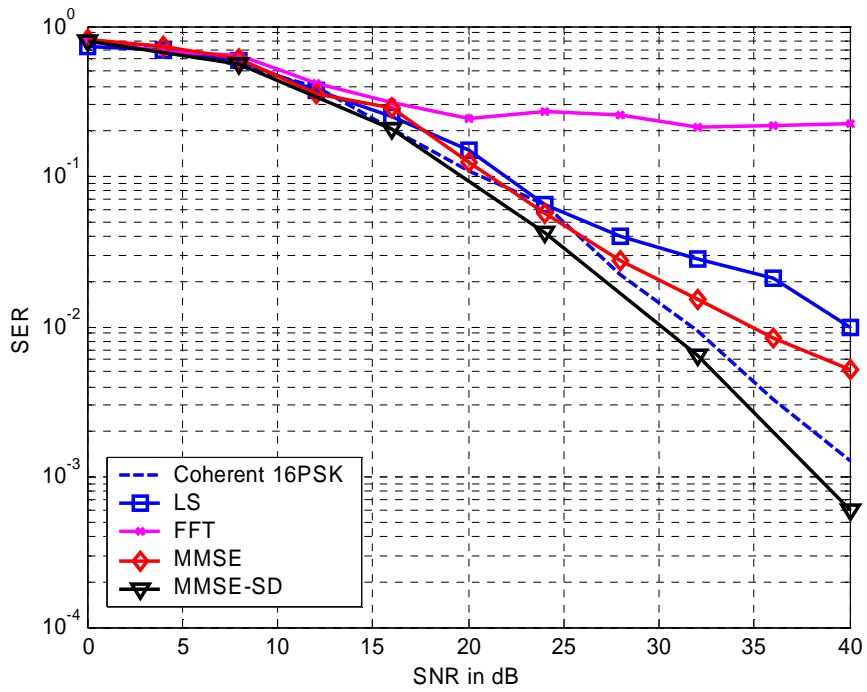


Figure 4.3 Performance of different detection techniques for MC-CDMA using 16PSK modulation. $f_dT = 0.1$, Spreading factor = 1, $N = 1024$

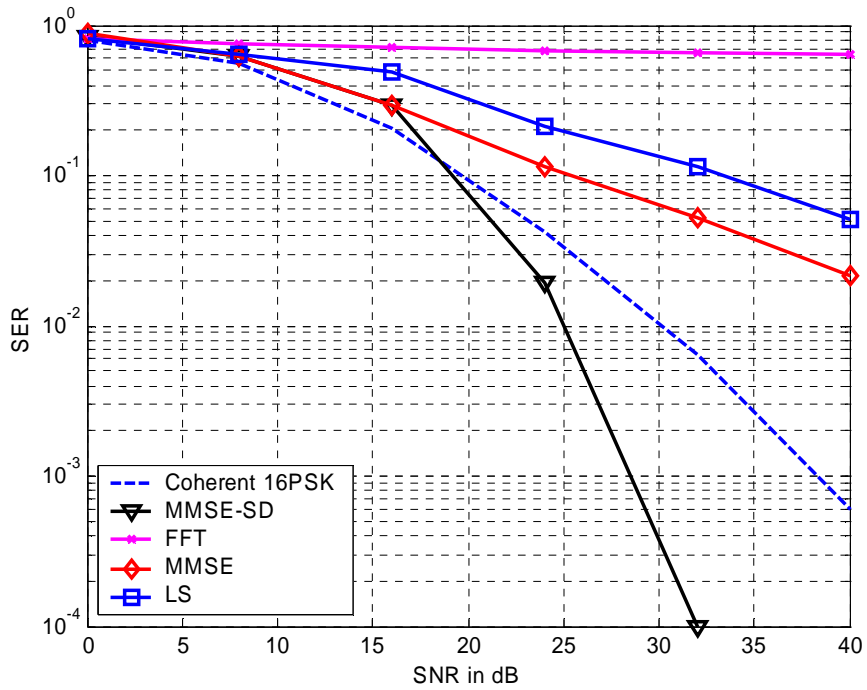


Figure 4.4 Performance of different detection techniques using 16PSK modulation. $f_dT = 1$, Spreading factor = 1, $N = 1024$

Also evident from Figures 4.3 and 4.4 is that the MMSE performance is better than single carrier BPSK in a flat fading channel while the MMSE performance is worse than the single carrier 16PSK in flat fading assuming ideal channel estimation.

Figures 4.5 and 4.6 show the performance of different detection techniques as a function of the Doppler. Figure 4.5 shows the performance in low to moderate Doppler spreads. As is seen from the figure, the performance of all the advanced detection techniques are the same for low Doppler spreads. The MMSE and LS techniques perform similarly while the FFT performance deteriorates with increased normalized Doppler. The performance of the successive detection technique improves with an increase in the normalized Doppler spread as it exploits diversity in time. This effect is clearly evident in Figure 4.6 where the performance is shown for normalized Doppler from 0.1 to 1. The performance of MMSE with Successive detection improves while the other detection techniques degrade with increasing Doppler. Also the performance of MMSE with successive detection is found to be better than Coherent 16PSK in a flat fading channel.

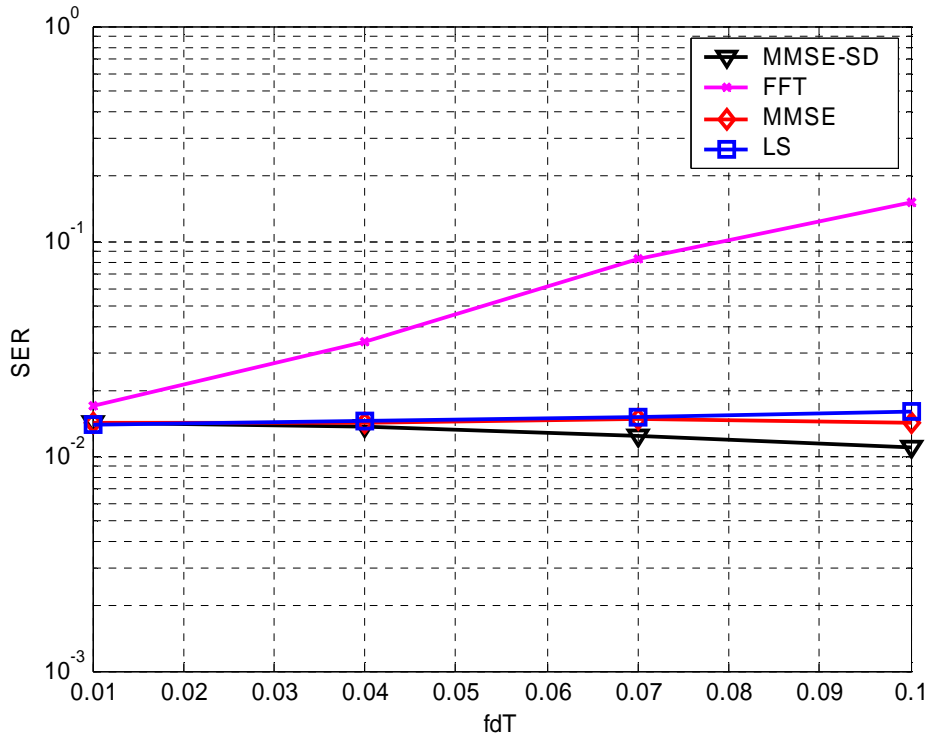


Figure 4.5 Performance using 16PSK modulation for varying $f_d T$. SNR= 30dB

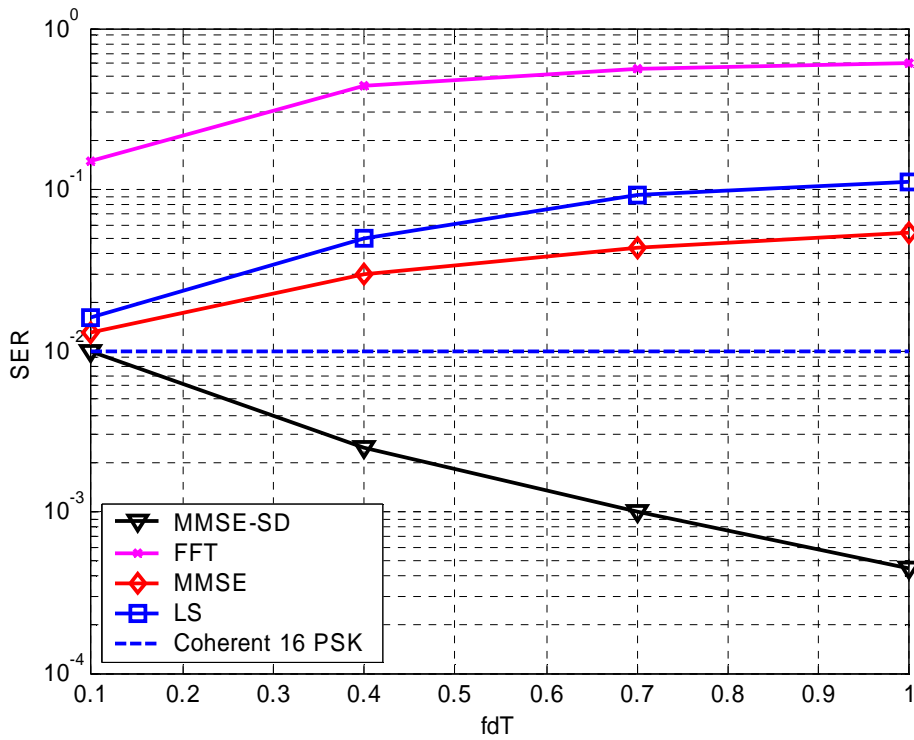


Figure 4.6 Performance using 16PSK modulation for varying $f_d T$. SNR= 30dB, Spreading factor = 1, N = 1024

In this section we have shown the performance of various detection techniques for MC-CDMA. MMSE combined with successive detection was found to perform the best as it exploits the time diversity of the channel while FFT detection is found to suffer significantly from ICI. In the following section robust channel estimation for MC-CDMA will be discussed in detail.

4.2 Robust Channel Estimation for MC-CDMA

A brief introduction to channel estimation techniques for Multicarrier systems was presented in Chapter 3. Coherent Multicarrier systems require channel estimation. This can be avoided by using differential detection, at the cost of about 3-4 dB performance loss. The channel estimators usually employ pilots and interpolation is performed to determine the channel coefficients for the data symbols. This interpolation can be performed in time or in frequency. If the channel properties like the channel impulse response length, maximum Doppler etc. are known apriori, then some MMSE type channel estimation can be performed to get more accurate channel estimates. Such MMSE channel estimators are found to perform much better than the conventional channel estimators which estimate coefficients by simple interpolation. In this section a time domain channel estimator will be described. The channel estimator is very robust to Doppler spread variations in the channel as will be shown in the performance results.

4.2.1 Review of Channel Estimation techniques

Several pilot assisted channel estimation techniques have been proposed for OFDM. The pilot spacing required for practical channel estimators are discussed in [Rin96]. This reference also discusses the channel estimators based on piecewise-constant and piecewise-linear interpolations between the pilots. In [Edf98] a frequency domain MMSE estimator is proposed and a low rank approximation to it using Singular Value Decomposition is studied. The MMSE estimator requires knowledge of the frequency correlation of the channel and the operating SNR. In [Li98] the MMSE channel estimator uses channel correlations in both time and frequency. Although it works very well in mismatched cases, the performance degrades if the assumed Doppler and delay spreads are smaller than the actual ones. A Maximum Likelihood Channel Estimator that does not require the channel statistics is proposed in [Neg98]. This MLE estimator does not require knowledge of the channel statistics and the operating SNR. A comparison between the MMSE and MLE channel estimator is studied in [Mor01a]. This reference also analyzes the tradeoffs in utilizing an MMSE or an MLE channel estimator and

compares their performance. A time domain channel estimation algorithm has been proposed in [Min00]. The relation between the algorithm and frequency domain based MMSE type channel estimation is also discussed. In this section we will discuss in detail the time domain channel estimator proposed in [Cho01] and study the performance in detail.

4.2.3 Time domain MMSE channel estimator

The time domain MMSE channel estimator requires knowledge of the channel parameters. A typical mobile radio channel can be described as a tapped delay line filter with time varying coefficients to model the time varying nature of the channel. The length of the tapped delay line channel model is determined by the delay spread of the channel. If the assumption of a Wide Sense Stationary Uncorrelated Scattering (WSSUS) model for the channel holds true, the channel is characterized by its multipath intensity profile and the scattering function. The multipath intensity profile is assumed to be exponentially distributed and the scattering function is determined by the time varying nature of the channel which in turn depends on the Doppler frequency. It is also assumed that the inverse Fourier transform of the Doppler spectrum is the zeroth-order Bessel function of the first kind. Using these assumptions the autocorrelation function of the channel is given as

$$E\{h(n_1, l_1)h^*(n_2, l_2)\} = c.J_0\left(\frac{2\pi f_d T(n_1 - n_2)}{N}\right)e^{-l_1/L}\delta(l_1 - l_2) \quad (4.15)$$

where, $h(n, l)$ is the tap gain of the l th tap at time n , c is a normalization constant and is given as $c\sum_l e^{-l/L} = 1$, f_d is the Doppler frequency and L is the number of taps.

The pilot symbols can be inserted in a variety of ways. Figure 4.7 shows an arrangement where an entire MC-CDMA block of symbols is composed of pilots. These pilot MC-CDMA symbols are inserted in a time interleaved fashion. We could have instead inserted the pilots between the data symbols within a MC-CDMA block. The time domain correlation of the channel is important in the former method while the frequency domain correlation is important in the latter method. Hence if the channel changes rapidly

in time choosing the former scheme would be a good choice and if the channel changes in frequency then the latter scheme might be a better choice.

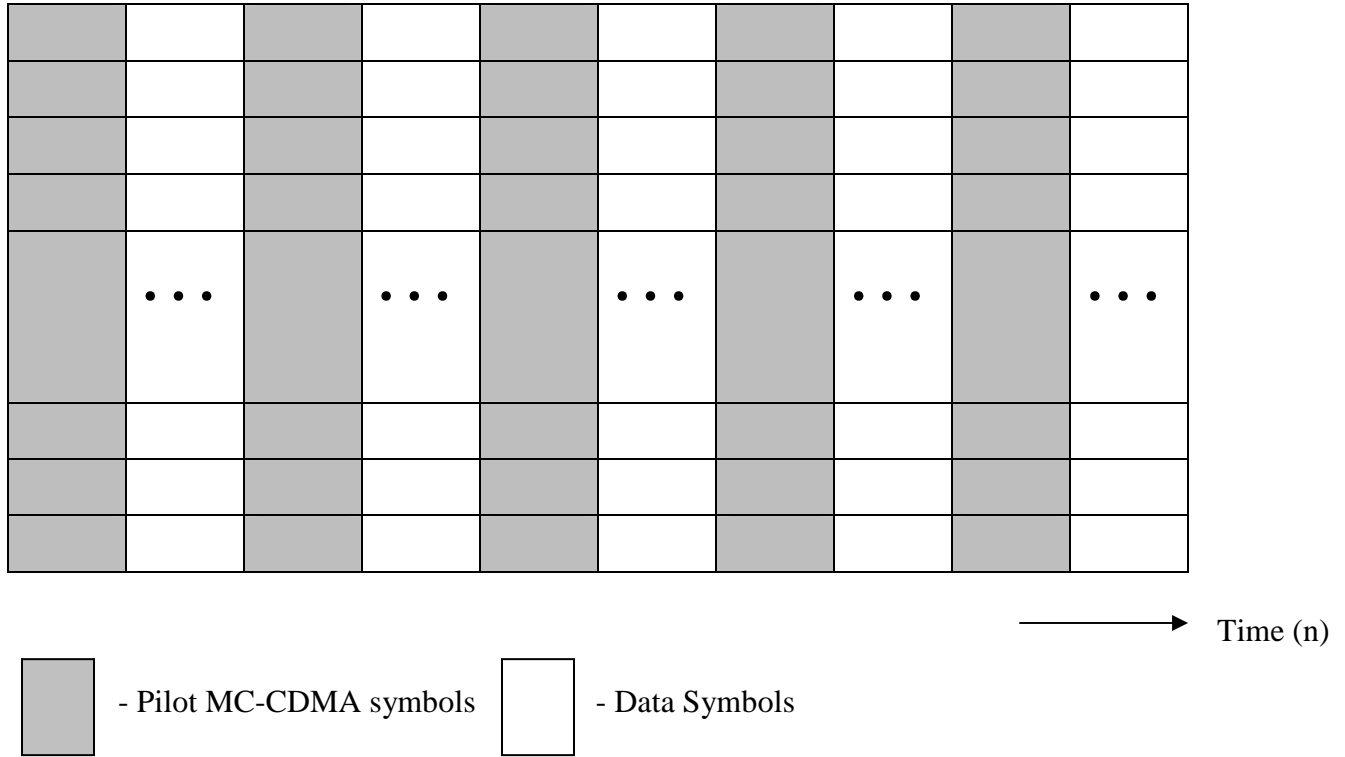


Figure 4.7 Pilot pattern used for channel estimation. Pilot symbols are time interleaved.

If an estimate of the channel statistics like the Doppler spread, Delay spread and the power delay profile of the channel are known then an estimate of the channel impulse response $h(n,l)$ can be found using the pilot MC-CDMA symbols. Another method of channel estimation is to find the coefficients at the pilot symbol locations and then interpolate for the data symbols. In the current method, instead of using any interpolation we estimate the channel impulse response, $h(n,l)$. The number of pilot symbols to be inserted between the data symbols is dependent on the time domain correlation of the channel which in turn depends directly on how fast the channel changes in time.

Using the pilot MC-CDMA symbols we form a vector \mathbf{y}_p containing all the pilot

MC-CDMA symbols. If we consider M MC-CDMA symbols in time and if we assume P symbols being pilot symbols, with each MC-CDMA symbol having N subcarriers, then the vector \mathbf{y}_p is of dimensions, $Lx(N*P)$. We then form a vector of channel impulse responses, containing the coefficients of the multipath for every sample within a MC-CDMA symbol. Thus the vector \mathbf{h} can be written as,

$$\mathbf{h} = [\mathbf{h}_1 \mathbf{h}_2 \mathbf{h}_3 \dots \mathbf{h}_M], \quad (4.16)$$

where \mathbf{h}_n 's can be given as

$$\mathbf{h}_n = [h(1,0) \dots h(1,l) \dots h(2,0) \dots h(2,l) \dots h(N-1,0) \dots h(N-1,l)] \quad (4.17)$$

The MMSE estimate of the channel coefficients are then given as,

$$\hat{\mathbf{h}} = \mathbf{R}_{\mathbf{h}\mathbf{y}_p} \mathbf{R}_{\mathbf{y}_p\mathbf{y}_p}^{-1} \mathbf{y}_p \quad (4.18)$$

The autocorrelation matrix $\mathbf{R}_{\mathbf{y}_p\mathbf{y}_p}$ and the cross correlation matrix $\mathbf{R}_{\mathbf{h}\mathbf{y}_p}$ are obtained from the channel correlation properties.

We have that, $\mathbf{R}_{\mathbf{y}_p\mathbf{y}_p} = E\{y(n_1)y^*(n_2)\}$

$$\begin{aligned} E\{y(n_1)y^*(n_2)\} &= E\left\{\left(\sum_{l=0}^L h(n_1,l)s(n_1-l) + w(n_1)\right)\left(\sum_{m=0}^L h(n_2,m)s(n_2-m) + w(n_2)\right)^*\right\} \\ &\quad \text{From (4.1)} \\ &= E\left\{\left(\sum_{l=0}^L h(n_1,l)s(n_1-l) + w(n_1)\right)\left(\sum_{m=0}^L h^*(n_2,m)s^*(n_2-m) + w^*(n_2)\right)\right\} \\ &= E\left\{\left(\sum_{l=0}^L h(n_1,l)s(n_1-l) \sum_{m=0}^L h^*(n_2,m)s^*(n_2-m) + w^*(n_2)w(n_1) + \dots\right.\right. \\ &\quad \left.\left.\sum_{m=0}^L h^*(n_2,m)s^*(n_2-m)w(n_1) + \sum_{l=0}^L h(n_1,l)s(n_1-l)w^*(n_2)\right)\right\} \end{aligned}$$

The cross correlation between the channel impulse response term $h(n,l)$ and the noise term $w(n)$ is zero and hence the above can be simplified as,

$$= E\left\{\left(\sum_{l=0}^L h(n_1,l)s(n_1-l) \sum_{m=0}^L h^*(n_2,m)s^*(n_2-m)\right)\right\} + E\{w^*(n_2)w(n_1)\}$$

$$= \sum_{l=0}^L J_0(2\pi f_d T(n_1 - n_2) / N) s(n_1 - l) s(n_2 - l)^* + \sigma^2 \delta(n_1 - n_2) \quad (4.19)$$

From (4.15)

We have to note here that there is a guard interval. Thus if n_1 and n_2 are coming from different symbols, we must take into account the guard interval.

Also, the cross correlation matrix,

$$\begin{aligned} \mathbf{R}_{\mathbf{h}_p} &= E \left\{ h(n_1, l) y^*(n_2) \right\} \\ &= c \sum_{l=0}^L J_0(2\pi f_d T(n_1 - n_2) / N) s(n_2 - l)^* \end{aligned} \quad (4.20)$$

The above can be proved from using Equations (4.1) and (4.15) in the same manner as the autocorrelation matrix. Again, the guard symbols must be considered while computing the cross correlation matrix. It is to be noted that $s(n)$ is the output of the IFFT block for the pilot symbols at the transmitter and is usually known at the receiver. This information is necessary for the channel estimation.

In the following sections we show by simulations the performance of the channel estimation algorithm for various channel conditions. The proper metric to quantify the performance of the channel estimation algorithm is usually the Mean Squared Error and is usually expressed in dB. The normalized Mean Square Error (NMSE) is defined as (Cho01),

$$\text{NMSE}(n) = \frac{\sum_l E \left\{ |h(n, l) - \hat{h}(n, l)|^2 \right\}}{\sum_l E \left\{ |h(n, l)|^2 \right\}} \quad (4.21)$$

The performance of the channel estimation algorithm is shown in Figure 4.8. We see that there is not much difference in the performance of the algorithm for low SNR values. The reason being that the Normalized MSE is small compared to the noise variance. Further-

more the FFT detection gives an error floor as expected. The performance also depends on the number of pilot symbols inserted between the data symbols. The MSE is reduced by having more pilot symbols but a corresponding decrease in information throughput is suffered.

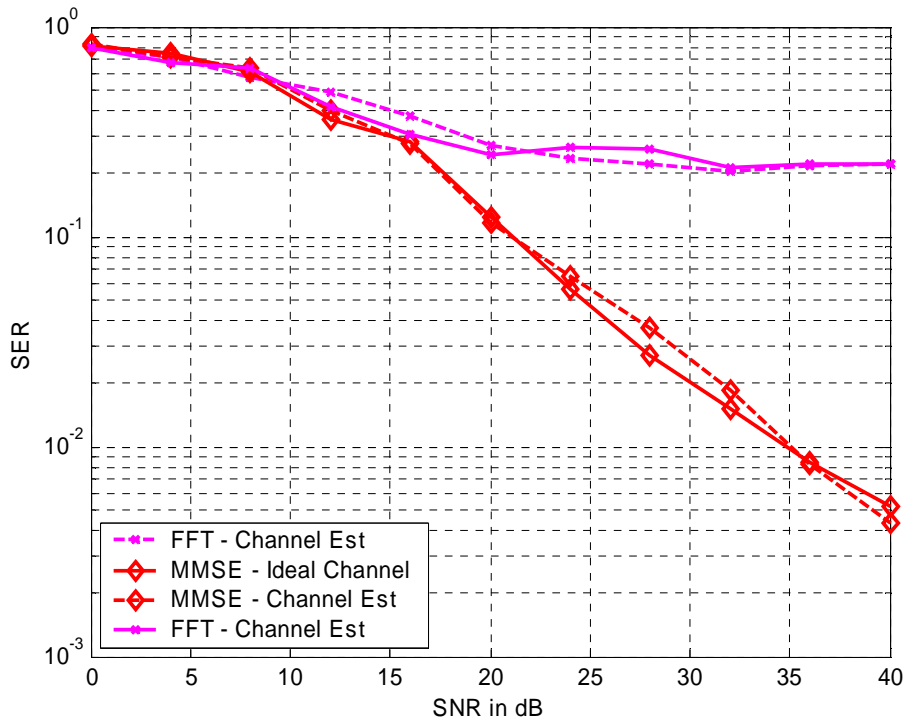


Figure 4.8 Performance of time domain Channel Estimator for FFT and MMSE detection with $f_d T = 0.1$, Spreading factor = 1, $N = 128$. 4 Data symbols were inserted for every Pilot symbol.

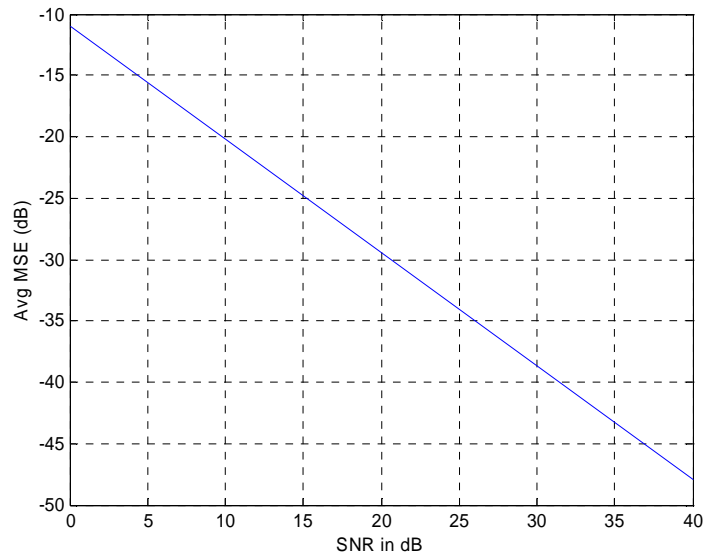


Figure 4.9 Normalized MSE for the channel estimator with $f_d T = 0.1$, 4 Data symbols for every Pilot symbol.

Figure 4.10 shows the performance of the channel estimator for the case of 10 Data symbols between Pilot symbols. The NMSE for this case is slightly higher than the NMSE for the previous case. Figure 4.12 shows the performance as a function of $f_d T$.

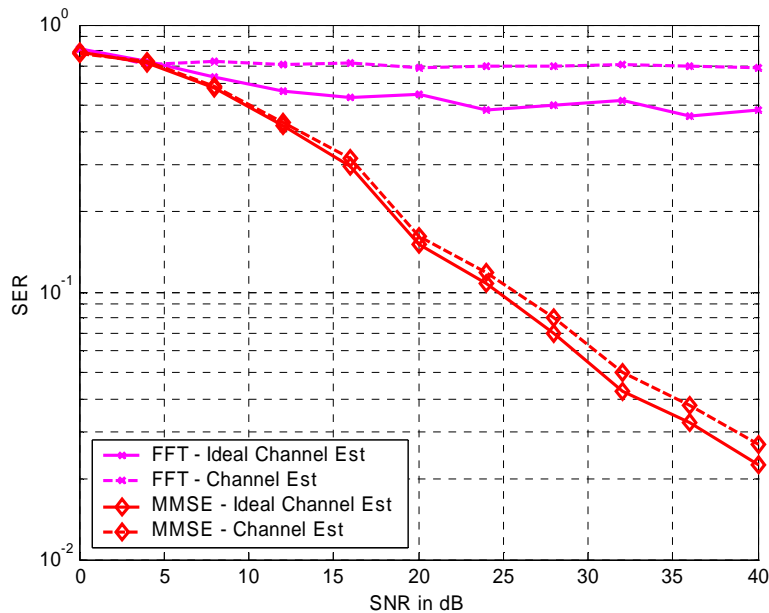


Figure 4.10 Performance of time domain MMSE Channel Estimator for FFT and MMSE detection with $f_d T = 0.3$, Spreading factor = 1, $N = 128$, 10 Data symbols were inserted for every Pilot symbol.

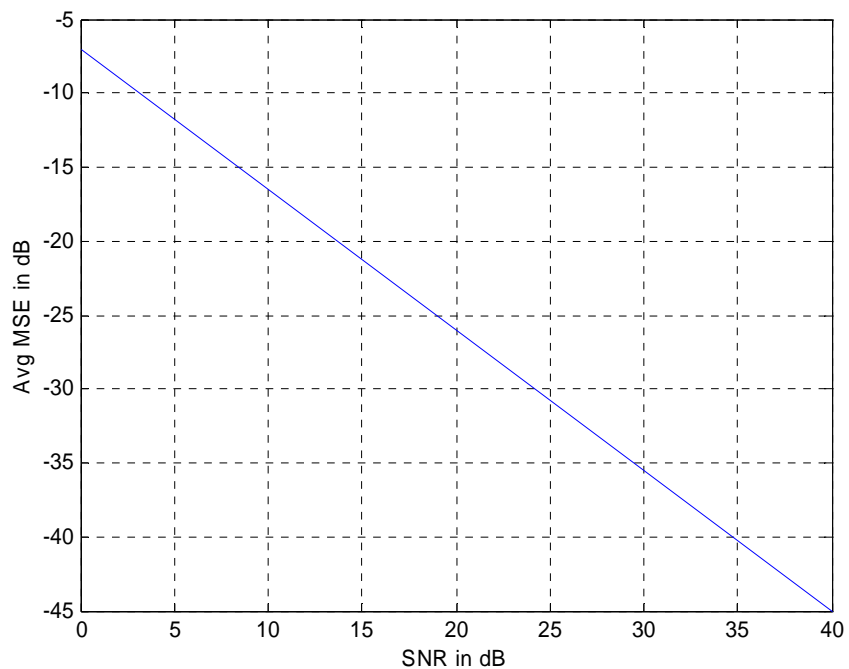


Figure 4.11 Normalized MSE for the channel estimator with $f_d T = 0.3$, $SF = 1$, $N = 128$, Data symbols for every Pilot symbol.

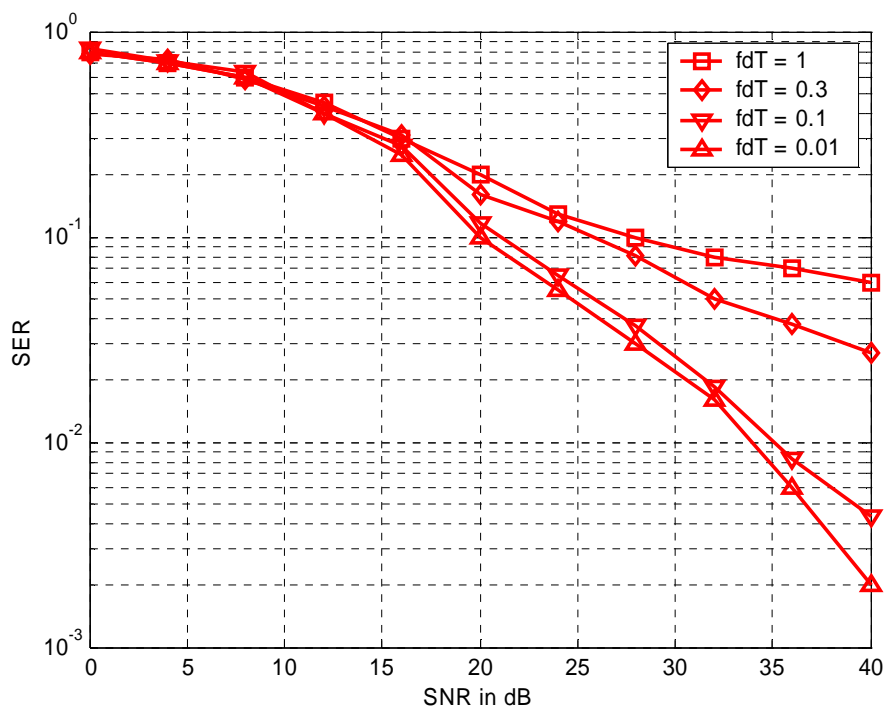


Figure 4.12 Performance as a function of normalized Doppler for the channel estimator with $f_d T = 0.1$, 5 Data symbols for every Pilot symbol.

4.2.4 Robustness of the Channel Estimator

The channel estimator discussed above requires apriori knowledge of the statistics of the channel namely the channel impulse response, the noise variance and the Doppler spread in the channel. Such channel statistics are usually not known and hence the estimator has to be robust to these channel parameter changes. A mismatch case was assumed for these channel parameters and then the performance of the channel estimator was studied. Form simulations we could observe that the channel estimator was very robust to these parameter values and the performance was even very close to the ideal channel parameter assumption case.

The following was the mismatch channel parameters that were assumed for the channel estimator.

| | Assumed conditions | Actual Conditions |
|---------------------------|--------------------|-------------------|
| SNR | 30 dB | 0 ~ 40 dB |
| $f_d T$ | 0.1 | 0.05 |
| Delay Spread | 4 samples | 2 samples |

Table 4.1 Mismatch condition assumed in the channel estimator

The channel estimator's performance using these mismatch cases is as shown in the Figure 4.13 for the MMSE detector.

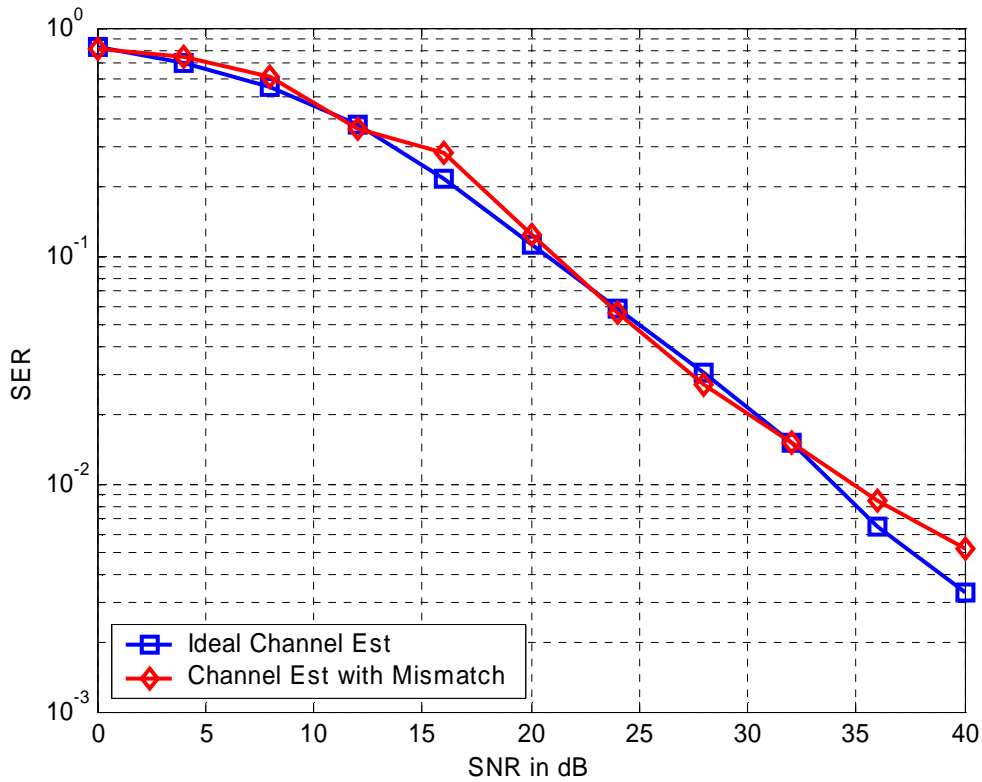


Figure 4.13 Performance of the channel estimator using the mismatch channel statistic values for MMSE detection, Spreading factor = 1, N = 128

The robustness of the channel estimator to changes in the assumed normalized Doppler spread is shown in Figure 4.15. The corresponding mismatch conditions are shown in Table 4.2 where we have assumed that the SNR and the Delay spread are the same as the actual values.

| | Assumed conditions | Actual Conditions |
|---------------------------|--------------------|-------------------|
| SNR | 30 dB | 30 dB |
| $f_d T$ | 0.1 | 0.01 ~ 1 |
| Delay Spread | 4 samples | 4 samples |

Table 4.2 Mismatch condition assumed in the channel estimator corresponding to Figure 4.14

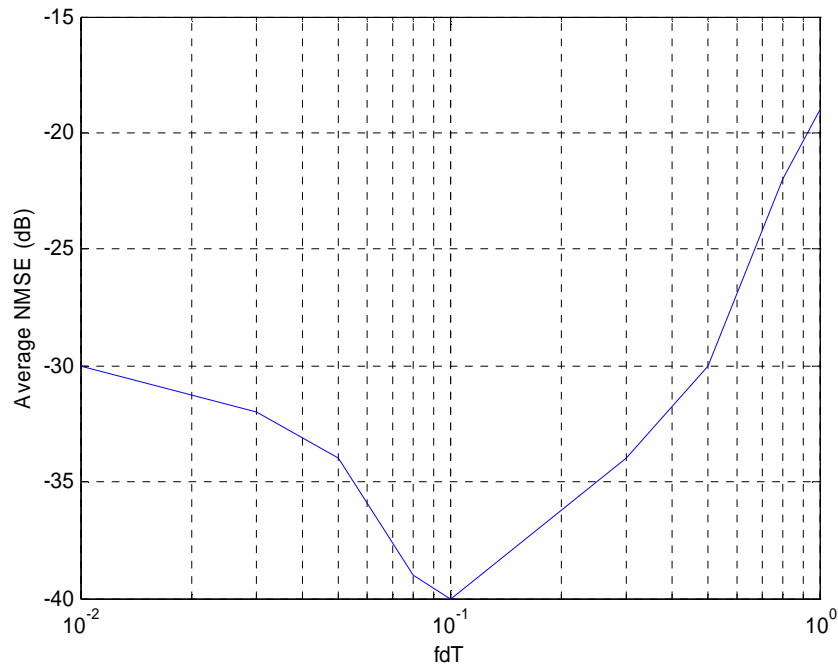


Figure 4.14 Performance of the channel estimator using the mismatch channel statistic values for MMSE detection, Spreading factor = 1, $N = 128$. The assumed normalized Doppler spread varied from the actual Doppler spread. 4 Data symbols for 1 pilot symbol.

We can see that Average NMSE is the least (about -40 dB) at $f_d T = 0.1$ which is the actual value. The plot is not symmetrical as the ICI at high $f_d T$ (close to 1) is more than that at low values. Thus the NMSE value is large with increase in $f_d T$. The robustness of the channel estimator to the delay spread is shown in Figure 4.15. The corresponding mismatch conditions are shown in Table 4.3 where we have assumed that the SNR and the $f_d T$ are the same as the actual values.

| | Assumed conditions | Actual Conditions |
|---------------------------|--------------------|-------------------|
| SNR | 30 dB | 30 dB |
| $f_d T$ | 0.1 | 0.1 |
| Delay Spread | 4 samples | 0 ~ 10 samples |

Table 4.3 Mismatch condition assumed in the channel estimator corresponding to Figure 4.15

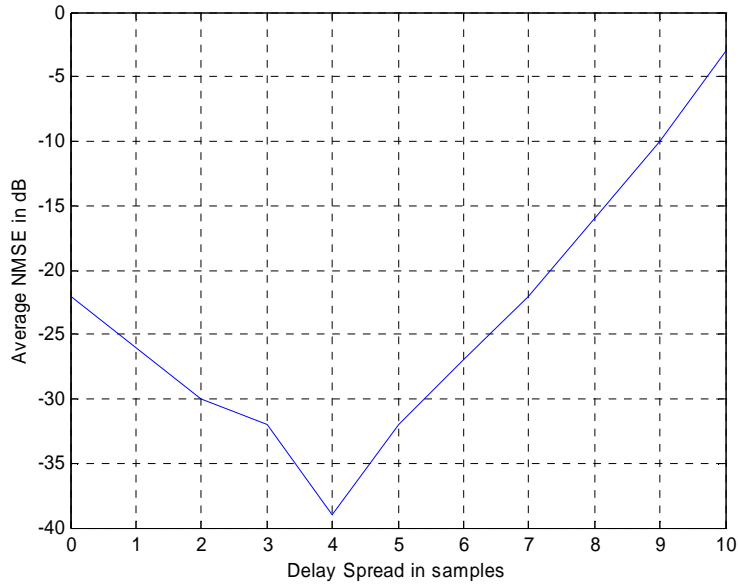


Figure 4.15 Performance of the channel estimator using the mismatch channel statistic values for MMSE detection, Spreading factor = 1, $N = 128$. Delay spread varied from actual.

4.3 Summary

In this chapter we have dealt with advanced detection techniques for multicarrier modulation. The problems with conventional FFT detection were explained. Hence improved detection methods like LS and MMSE were discussed. The time varying channel provides time diversity which can be exploited using successive detection methods. The performance of these detection techniques were shown for various channel conditions. MMSE combined with successive detection was found to perform the best while FFT was found to suffer severely from ICI. Time domain MMSE channel estimation for MC-CDMA was also studied. The channel estimator attempts to estimate the channel impulse response for each tap as a linear combination of the received signal. The estimator requires knowledge of channel statistics but was found to perform very well even in the case of mismatch between the assumed and the actual channel conditions. The performance of the channel estimator was shown through simulations and the corresponding Normalized Mean Square Error was also plotted. Interference rejection techniques for MC-CDMA systems employing multiple antennas will be discussed in Chapter 6.

Chapter 5

Fundamentals of Antenna Arrays and Beamforming

The necessity to improve the capacity of wireless communication systems has led to the need for exploiting the spatial characteristics of the wireless channel. An effective means to exploit the spatial dimension is through the use of adaptive antenna arrays also referred to as *intelligent antennas* or *smart antennas* [Bue99]. While a lot of research has gone into the improvement in capacity achieved due to the use of smart antennas, recent advances in digital signal processing capabilities have made implementing these advanced receivers a possibility. In this chapter we discuss some of the basic concepts behind smart antennas and show their performance in the presence of interference.

5.1 Introduction

The two main factors that make mobile radio reception difficult is the presence of multipath fading and co-channel interference. The use of smart antennas can improve performance in these hostile environments. Smart antennas can be broadly classified into two categories, namely the phased array and the diversity array. Elements in a phased array are placed at a distance less than or equal to half a wavelength while those in a diversity array are placed at a much larger distance. As a result, the assumption that the received signal is a plane waves holds true for a phased array but not for a diversity array. A phased array consists of a set of antenna elements that are spatially distributed at known locations with reference to a common fixed point. By changing the phase and amplitude of the exciting currents in each of the antenna elements it is possible to create gains and nulls in any direction [Pil89]. The signals received in these elements are typically combined at baseband using complex weights. Adaptive algorithms can be used to adapt the weights based on some optimization criteria such as maximization of output SNR. Also there are algorithms by which we can maximize the output SINR. In such a

system we maximize the antenna response in the direction of the desired user and minimize it in the direction of the interferer.

Various array geometries are possible for the antenna elements with the most common of them being linear, circular and planar arrays. In a linear array the centers of all array elements are aligned in a straight line. If the spacing between the elements is uniform it is called a uniformly spaced linear array. A circular array is one in which the centers of the array elements lie on a circle. On the other hand if the centers of the array elements all lie in the same plane it is called a planar array. Linear and circular arrays are special cases of the planar array.

The radiation pattern of the array is determined by the radiation patterns of the individual elements, their orientation in space and the amplitude and phase of the feeding currents. If each element of the array is an isotropic source, the radiation pattern obtained will be solely dependent on the array geometry and the feeding currents. The radiation pattern thus obtained is called the *array factor*. If the elements of the array are similar and if they are non-isotropic, the radiation pattern is computed from the principle of pattern multiplication as the product of the array factor and the individual element pattern [Stu81]. For the purpose of this research we considered a uniform linear array.

5.1.1 Difference between Phased and Diversity Array

Phased arrays are typically used for interference rejection while diversity arrays are used for combating multipath fading in mobile wireless channels. In diversity arrays, the elements are spaced sufficiently apart (typically $> 10\lambda$) so that the fading envelopes seen at the antenna elements are uncorrelated or slightly correlated. The main idea behind diversity arrays is that such uncorrelated (or slightly correlated) branches will have very low probability of simultaneously experiencing a deep fade. Thus having more elements increases the probability that at least one element will produce sufficient SNR for reliable decoding of the information. Additionally in diversity arrays there is no geometric interpretation of the array response and the concept of beam pattern is invalid. However, a very important result is that the combining approaches used in diversity arrays are

similar to the beamforming approaches used in phased arrays because several of these algorithms have the same maximization criteria. Thus the weights used in phased arrays to maximize the SNR are simply the same as the maximal ratio combining (MRC) solution for diversity arrays. A more detailed discussion of these algorithms will be presented.

5.2 Uniform Linear Array

Figure 5.1 shows a simple uniform linear antenna array. We will attempt to express the received signal in each of the element in terms of the signal received in the first element or the reference element.

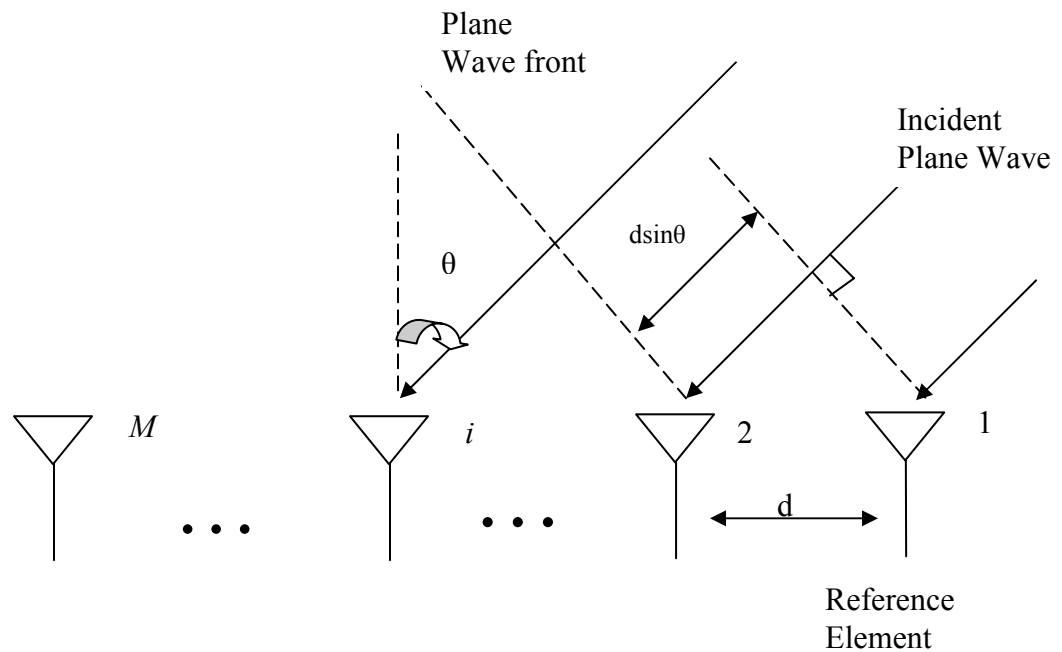


Figure 5.1 A Uniform Linear Antenna Array showing the incident Plane wave

In the above figure we have an M element uniform linear array, which receives the signal from a direction θ relative to the array broadside. This angle is called the Angle-of-Arrival (AOA) or the Direction-of-Arrival (DOA) and is measured clockwise from the broadside of the array. The band pass representation of the received signal at the first element can be expressed as,

$$\tilde{x}_1(t) = s(t) \cos(2\pi f_c t + \alpha(t) + \gamma) \quad (5.1)$$

where $s(t)$ is the amplitude of the received signal which may or may not be corrupted by a fading channel, f_c is the carrier frequency, $\alpha(t)$ is the phase information and γ the random phase introduced due to the channel. The complex envelope representation of the above signal can be written as

$$x_1(t) = s(t) \exp\{j(\alpha(t) + \gamma)\} \quad (5.2)$$

The received signal and its complex envelope are related by the following equation,

$$\tilde{x}_1(t) = \text{Re}[x_1(t) \exp(j2\pi f_c t)] \quad (5.3)$$

Now we assume that the signals originate from a very far distance and hence a plane wave associated with the signal advances through a non-dispersive medium that only introduces propagation delay. Hence the signal at any element can be expressed as a time advanced or time delayed version of the signal at the reference element. From Figure 5.1 the signal at the reference element would travel a distance $d \sin \theta$ further to reach the second element. The corresponding lag in time can be represented as

$$\tau = \frac{d \sin \theta}{c} \quad (5.4)$$

where c is the velocity of light. The signal at the second element is thus given by

$$\tilde{x}_2(t) = \tilde{x}_1(t - \tau) = s(t - \tau) \cos(2\pi f_c (t - \tau) + \alpha(t - \tau) + \gamma) \quad (5.5)$$

Now if the carrier frequency is large compared to the message signal bandwidth the received signal can be considered to be quasi-static and thus the above equation can be written as

$$\tilde{x}_2(t) = s(t) \cos(2\pi f_c (t - \tau) + \alpha(t) + \gamma) \quad (5.6)$$

The complex envelope of the received signal can thus be expressed as,

$$\tilde{x}_2(t) = s(t) \exp(j(-2\pi f_c \tau + \alpha(t) + \gamma)) \quad (5.7)$$

$$= x_1(t) \exp(-j2\pi f_c \tau) \quad (5.8)$$

Thus we see that the time delay due to propagation manifests in a phase shift in the received signal at the reference element.

Now using the expression for the time delay τ in the above expression we have,

$$\tilde{x}_2(t) = x_1(t) \exp(-j2\pi f_c \frac{d \sin \theta}{c}) \quad (5.9)$$

$$= x_1(t) \exp(-j2\pi \frac{d \sin \theta}{\lambda}) \quad (5.10)$$

Now for any i th element in the array, the received signal is given as,

$$\tilde{x}_i(t) = x_1(t) \exp(-j2\pi(i-1) \frac{d \sin \theta}{\lambda}) \quad i = 1, 2, \dots, M \quad (5.11)$$

Let $\mathbf{y}(t) = [y_1(t), y_2(t), \dots, y_M(t)]^T$ be the received signal at the antenna elements and let us define a vector, $\mathbf{a}(\theta) = [1, \exp(\frac{j2\pi d \sin \theta}{\lambda}), \dots, \exp(\frac{j2\pi(M-1)d \sin \theta}{\lambda})]^T$.

The complex envelope of the received signal in the array is thus expressed as,

$$\mathbf{y}(t) = \mathbf{a}(\theta)x_1(t) \quad (5.12)$$

The vector $\mathbf{a}(\theta)$ is called the *steering vector* or the *array response vector*. In the case we considered above, the array steering vector is a function of the angle of arrival only. Usually the steering vector is also a function of the array geometry, signal frequency and the individual element response. The collection of steering vectors for all angles and frequencies is called *array manifold*. For the case of uniform linear array the array manifold can be determined analytically. In practice however the array manifold is measured as a point source response of the array for various angles and frequencies. This process of obtaining the array manifold is called *array calibration*. In all our discussions above, the inverse bandwidth of the arriving signal is assumed to be much larger than the propagation across the array. This is called the narrowband signal assumption and is what we have assumed throughout this work.

Suppose we have k input signals $[s_1(t), s_2(t), \dots, s_k(t)]$ arriving at the array with different Angles-of-Arrivals (θ_i) and the same central frequency (f_c). In this case, the input data vector can be thought of as the superposition of all the impinging signals and noise. Thus the input data vector can be expressed as,

$$\mathbf{y}(t) = \sum_{j=1}^k \mathbf{a}(\theta_j) s_j(t) + \mathbf{n}(t) \quad (5.13)$$

In the above expression $\mathbf{a}(\theta_i)$ are the corresponding array vectors of each of the signals and $\mathbf{n}(t)$ is an $M \times 1$ vector of noise components with an expected value . The above can be written in a matrix form as follows,

$$\mathbf{y}(t) = \mathbf{A}(\theta)\mathbf{s}(t) + n(t) \quad (5.14)$$

where $\mathbf{A}(\theta)$ is a $M \times k$ matrix containing the steering vectors and

$$\mathbf{s}(t) = [s_1(t), s_2(t), \dots, s_k(t)]^T.$$

Now in general beamforming problems we are interested in determining the input signals $\mathbf{s}(t)$ from the received signal vector $\mathbf{y}(t)$. These beamforming algorithms will be discussed later in the chapter.

5.3 Beamforming

Often times in mobile wireless environments, the desired signal and the interference occupy the same frequency band. Unless the signals have low correlation (like in CDMA systems) temporal processing will not be effective in interference rejection. However the desired signal and interference arrive from different directions and hence have different angles-of-arrival. Beamforming is the process of forming beams towards the direction of the desired user while simultaneously suppressing signals originating from other directions. Thus beamforming can also be looked upon as the spatial filtering of signals using their spatial signature properties.

A beamformer combines sampled data from each antenna element the same way an FIR filter would combine temporally sampled information. Beamformers are of two general types, a narrowband beamformer and a wideband beamformer. A narrowband beamformer is shown in the Figure 5.2. The output of the beamformer is given by,

$$z(k) = \sum_{i=1}^M w_i^* y_i(k) \quad (5.15)$$

where the complex weights w are used to steer the beam towards the desired user and steer nulls towards interferers. The above equation can be written in vector form as

$$z(k) = \mathbf{w}^H \mathbf{y}(k) \quad (5.16)$$

A wideband beamformer is often used when signals of wide band are of interest and is more complex than a narrow band beamformer. [Van88].

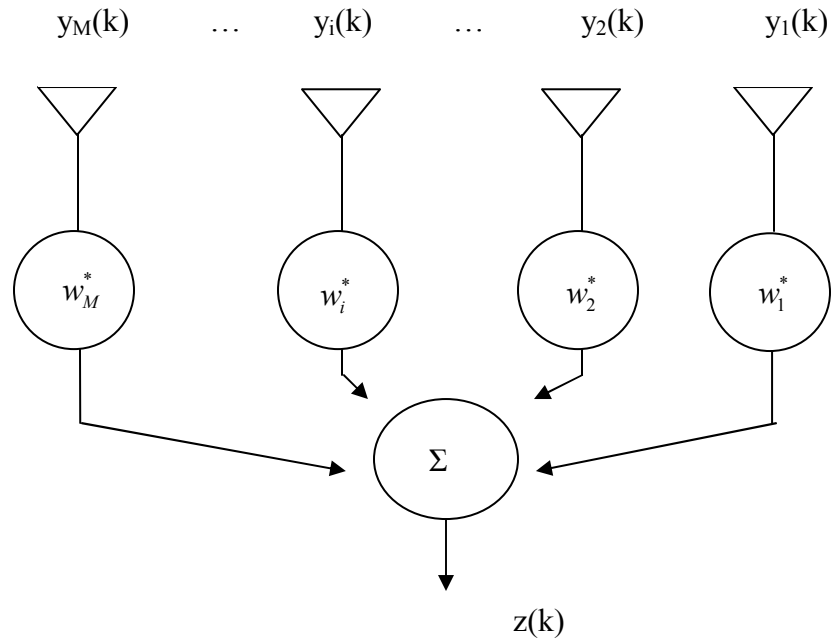


Figure 5.2 Narrowband beamformer

5.4 Analogy to FIR filter

A beamformer is used to separate the desired user signal from interferer using the spatial information. A straight forward analogy of this to an FIR filter will provide us insight into a beamformer. To illustrate this point we use the sinusoidal energy retrieval problem in the time domain and compare it with the beamforming problem in the space domain. Let us consider a sinusoidal signal with k different frequencies with additive noise. The expression for the signal can be given by,

$$x(t) = \sum_{i=1}^k b_i \exp(j2\pi f_i t + \phi_i) + n(t) \quad (5.17)$$

where b_i , f_i and ϕ_i are the amplitude, frequency and phase of the i th sinusoid respectively.

If we suppose that the above signal is sampled at a rate T_s irrespective of the frequencies of the sinusoids and if $x(m)$ represents the signal at time instant mT_s , then $x(m)$ is given as,

$$x(m) = \sum_{i=1}^k b_i \exp(j2\pi f_i(mT_s) + \phi_i) + n(mT_s) \quad (5.18)$$

Suppose this sampled signal is fed to an FIR filter with $(M-1)$ delay elements. Then at time instant mT_s , the filter input and the output of the delay elements can be written as

$$\mathbf{x}(m) = \sum_{i=1}^k \mathbf{a}(f_i) s_i(m) + \mathbf{n}(m) \quad (5.19)$$

where $\mathbf{x}(m) = [x(m), x(m-1), \dots, x(m-M+1)]^T$, $\mathbf{n}(m) = [n(mT_s), \dots, n((m-M+1)T_s)]^T$,

$$\text{and } \mathbf{a}(f_i) = \begin{bmatrix} 1 \\ e^{j2\pi T_s f_i} \\ \vdots \\ e^{j2\pi(M-1)T_s f_i} \end{bmatrix} \quad (5.20)$$

$$\text{Also } s_i(m) = b_i \exp(j(2\pi f_i(mT_s) + \phi_i)) \quad (5.21)$$

Comparing equations (5.20), (5.21) with that of the (5.13) and (5.14) we see that the normalized element spacing d/λ of the beamformer corresponds to the sampling period T_s of the temporal filter and the sine of the Angle-of-arrival (θ_i) of the beamformer corresponds to the temporal frequency (f_i) of the FIR filter input.

As the functionalities of the FIR filter and a Uniform Linear Array are similar, the Nyquist Sampling theorem applied to the FIR filter in time domain can be applied to the beamformer in the space domain. According to this theorem a band limited signal with highest frequency f can be uniquely determined if the sampling frequency is at least $2f$. If we sample at any frequency less than $2f$ aliasing will occur. In the space domain, the sampling rate corresponds to the inverse of the normalized element spacing, and the highest frequency corresponds to 1 ($\sin \theta_i$ is always less than 1). Thus the spatial Nyquist theorem can be expressed as,

$$\frac{1}{d/\lambda} \geq 2 * 1$$

$$\text{Equivalently, } d \leq \frac{\lambda}{2} \quad (5.22)$$

We see from the above expression that the element spacing must not be greater than half the carrier wavelength to avoid spatial aliasing. Spatial aliasing is the inability to distinguish two different signals arriving from different spatial locations. Conversely spacing the elements too close will result in mutual coupling effects. Hence the spacing must be large enough to avoid mutual coupling effects. For uniform linear arrays, aliasing can still happen if the signals are arriving at complimentary angles with respect to the bore sight. This ambiguity can be avoided by using circular arrays instead of linear ones.

Using the analogy presented before, the beamformer response can be determined using the corresponding FIR filter response for a sinusoid of a particular frequency f . The frequency response of an FIR filter with weights w_i^* and $M-1$ taps is given by,

$$H(e^{j2\pi f}) = \sum_{i=1}^M w_i^* e^{-j2\pi f T_s (i-1)} \quad (5.23)$$

We have discussed before that the f and T_s of the harmonics retrieval problem in a FIR filter is equivalent to $\sin\theta$ and d/λ respectively for the beamformer. Hence the beamformer response can be obtained from equation (5.23) by substituting the appropriate values.

The beamformer response is thus given by,

$$g(\theta) = \sum_{i=1}^M w_i^* e^{-j \frac{2\pi(i-1)d \sin\theta}{\lambda}} \quad (5.24)$$

The above equation gives the beamformer response for a particular angle of arrival, θ . Thus if we have several signals coming in from different spatial locations and we want to extract signals coming from a direction θ_i , then we need to find proper weights so that the beamformer response is maximum in the direction of θ_i and is minimum in the directions-of-arrival of other signals.

5.5 Adaptive Antenna Arrays

In mobile radio environments, the users keep moving and hence the DOAs of the users are time-varying. Also the parameters of the user's signals vary in time due to the presence of cochannel interference, noise and multipath associated with the channel. Fixed weights will not track these changes in the time varying channel. An adaptive antenna array can change its beam pattern in response to the changing signals. This kind of an antenna system usually works with some internal feedback whereby the system can modify the antenna patterns.

The weights used must be changed using some adaptive algorithm. Such algorithms are usually designed to meet some performance criteria and then generating a set of equations such that the performance criteria are met. Some of the most frequently used performance criteria are the Mean Square Error (MSE), the Maximum Likelihood (ML), Maximum Signal to Noise Ratio (MSNR) and Maximum Signal to Interference Noise Ratio (SINR). These performance criteria are usually expressed as cost functions and the weights are adapted iteratively until the cost functions converge to a minimum value. Once the cost function is minimized we can be assured that the performance criterion is met and the algorithm is said to have converged.

There are several factors that are to be considered while choosing an adaptive algorithm like the convergence rate of the algorithm, complexity and robustness. The convergence rate is the number of iterations required for the convergence of the algorithm. In mobile environments, convergence rate is important as it is important to converge to optimum before the channel conditions change. The complexity issues come into play when we need to determine the number of DSP cycles needed for algorithm implementation. Finally the algorithm we choose should be robust as it should be able to perform fairly well even in cases where the input data may be ill-conditioned.

5.6 Optimum Beamforming

The complex weights for each element of the array can be calculated for the optimization of some property of the received signal. The weights that are obtained are not necessarily those that maximize beam pattern in the direction of the desired user. Rather they

optimize the cost function in question. Adaptive beamforming is an approximation of optimum beamforming.

If we consider the performance criteria is to minimize the Mean Square Error between the received and the transmitted signals, the cost function to be minimized is given as,

$$J = E[|d(n) - y(n)|^2] \quad (5.25)$$

where $E[.]$ denotes the ensemble average.

Substituting for the output of the beamformer as $y(n) = \mathbf{w}^H \mathbf{x}(n)$ and taking of the gradient of the cost function and setting it to zero, we get

$$\nabla J = -2\mathbf{r}_{xd} + 2\mathbf{R}_{xx}\mathbf{w} = 0 \quad (5.26)$$

where $\mathbf{R}_{xx} = E[\mathbf{x}(n)\mathbf{x}(n)^H]$ is the $M \times M$ correlation matrix of the input signal $\mathbf{x}(n)$. Also $\mathbf{r}_{xd} = E[\mathbf{x}(n)d^*(n)]$ is the cross-correlation vector between the sensor inputs and the desired signal $d(n)$. Solving equation (5.26) gives the expression for the optimum weights for MMSE as,

$$\mathbf{w}_{opt} = \mathbf{R}_{xx}^{-1}\mathbf{r}_{xd} \quad (5.27)$$

The above equation is also known as the Wiener-Hopf equation or the Optimum Wiener solution.

5.7 Adaptive Beamforming algorithms

Adaptive algorithms determine the weights iteratively approximating the optimum weights. The reason being that computing optimum weights using equation (5.27) involves ensemble averaging and matrix inversions which can consume more DSP cycles. Some early work on adaptive beamforming can be found in [How59]. Several beamforming algorithms have been proposed since then. The following sections summarize some of the most common and widely used beamforming techniques.

5.7.1 Least Mean Squares (LMS)

The LMS algorithm is an MMSE weight adaptation algorithm that uses the steepest descent algorithm. The weight vectors are calculated recursively using the following equations,

$$\begin{aligned}
w(k+1) &= w(k) + \Delta x(n)e(n) \\
\text{where} & \\
e(n) &= d^*(n) - x^H(n)w(n)
\end{aligned} \tag{5.28}$$

In the above equation, Δ is the step-size and determines the rate of convergence of the algorithm. The choice of Δ depends on the eigen-spread of the covariance matrix, R_{xx} . The LMS algorithm requires knowledge of the transmitted signal. This is usually accomplished by sending periodically some known pilot sequences that is usually known to the receiver.

5.7.2 Recursive Least Squares (RLS) Algorithm

The RLS algorithm uses weighted sums for estimating R_{xx} and r_{xd} using the following equations,

$$\begin{aligned}
\tilde{\mathbf{R}}_{xx} &= \sum_{i=1}^N \gamma^{n-1} x(i)x^H(i) \\
\tilde{\mathbf{r}}_{xd} &= \sum_{i=1}^N \gamma^{n-1} d(i)^* x(i)
\end{aligned} \tag{5.29}$$

The matrix inversion is obtained recursively and the weight update equation is given by

$$w(n) = w(n-1) + q(n)[d^*(n) - w^H(n-1)x(n)] \tag{5.30}$$

Here,

$$q(n) = \frac{\gamma^{-1} \mathbf{R}_{xx}^{-1}(n-1)x(n)}{1 + \gamma^{-1} x^H(n) \mathbf{R}_{xx}^{-1}(n-1)x(n)} \tag{5.31}$$

where,

$$\mathbf{R}_{xx}^{-1}(n) = \gamma^{-1} [\mathbf{R}_{xx}^{-1}(n-1) - q(n)x(n) \mathbf{R}_{xx}^{-1}(n-1)] \tag{5.32}$$

The RLS algorithm converges about 10 times faster than the LMS algorithm provided the SINR is high. It requires an initial estimate of \mathbf{R}_{xx}^{-1} matrix and a reference signal.

5.7.3 Direct Matrix Inversion

In this method the optimum weight computation equation 5.27 is used except that the \mathbf{R}_{xx} and \mathbf{r}_{xd} are the data samples over a finite interval.

Thus the estimates are given by,

$$\begin{aligned}\hat{\mathbf{R}}_{xx} &= \sum_{i=N_1}^{N_2} x(i)x(i)^H \\ \hat{\mathbf{r}}_{xd} &= \sum_{i=N_1}^{N_2} d(i)^* x(i)\end{aligned}\quad (5.33)$$

The DMI algorithm would converge to optimum, faster than the LMS algorithm but it is computationally complex.

Figure 5.3 shows the beam pattern of a 4-element beam former. From the figure it is evident that we can place nulls in spatial locations where the interferers are present while simultaneously increasing the gain in the direction of the desired user. It is to be noted that an N element beamformer can ideally remove up to $(N-1)$ interferers. Overloaded array processing algorithms might be needed if we have to remove more than N interferers.

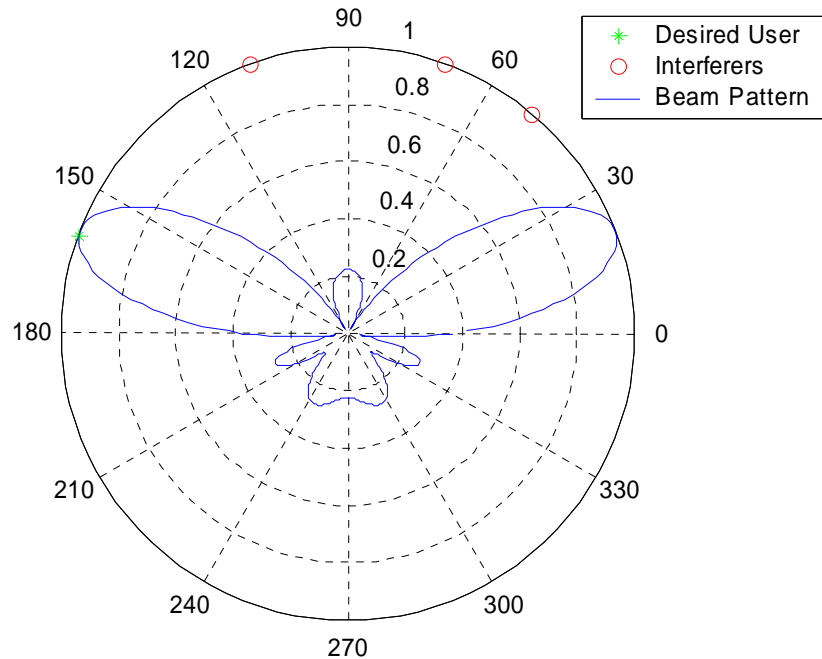


Figure 5.3 Beam pattern of a 4 element ULA with 3 interferers in AWGN channel. Weight calculated using Direct Matrix Inversion algorithm

5.7.4 Decision Directed algorithms

The algorithms discussed above all require the knowledge of the transmitted signals. In decision directed algorithms the weights can be updated using any of the above techniques, but the reference signal is obtained by demodulating $y(n)$. This means that no external reference is required, but convergence is not guaranteed because the demodulated $y(n)$ may not correspond to the original data symbols $d(n)$.

For the purpose of this research we focus only on MMSE techniques which are pilot assisted because pilot assisted beamforming techniques usually perform better and are reliable compared to blind algorithms. Also all recent wireless standards provide some overhead symbols for synchronization purposes and hence these pilot symbols can be used for beamforming as well.

5.8 Diversity Combining

The above sections discussed the performance of phased arrays and the different beamforming algorithms for interference rejection. Additionally signals from various elements can be combined to improve the performance in fading channels. The following sections discuss some of the most common diversity combining techniques.

5.8.1 Selection Combining

In selection combining, the branch with the largest SNR is selected and that element's signal is used for the decoding process. Hence the larger the number of elements the better the performance of the selection combining process.

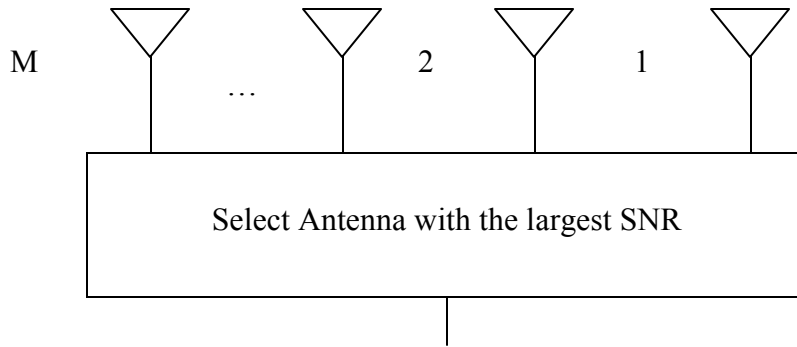


Figure 5.4 Selection Diversity

5.8.2 Maximal Ratio Combining (MRC)

MRC takes better advantage of the diversity provided by all branches. In MRC the elements are weighted with their instantaneous SNRs. The branches are co-phased to get maximum advantage of diversity combining before the summation process. This summed signal is used for the decoding process. The performance of MRC is much better than that of the selection combining. However it is more complex since it requires SNR estimation and weight updates.

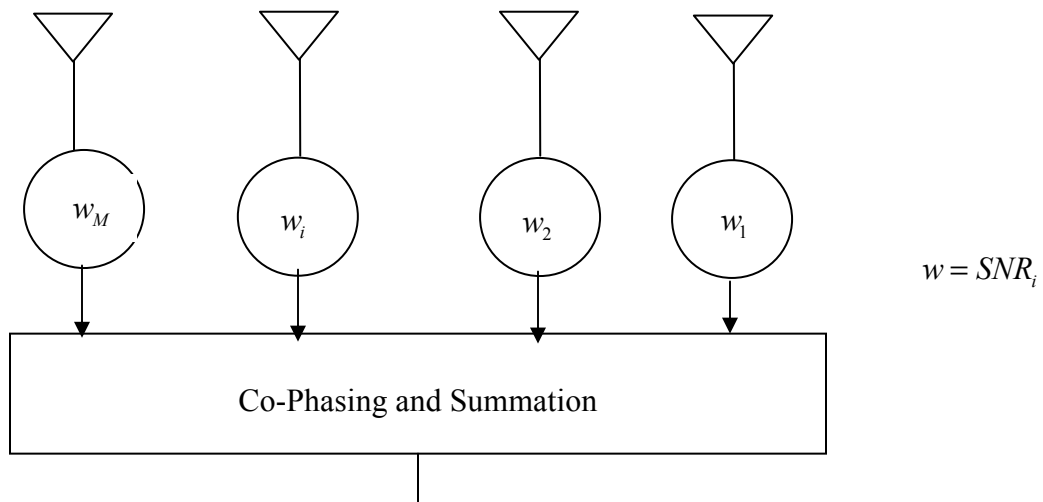


Figure 5.5 Diversity Combining

5.8.3 Equal Gain Combining (EGC)

EGC is a variant of the Maximal Ratio Combining technique. The weights are all set to the same value and are not changed after that. Then the signals are co-phased as in MRC before the summation process.

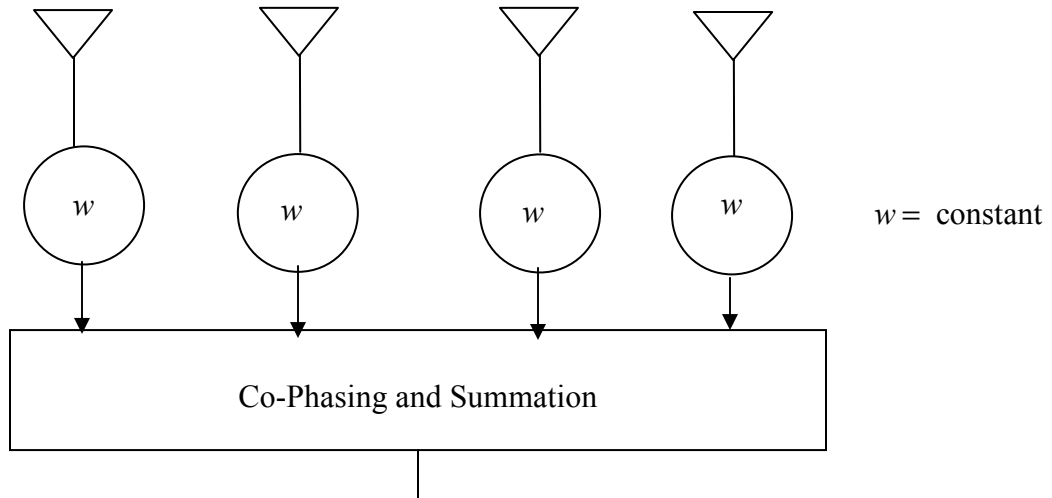


Figure 5.6 Equal Gain Combining

Figure 5.7 shows the BER performance of the MRC diversity combining in a flat fading channel for QPSK modulation.

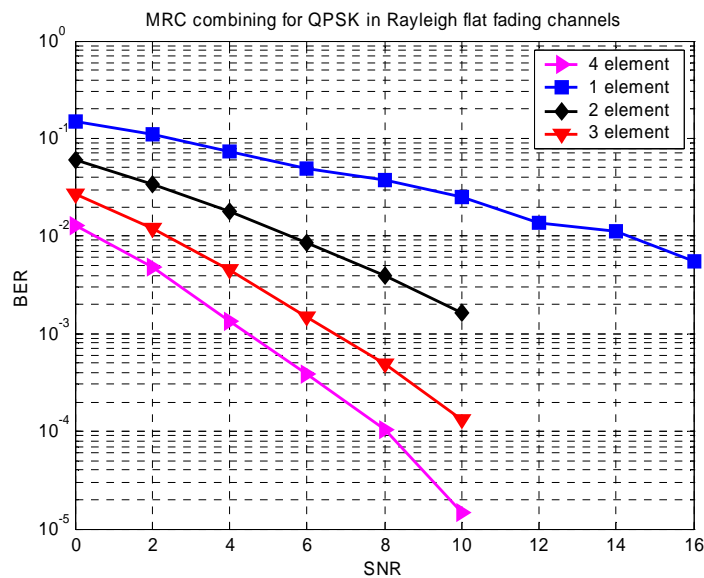


Figure 5.7 Performance of Maximal Ratio Combining in uncorrelated Rayleigh fading channels.

We see that as we increase the number of elements the diversity advantage improves the performance although it follows the law of diminishing returns.

5.9 Summary

In this chapter we presented some fundamentals concepts on beamforming and adaptive antenna arrays. Optimum beamforming and adaptive algorithms were also discussed. MMSE algorithms were discussed which is the main focus of our research. Diversity combining techniques were also discussed and performance results were shown. In subsequent chapters we will discuss the performance of these beamforming algorithms in the context of an OFDM signal.

Chapter 6

Beamforming for MC-CDMA systems

In the previous chapters we investigated performance improvement using multiple antenna systems in a multipath fading channel and in the presence of interference. In this chapter we study the performance of these multiple antenna systems for a MC-CDMA signal. We assume here a reverse link scenario with an adaptive array at the base station and study different ways which we can combine the signals at the array for effective interference rejection. As was discussed previously, the spreading involved in MC-CDMA has interference rejection capabilities but is not sufficient in the case of strong interferers. Hence we need to use beamforming algorithms in cases where we need to reject strong interferers. Although there are many beamforming algorithms, the main channel parameters like the angle spread, delay spread and the Doppler spread make the interference rejection problem more difficult. Hence this chapter examines some ways to do beamforming for OFDM systems under harsh channel conditions. We propose some new and effective ways that can be used as demanded by the channel conditions.

We start with a brief review of all algorithms that have been previously studied in Section 6.1. Section 6.2 describes the frequency domain beamforming and Section 6.3 presents performance results for frequency domain beamforming in a flat fading channel. Section 6.4 analyzes the performance of frequency domain beamforming in a frequency selective channel while Section 6.5 gives a brief summary of a sub-band beamforming technique. Section 6.6 describes time domain beamforming while Sections 6.7 and 6.8 describe the MMSE space and frequency beamforming technique. Section 6.9 concludes the chapter by summarizing some of the important results that have been presented in this chapter.

6.1 Literature review

Much of the early work focused on multiple antenna receivers for OFDM systems. We cite those works here on MC-CDMA beamforming since an MC-CDMA system is essentially an OFDM system with some spreading involved. [Kim00] studied the performance of adaptive LMS weight formation for OFDM systems. The research dealt with the performance in an AWGN channel. [Li99] proposed an adaptive MMSE beamforming algorithm that involves channel parameter estimation for all users. The algorithm involves instantaneous channel correlation estimation that can be used for the MMSE diversity combiner. One of the earliest works can be found in [Voo98]. In that work, the authors looked into the Sample Matrix Inversion algorithm with pilot interpolation for computing the sample covariance matrix. This method guarantees good performance if the channel does not change in frequency and is relatively flat.

6.2 Frequency Domain Beamforming

The combining of multicarrier signals in various elements of the receiver array can be done in many different ways. The simplest method is to combine them in frequency after the FFT operation in the receiver. This is usually done because the pilots used for timing synchronization and channel estimation are usually inserted in the frequency domain at the transmit side and hence it is necessary to get back those pilot symbols after the FFT operation at the receive side and then proceed with combining. Another approach would be to combine the signals in the receive elements in time and then perform an FFT operation. We call this approach time-domain beamforming, which we will discuss in Section 6.6.

A typical frequency domain beamforming approach is shown in the Figure 6.1.

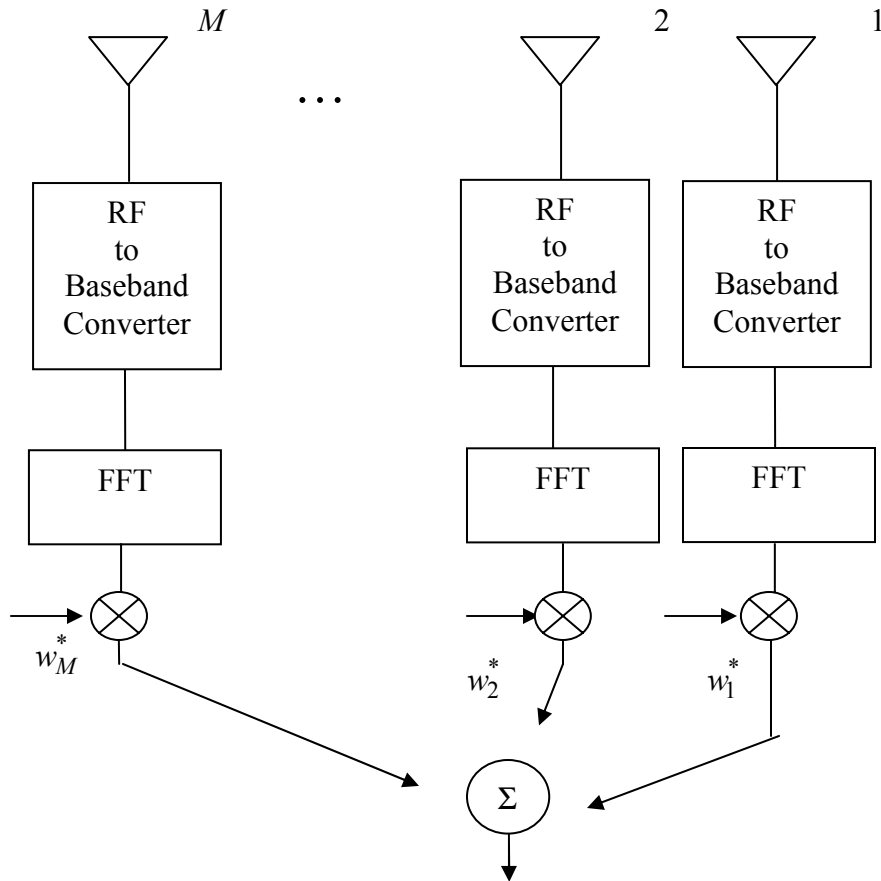


Figure 6.1 Frequency Domain beamformer

6.2.1 Model of the Received signal

Let us assume that the transmitted signal is

$$s(n) = \sum_{k=0}^{N-1} x_k e^{j2\pi nk/N} \quad 0 \leq n \leq N-1 \quad (6.1)$$

where N is the number of subcarriers. Here x_k are the individual modulated symbols in the subcarriers.

If we consider a multipath channel with L paths, the received signal can be modeled as the sum of these paths and can be expressed as (from Equation 4.1)

$$y(n) = \sum_{l=0}^L h(n,l)s(n-l) + w(n) \quad (6.2)$$

Here L is the number of multipaths, $h(n,l)$ represents the time varying nature of the channel coefficients for each path, l , $w(n)$ is the additive white Gaussian noise and $s(n)$ represents the output of the IFFT at the transmitter.

We assume an M element antenna array and the received signal at each of the antenna elements can be written as (from Equation 5.11)

$$y_m(n) = \sum_{l=0}^L h(n,l) s(n-l) \exp\left(\frac{-j2\pi(m-1)d \sin \theta}{\lambda}\right) + w_m(n) \quad (6.3)$$

In the above expression the subscript m refers to the m th element of the array and we assume a phased array with no angle spread.

Using the expression for $s(n)$ from equation 6.1, we get

$$\begin{aligned} y_m(n) &= \sum_{l=0}^L \sum_{k=0}^{N-1} x_k \exp\left(\frac{j2\pi(n-l)k}{N}\right) h(n,l) \exp\left(\frac{-j2\pi(m-1)d \sin \theta}{\lambda}\right) + w_m(n) \\ &= \sum_{k=0}^{N-1} x_k \exp\left(\frac{j2\pi nk}{N}\right) \sum_{l=0}^L h(n,l) \exp\left(\frac{-j2\pi lk}{N}\right) \exp\left(\frac{-j2\pi(m-1)d \sin \theta}{\lambda}\right) + w_m(n) \end{aligned} \quad (6.4)$$

We can define the following ,

$$H_k(n) \equiv \sum_{l=0}^L h(n,l) \exp\left(\frac{-j2\pi lk}{N}\right) \quad (6.5)$$

which is the Fourier transform of the channel impulse response at a particular time n . We can thus rewrite equation (6.4) as

$$y_m(n) = \sum_{k=0}^{N-1} x_k H_k(n) \exp\left(\frac{j2\pi nk}{N}\right) \exp\left(\frac{-j2\pi(m-1)d \sin \theta}{\lambda}\right) + w_m(n) \quad (6.6)$$

In general the received vector in all the M elements of the array can be written as

$$\mathbf{y}(n) = \sum_{k=0}^{N-1} x_k H_k(n) \exp\left(\frac{j2\pi nk}{N}\right) \mathbf{a}(\theta) + \mathbf{w}(n) \quad (6.7)$$

Here $\mathbf{a}(\theta) = [1, \exp(\frac{j2\pi d \sin \theta}{\lambda}), \dots, \exp(\frac{j2\pi(M-1)d \sin \theta}{\lambda})]^T$ is the vector containing the phase shifts experienced by the signal while traversing through the array. $\mathbf{A}(\theta)$ is also called the array steering vector or the array response vector as discussed in Chapter 5 and $\mathbf{w}(n)$ is the vector containing the additive noise in each of the antenna elements in the array. As before we assume that the auto-correlation matrix of the noise vector is defined as

$$\begin{aligned} \mathbf{R}_{ww} &= E\{\mathbf{w}(n)\mathbf{w}^\dagger(n)\} \\ &= \sigma^2 \mathbf{I} \end{aligned} \quad (6.8)$$

The output of the FFT block at m th antenna element for the k th subcarrier can be expressed as (from Equation 6.6)

$$Z_{m,k} = \sum_{k=0}^{N-1} y_m(n) \exp(\frac{-j2\pi nk}{N}) = \sum_{k=0}^{N-1} x_k H_k(n) \exp(\frac{-j2\pi(m-1)d \sin \theta}{\lambda}) + W_{m,k}(n) \quad (6.9)$$

where $W_{m,k}(n)$ is the Fourier transform of the additive noise component at the m th antenna element for the k th subcarrier.

6.2.2 MMSE Beamforming

We use the received signal at the array and form weights that yield the optimum output signal. In the optimum weight computation, equation (5.27) is used. The \mathbf{R}_{xx} and \mathbf{r}_{xd} are computed after the FFT operation on the data samples at the output of each of the antennas in the array. Sufficient pilots are inserted in the transmitter so that sufficient statistics are available at the receive side for proper estimation of \mathbf{R}_{xx} and \mathbf{r}_{xd} . We will later discuss the performance improvement achieved due to the use of some advanced detection techniques before beamforming.

The weights are then used to combine this signal after the FFT operation and this combined signal is given by,

$$\mathbf{P} = \mathbf{w}^H \mathbf{Z} \quad (6.10)$$

where \mathbf{w} is the weight vector obtained using the MMSE criterion, $\mathbf{Z}_{m \times n}$ is a matrix of the output of the detection blocks at each of the receive elements and \mathbf{P} is the vector containing the combined signal. The vector \mathbf{P} is then used for despreading and symbol decoding after parallel to serial conversion.

We evaluated the performance of this beamforming algorithm in a variety of channel conditions and the results will be presented in the following sections. Frequency domain beamforming using the MMSE criteria can remove the multiplicative distortion introduced by the channel in a flat fading environment (i.e. when the channel frequency response does not change in the frequency range of the desired signal). This can save us from estimating the channel and compensating for it through some complex equalization procedure. The channel compensation can be very difficult to perform when there are interferers, with power levels higher than that of the desired signal level. The spreading associated with MC-CDMA also helps in interference suppression.

6.3 Performance results in a flat fading channel

For the purpose of evaluating the beamforming algorithm we first consider a flat fading channel and study the performance. Simulations were generally carried out as explained in Chapter 2 with a 4-element receive array. The results were obtained by changing parameters like angle spread, Doppler spread, the number of pilots necessary for weight computation, the angle separation between the desired user and interferer and the spreading factor, etc. As was explained in the previous section we did not perform any explicit channel estimation and channel compensation as the single weight vector performs both the interference suppression as well as the channel compensation. The \mathbf{r}_{xd} vector that is estimated using the pilot symbols can be thought of as the vector that provides the channel information and the covariance matrix \mathbf{R}_{xx} can be thought of as providing the necessary interference suppression.

6.3.1 Effect of the number of pilots

The MMSE beamforming algorithm is dependent on the number of pilots inserted at the transmit side for proper weight computation at the receiver. Figure 6.2 shows the performance difference in having different numbers of pilots per block.

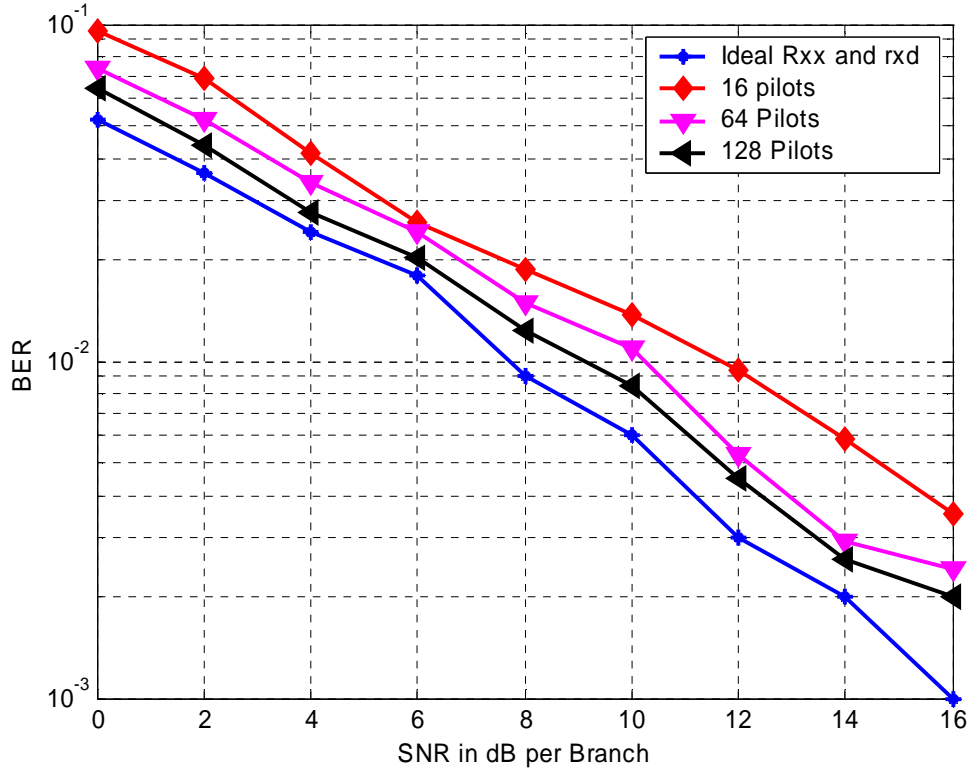


Figure 6.2 Effect of Number of Pilots on the algorithm's performance.

($N=1024$, $SIR = -10\text{dB}$, $f_d T = 0.01$, $SF = 1$, Angle Spread $\Delta=0$. Separation of 40 degrees between the desired user and interferer.)

As we see above the number of pilots inserted has an effect on the performance of the algorithm. Increasing the number of pilots results in better estimation and thus improved performance. However, increasing the number of pilots per block results in increased overhead. Thus there is a trade off between performance and the overhead necessary.

6.3.2 Effect of the desired user and interferer angle separation

The beamforming algorithm discussed above depends on pilot information and the spatial signature being different for the desired user and interferer. The following results investigate the separation between the desired user and interferer necessary for good BER performance.

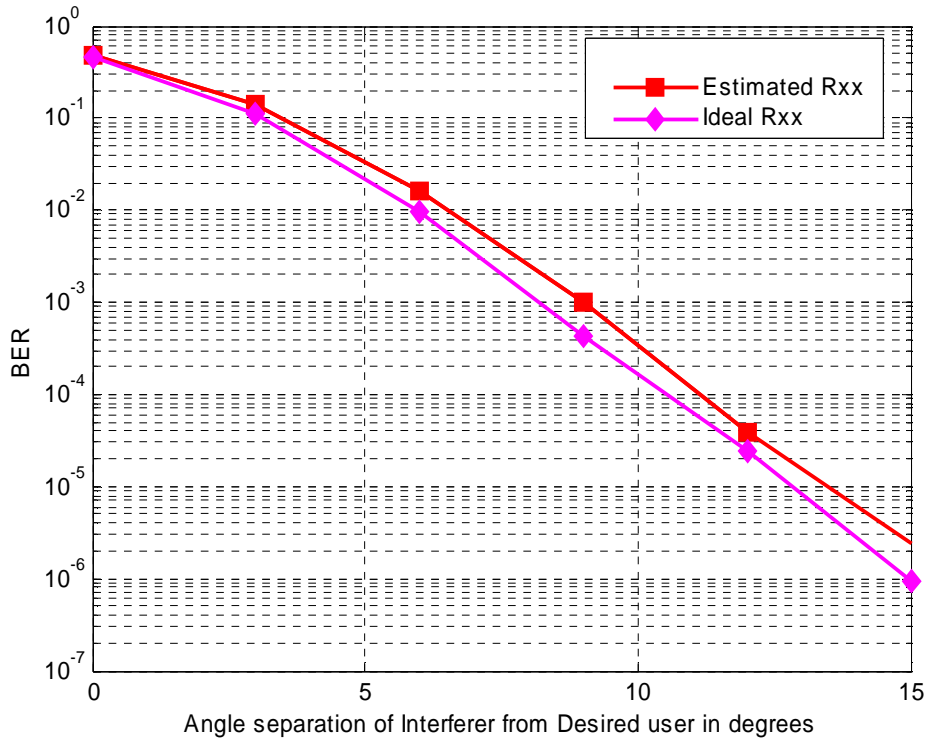


Figure 6.3 Effect of angle separation in degrees in an AWGN channel. SNR = 30dB, N=1024, SF = 1, Number of Pilots = 25, SIR = -10dB.

Figure 6.3 shows the performance in an AWGN channel for varying angle separation. Also a comparison is made with the ideal \mathbf{R}_{xx} estimation which is the case of having all pilots in an MC-CDMA block. The \mathbf{r}_{xd} vector is estimated in both the cases. We can see that there is little difference between the estimated and ideal \mathbf{R}_{xx} cases. The performance is the worst for 0 degree separation between the users as the spatial signatures are the same for the desired user and the interferer. Similar results are shown for a flat fading channel in Figure 6.4. We see that the BER performance is the same after about 20 degrees separation and we can expect the same performance for separation angles larger than 20 degrees.

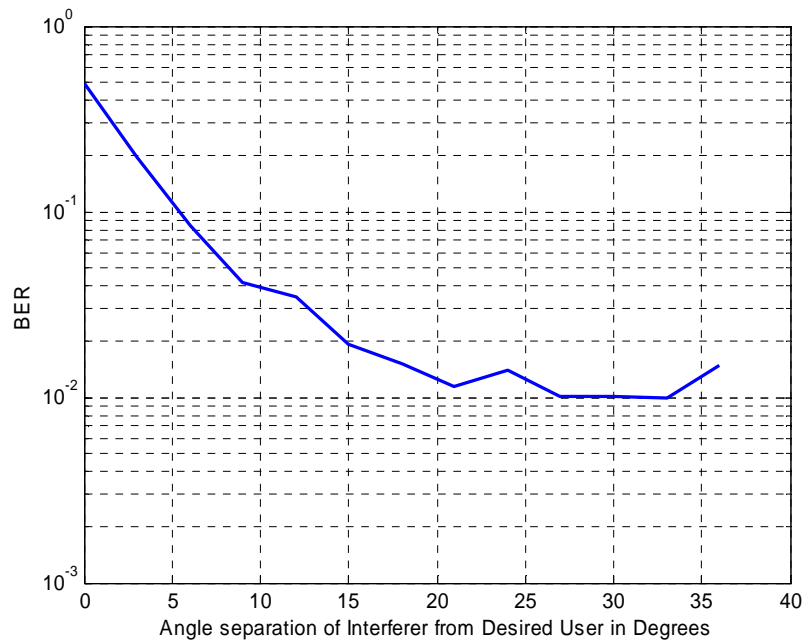


Figure 6.4 Effect of angle separation in degrees in a Rayleigh fading channel. SNR = 8dB, N=1024, SF = 1, Number of Pilots = 128, $f_d T = 0.01$, SIR = -10dB

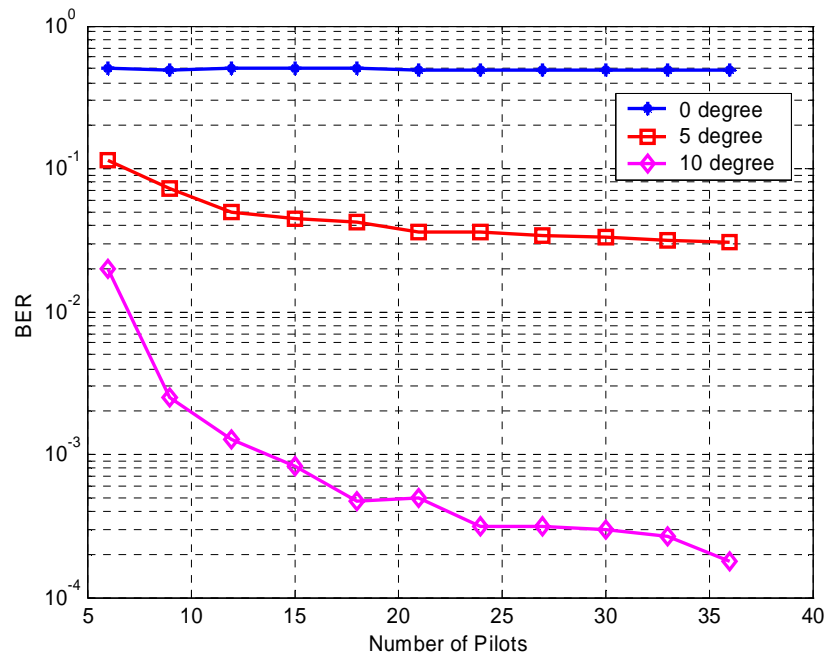


Figure 6.5 Effect of angle separation and number of pilots in an AWGN channel. SNR = 30dB, N=1024, SF = 1, SIR = -20dB

6.3.3 Effect of Spreading factor in Beamforming performance

The results above focused on the number of pilots necessary and the angle separation required between the user and interferer for guaranteed BER performance. In this section we study the effect of varying the spreading factor and the associated performance improvement. In cases where there is a very small angle separation between the desired user and the interferer, varying the spreading factor can help improve performance and as shown in Figure 6.6. The figure also shows the performance improvement due to the angle spread in the channel.

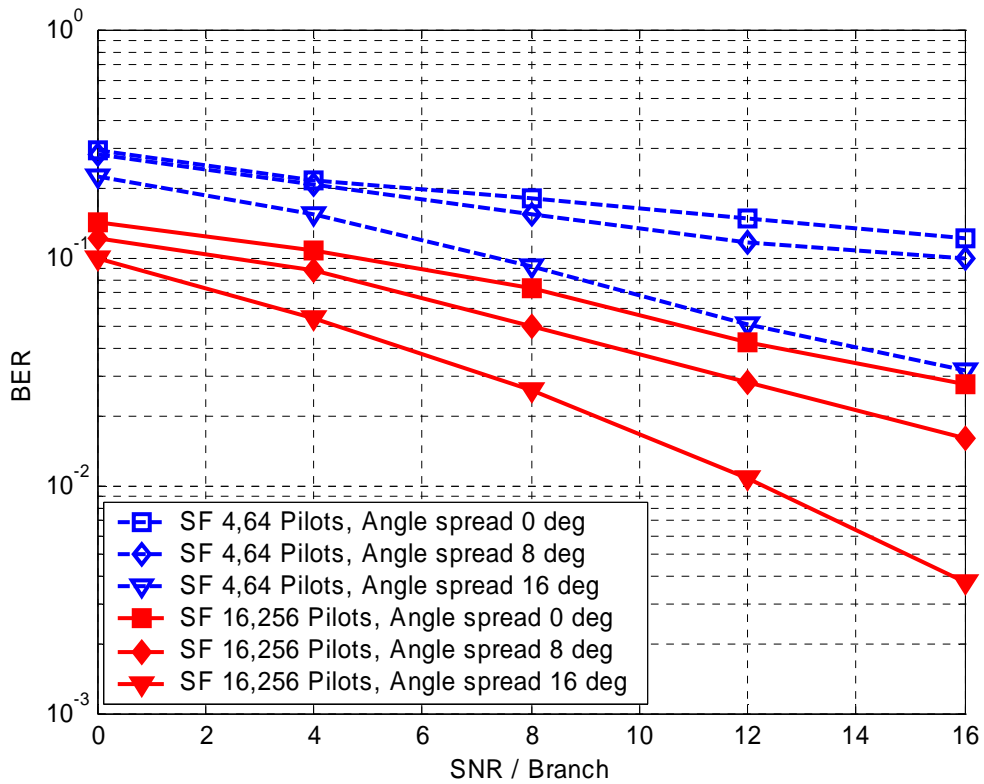


Figure 6.6 Effect of angle spread in degrees and varying spreading code length in a Rayleigh fading channel. $N=1024$, $f_d T = 0.01$, $SIR = -20\text{dB}$. User separation is 10 degrees.

We see that increasing angle spread provides better diversity advantage and increasing the spreading factor provides better interference suppression.

Figure 6.7 shows the performance of MMSE beamforming and Maximal Ratio Combining (MRC). We can see that in presence of interference MMSE beamforming performs better than MRC. The reason can be attributed to the fact that MRC maximizes the output signal to noise ratio and does not provide any interference suppression. We thus observe some error floor. The performance of MRC can however be improved by increasing the spreading code length. On the other hand MMSE beamforming with sufficient pilots can provide better performance. There is approximately 6dB performance improvement with a 4 element array compared to the single element case with no interference. There is little to no performance improvement by increasing the spreading code length as we get sufficient interference suppression with lower spreading codes themselves.

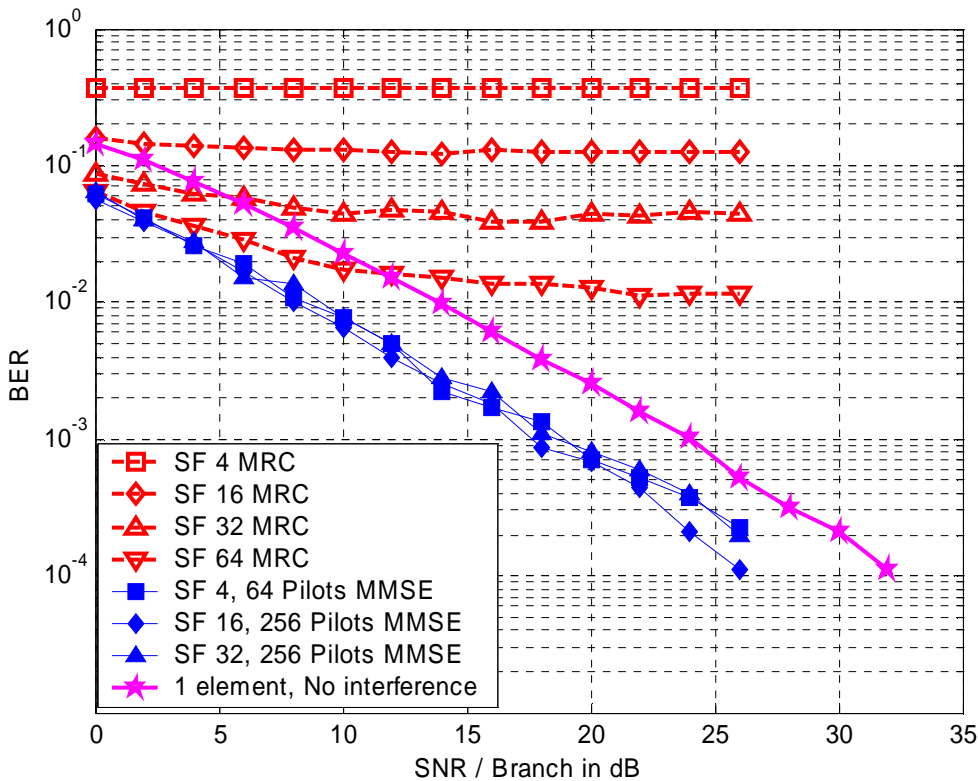


Figure 6.7 Performance comparison of MMSE beamforming with MRC. $N=1024$, $f_dT = 0.01$, $SIR = -20\text{dB}$. User separation is 40 degrees.

The effect of varying the interference power levels on the algorithm's performance is studied in Figure 6.8. As one would expect the performance degrades with increasing interferer power levels.

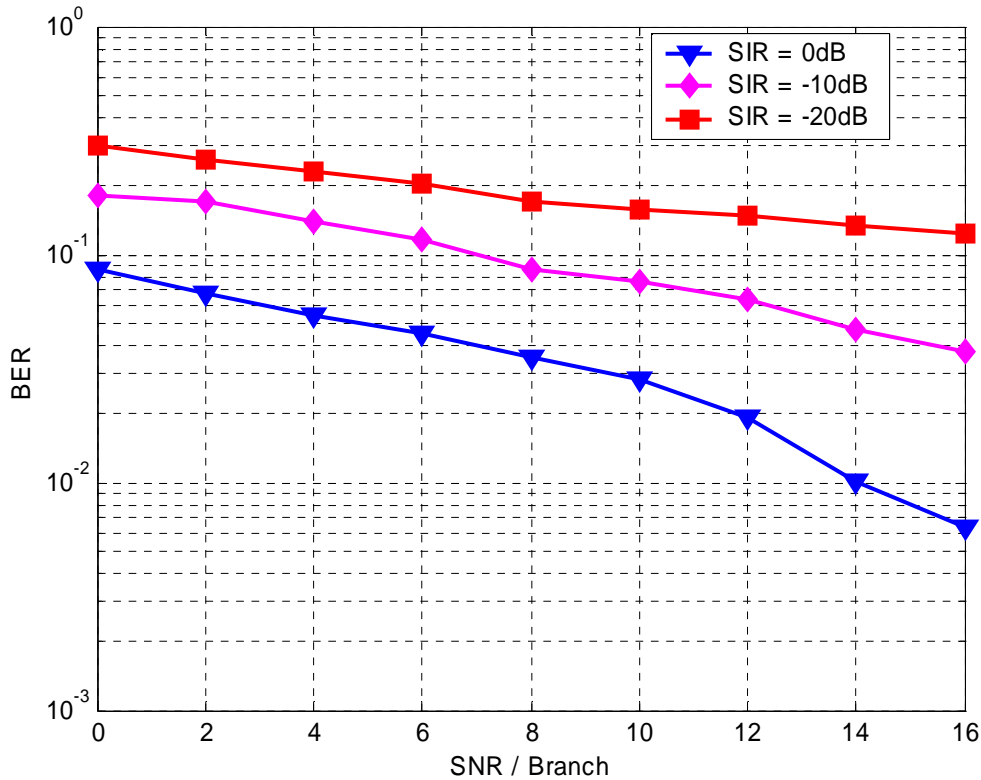


Figure 6.8 Performance of MMSE beamforming with varying SIR. ($N=1024$, $f_d T = 0.01$, $SF = 4$. User separation is 10 degrees, Angle spread $\Delta = 0$)

The impact of Doppler on the performance of multicarrier systems has been studied elaborately in Chapter 3. Figure 6.8 shows the performance of MMSE beamforming in the presence of large time variations in the channel. As we would expect the time variations disrupt the orthogonality between subcarriers and the pilot symbols are corrupted. This leads to performance degradation as is shown in Figure 6.9.

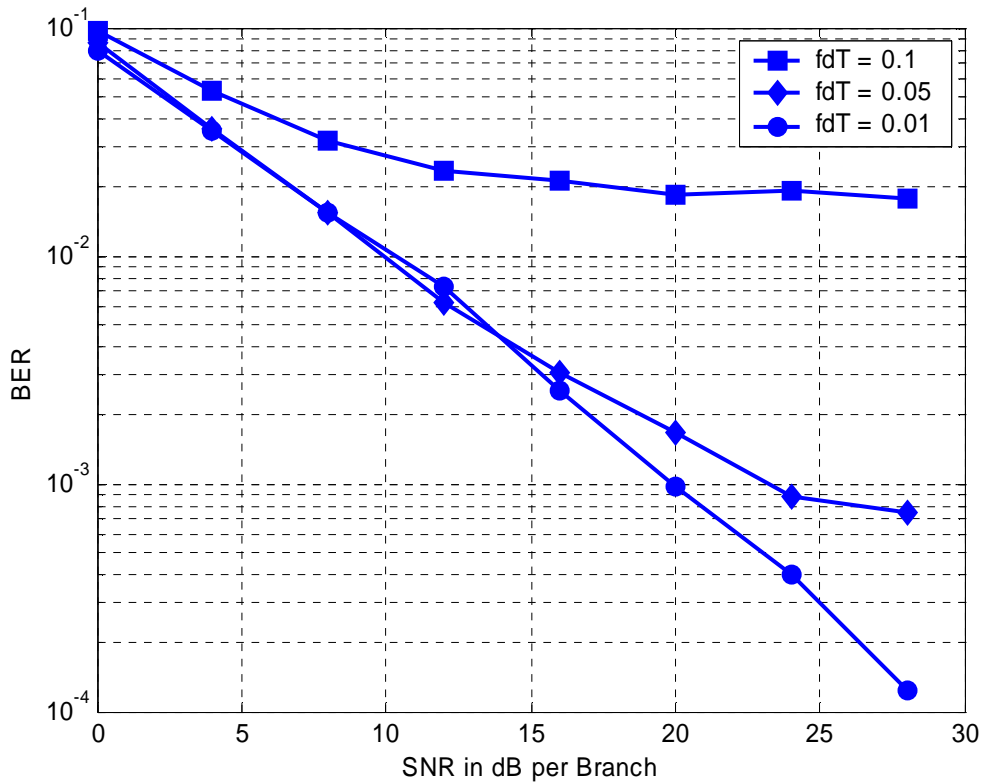
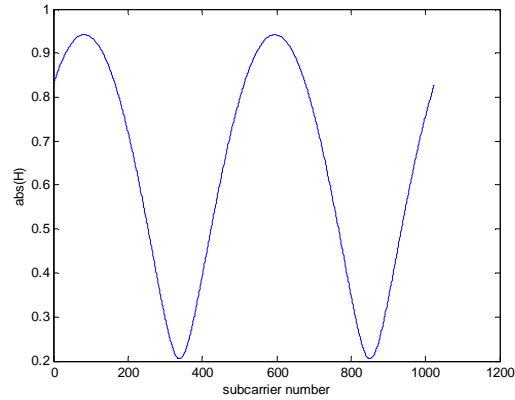


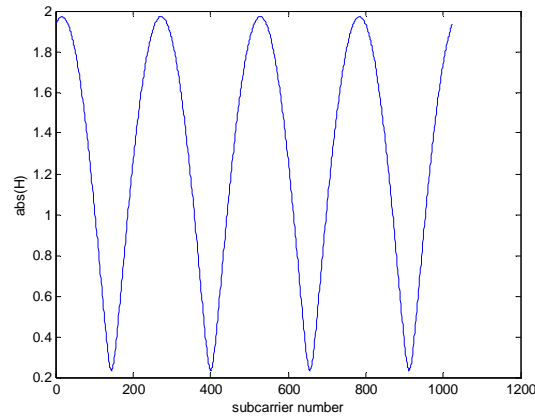
Figure 6.9 Performance of MMSE beamforming with increase in normalized Doppler spread values. ($N = 1024$, User separation = 40 degrees and SF = 4, Angle spread $\Delta = 0$)

6.4 Performance results in Frequency selective fading

We considered a two-ray path model for the multipath channel. The two paths are considered to have the same power and the corresponding frequency response of the channel is as shown in Figure 6.10. We can see that the frequency selectivity of the channel increases as we increase the delay spread due to the channel. Unlike flat fading channels the frequency response changes rapidly within the frequency range of interest and hence the beamformer would not be able to track changes in the channel frequency response for good performance.



(a)



(b)

Figure 6.10 Frequency Response of the channel (a) Delay spread = 200ns, (b) Delay spread = 400ns. $N = 1024$

The performance of the frequency domain beamforming algorithm depends on how selective the channel is in frequency. As mentioned earlier, large delay spreads cause significant variations in the channel amplitude and phase across frequency and hence the beamformer might not be able to track changes in frequency within the frequency range of interest. A possible solution to this is to insert a large number of pilot symbols so that the channel variations can be tracked. This could be avoided if many beamformers are used instead of one. However, there is a trade-off in decreasing through-put by inserting more pilot symbols. The performance of the algorithm in a frequency selective channel is

shown in Figure 6.11. We can see that there is an error floor for large SNR values and this error floor worsens with increasing delay spread.

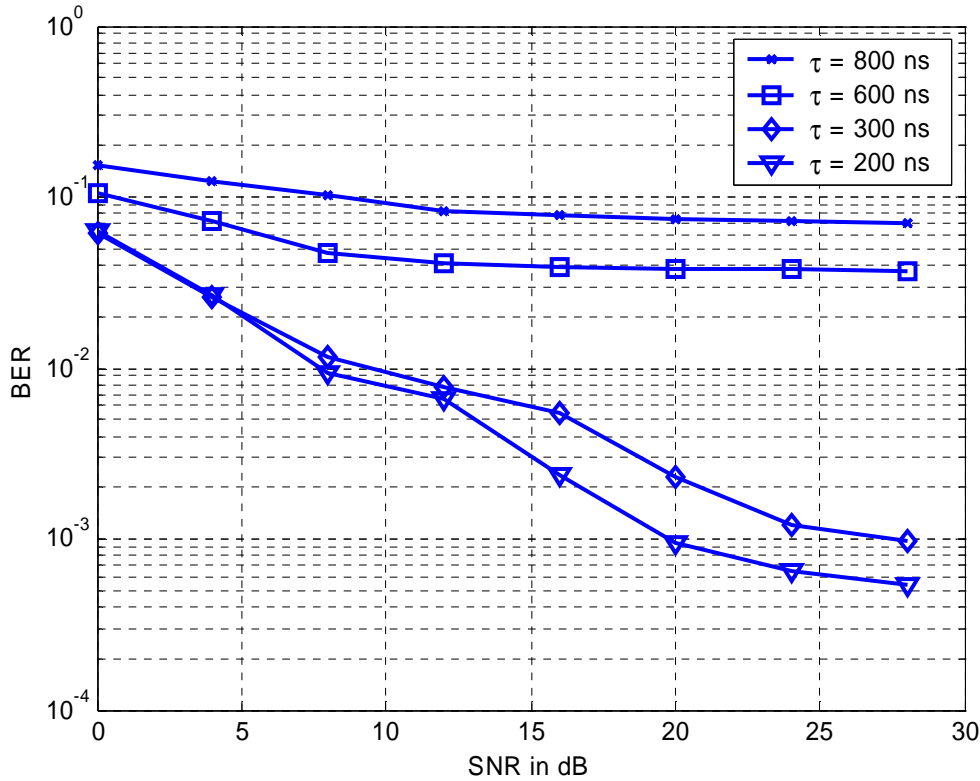


Figure 6.11 Performance of frequency domain beamforming with various values of delay spread (τ). $N = 1024$, $SIR = -10$ dB, $SF = 4$, $f_d T = 0.01$, Angle Spread (Δ) = 0°

The effect of a mixture of various channel parameters such as angle spread and Doppler spread on the performance of the beamforming algorithm is studied in Figure 6.12. Larger angle spread provides decorrelation at the receive antenna elements and thus improves performance as the beamforming algorithm exploits the diversity advantage. Large time variations in the channel result in loss of subcarrier orthogonality and results in more Inter-Carrier interference as discussed in Chapter 4. The performance degradation due to this is obvious. This necessitates the need for some robust detection along with beamforming and this will be discussed in detail in the following sections.

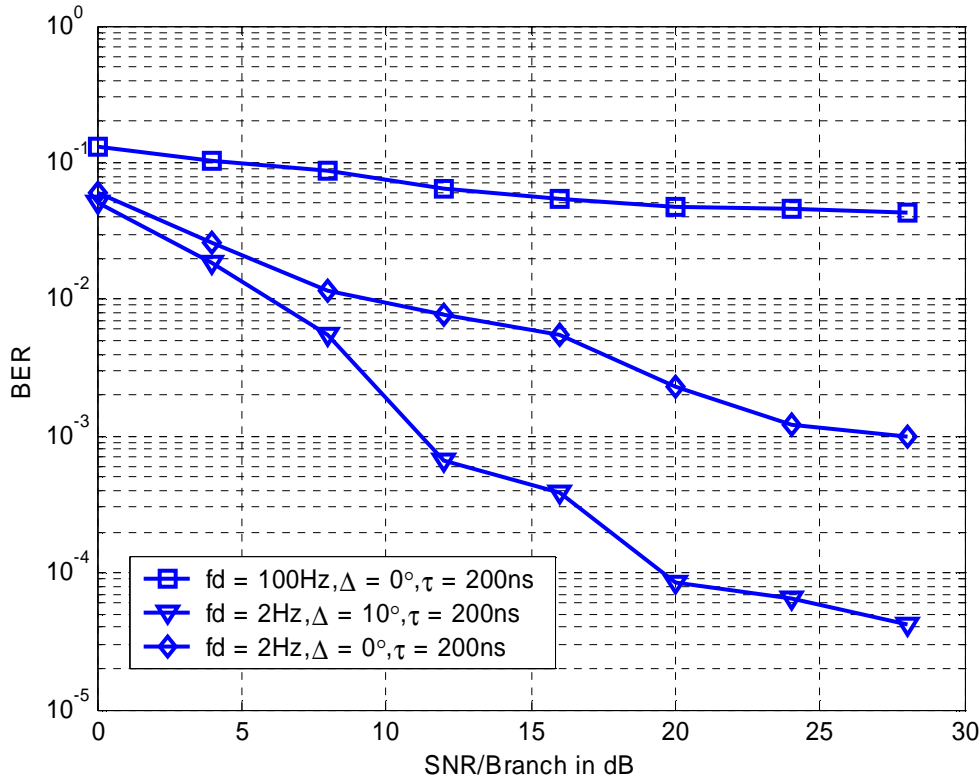


Figure 6.12 Performance of frequency domain beamforming with various values of Angle Spread (Δ) and Doppler spread. $N=1024$, $SF=4$, $SIR=-10\text{dB}$

6.5 Sub-band Beamforming

We discussed in previous sections the effect of delay spread on the beamforming algorithm's performance. We also observed that the performance of frequency domain beamforming degrades with increasing delay spread. For low to moderate delay spread values the frequency domain beamforming algorithm works well. A more robust technique will be to use multiple beamformers to track the fast changing channel. The multiple beamformer forms more than one set of weights for an OFDM symbol. The advantage is that by forming weights for a small fraction of subcarriers the weights can track the changes in the channel across frequency and the error floor that would result due to large delay spreads can be removed completely. This technique is studied

elaborately in [Che02] and a block diagram of the sub-band beamforming concept is shown in Figure 6.13.

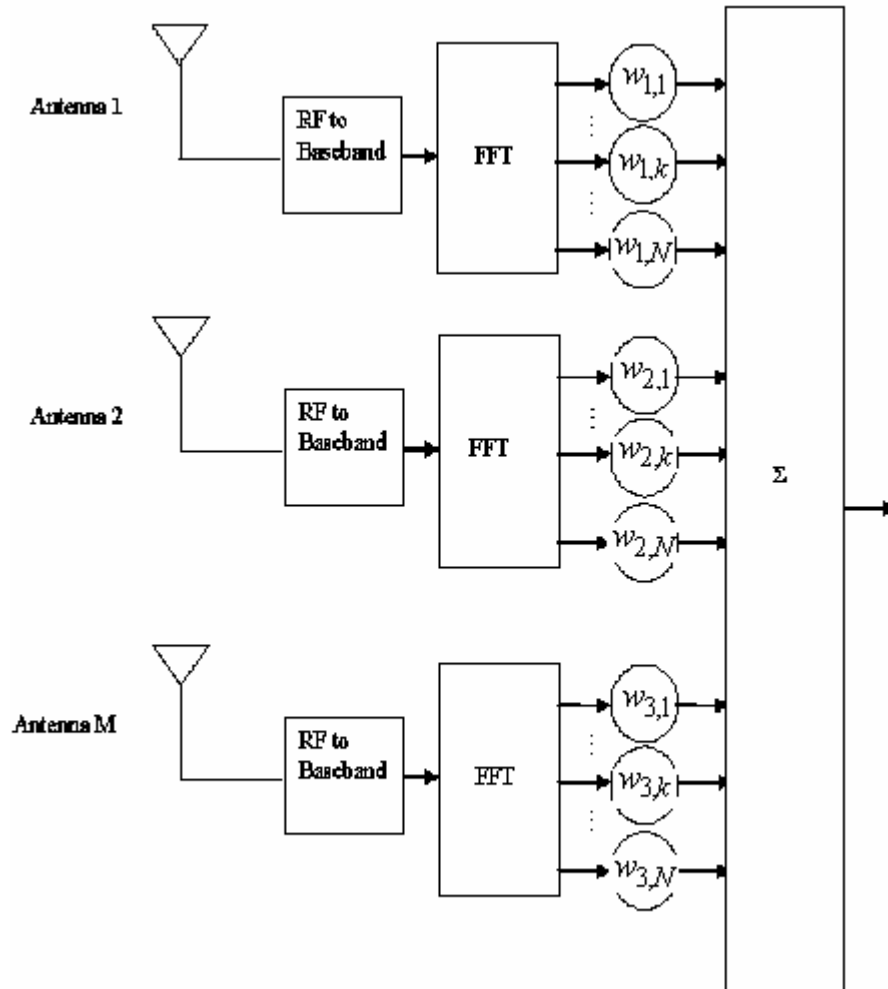


Figure 6.13 Sub-band beamforming for OFDM systems

From Figure 6.13 we see that we attempt to form unique weights for each subcarrier so that the channel changes can be tracked efficiently. Alternatively, we could form a set of weights for a group of subcarriers if the channel frequency selectivity is not very severe. Although this method in [Che02] does perform very well in time dispersive channels, the algorithm assumes a slow time varying channel which may not always be the case. Also the algorithm uses about 12 pilot OFDM symbols in a frame of 100 OFDM symbols to form the proper weights. This can be effective only when the channel is assumed to be

static for the entire duration of about 100 OFDM symbols. Also having 1024 or 512 beamformers in a 1024 subcarrier system can be prohibitively complex.

Figure 6.14 shows the performance of sub-band beamforming in a frequency selective channel. As explained before we attempt to form more than one weight vector for an OFDM symbol. Increasing the number of beamformers per OFDM symbol can track changes in frequency very well and the performance improvement is clearly evident. In Figure 6.14 we can see that by increasing from a single beamformer to about 32 beamformers the BER is improved dramatically.

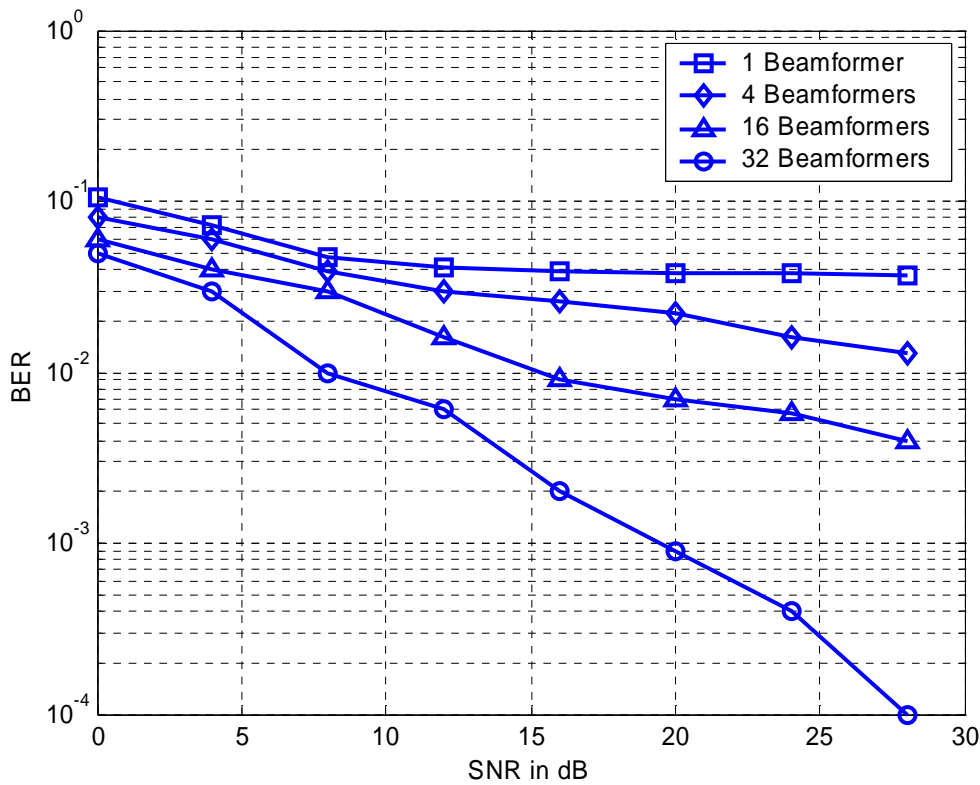


Figure 6.14 Performance of Sub-band domain beamforming. (Angle Spread (Δ) = 0, $f_d T = 0.01$. $N = 1024$, $SF = 4$, $SIR = -10\text{dB}$, $\tau = 600\text{ns}$).

6.6 Time Domain Beamforming

In this technique, the weights are computed in time (i.e., before the FFT block). Further, after the received signal in time is combined using these weights, the FFT is performed for demodulation. Since the pilot vectors are inserted in frequency domain at the

transmitter, the \mathbf{r}_{xd} vector is computed by performing the FFT operation on the received signal. Alternatively, the pilots could be transformed to the time domain. The \mathbf{r}_{xd} vector is normalized with the value of the reference element. Then channel estimation and channel compensation are done to undo the effects of the channel in the reference element. The Figure 6.15 below shows the block diagram of the time domain beamformer. The channel estimation was performed using a cubic Spline interpolation of the channel estimates at the pilot positions.

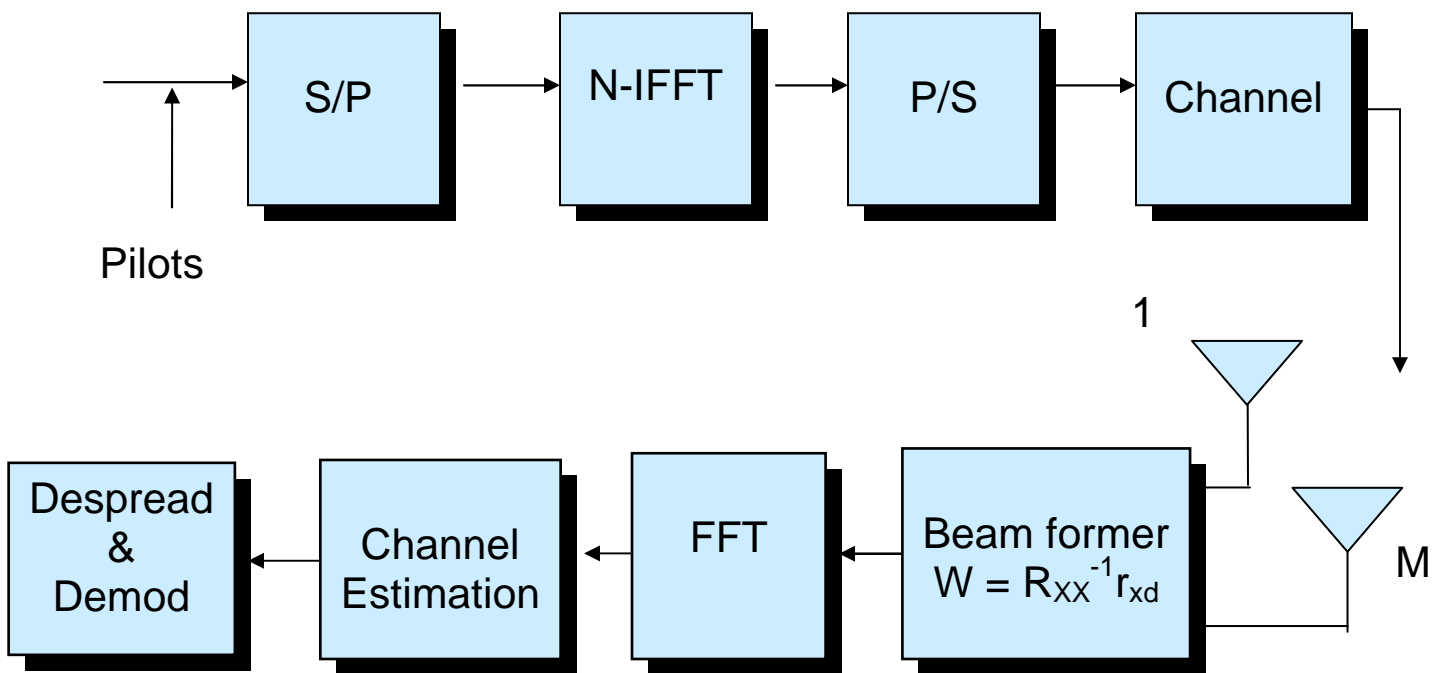


Figure 6.15 Block diagram of Time domain Beamforming

The performance of time domain beamforming in a flat fading channel is shown in Figure 6.16. We could observe that the performance is the same as that of the frequency domain beamforming under similar channel conditions.

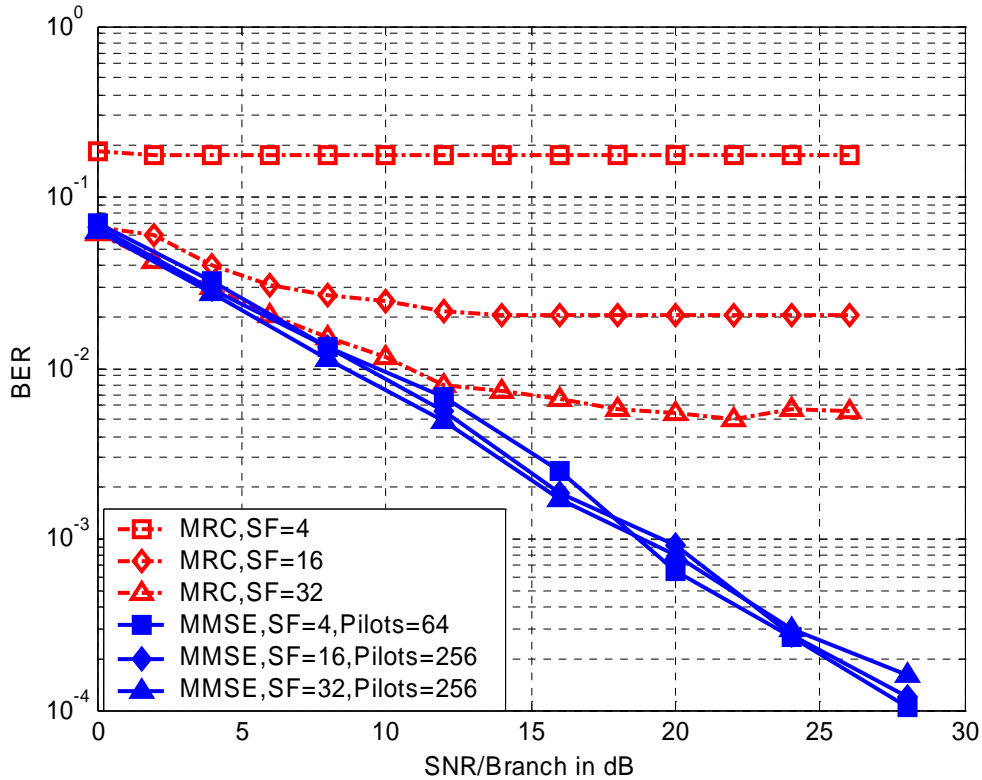


Figure 6.16 Performance of Time domain Beamforming in flat fading channel.

$f_d T = 0.01$, $N=1024$, $SF = 4$, $SIR = -20\text{dB}$

The performance of the time domain beamforming with and without channel estimation is shown in Figure 6.17. Channel estimation for multicarrier systems has already been discussed in Chapters 3 and 4. We see about a 3-4 dB performance loss by performing actual channel estimation as compared to ideal channel estimation.

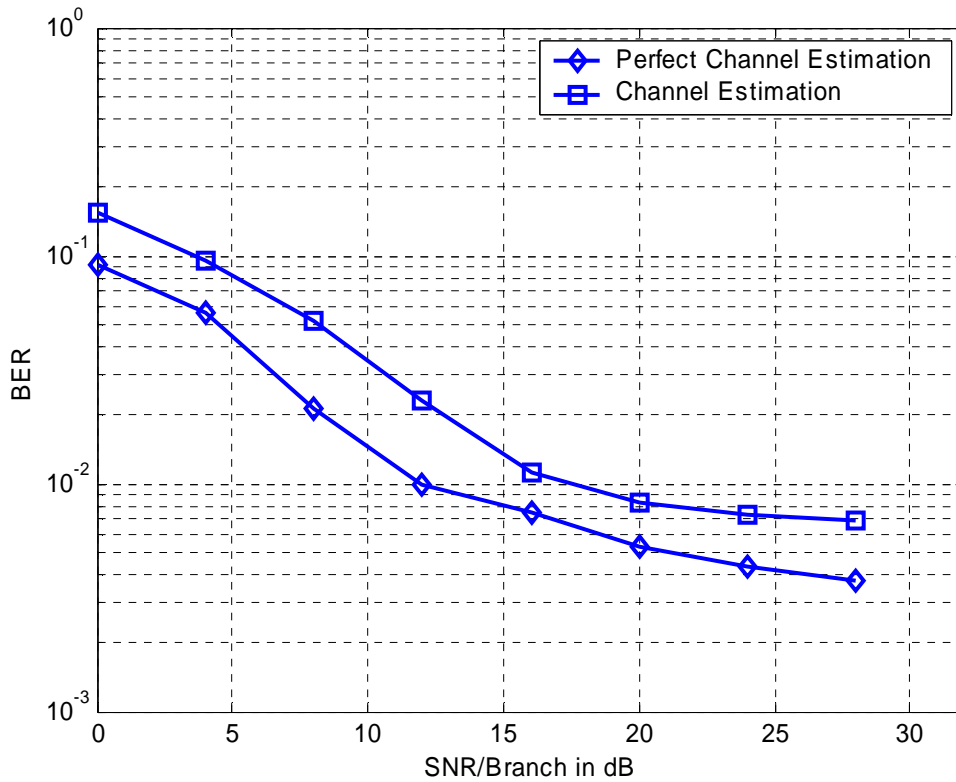


Figure 6.17 Performance of time domain beamforming in frequency selective channel with Channel Estimation. $f_d T = 0.01$, $N = 1024$, Angle spread (Δ) = 0° , Delay spread (τ) = 200ns, SIR = -10dB

6.6.1 Comparison between the time domain and frequency domain beamforming

The frequency and time domain beamformer performances are similar in a flat Rayleigh fading channel. The frequency domain beamformer works well when the channel delay spread is low. The same is true for time domain beamformer. Since we normalize the $\mathbf{r}_{\mathbf{x}d}$ vector, the time domain beamformer performance worsens if the angle spread is high. This is due to channel decorrelation at the antenna elements and hence combining results in an error floor. The frequency domain beamformer works well when the angle spread is high. This is because it exploits the diversity advantage due to decorrelation. This comparison can be observed clearly in Figure 6.18. The effect of Doppler is the same for both the beam-formers as the high ICI will result in error floors due to the loss of subcarrier orthogonality. In terms of complexity the beamformers are similar. However, the time-domain beam-former requires additional channel estimation after the FFT block.

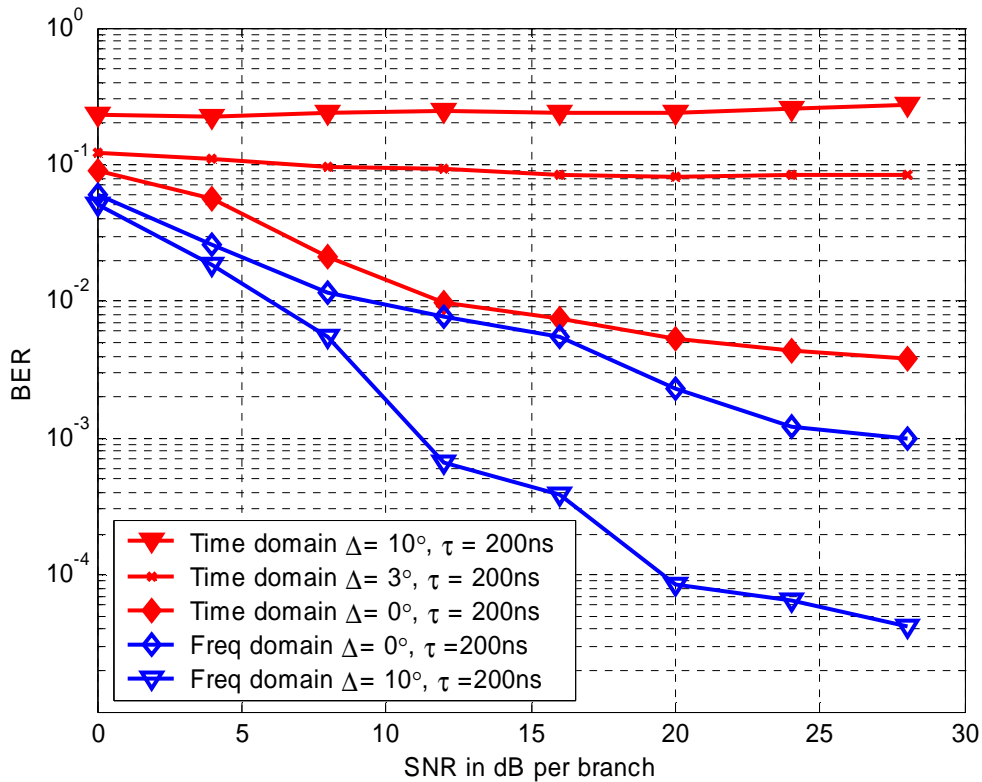


Figure 6.18 Performance Comparison of Time domain and Frequency domain beamforming in different angle spread environments. ($N = 1024$, Spreading factor = 4, $f_d T = 0.01$, SIR = -10dB)

In the sections above we studied the performance of beamforming algorithms and their effectiveness in various channel conditions. We could conclude that the techniques discussed above were not robust to time variations of the channel. Both time and frequency domain beamforming would result in error floor at high Doppler spreads. Hence we propose a synergistic use of appropriate detection techniques with beamforming which will be discussed in the section that follows.

6.7 MMSE in Space and Frequency for OFDM systems

A major concern with OFDM and other Multicarrier modulation schemes is the problem of Inter Carrier Interference (ICI). Time variations in the fading channel may lead to a loss of sub-channel orthogonality and a resulting error floor may result which increases with Doppler frequency. Hence, appropriate compensation techniques have to be applied to mitigate the effects of the Doppler spread. Thus we propose the use of MMSE detection followed by MMSE beamforming to mitigate the effects of Doppler spread as well as interference. Simulation results have shown that the error floor due to high Doppler can be removed. A typical block diagram of this technique is shown in Figure 6.19.

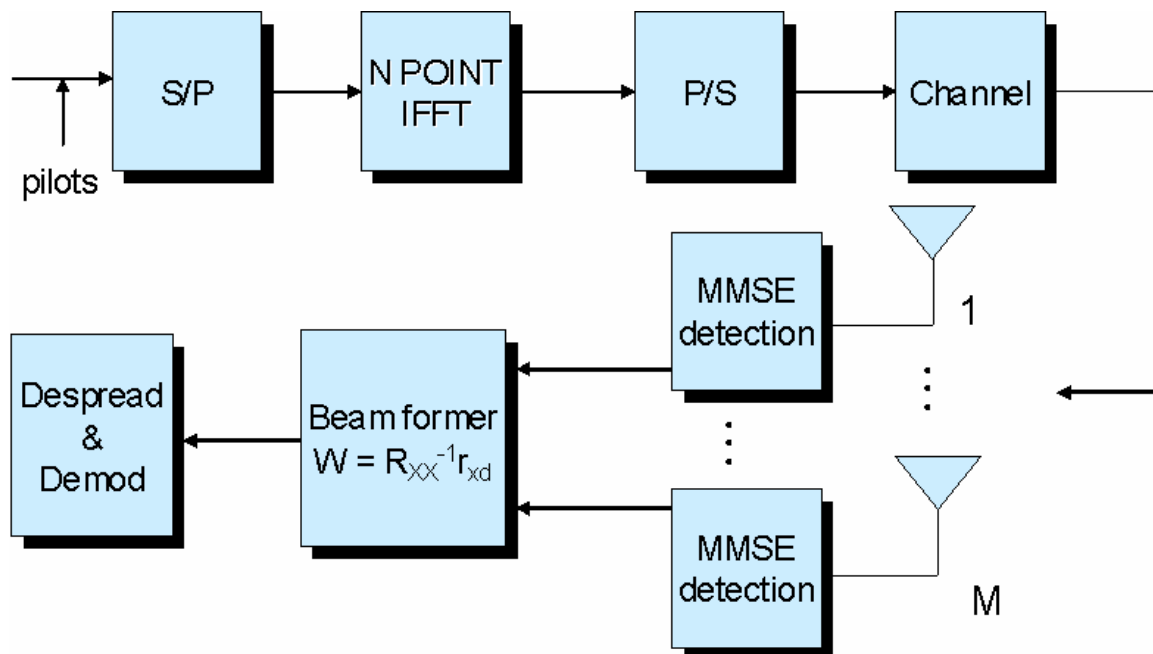


Figure 6.19 Block Diagram of MMSE in Space and Frequency for OFDM systems

The primary difference between the above technique and the frequency domain beamforming algorithm is that MMSE detection compensates for the lack of orthogonality between the subcarriers. A potential drawback of this technique is that the MMSE detection requires knowledge of the operating SNR and is more complex than simple FFT detection. The performance of MMSE in space and frequency in a flat fading channel is shown in Figure 6.20.

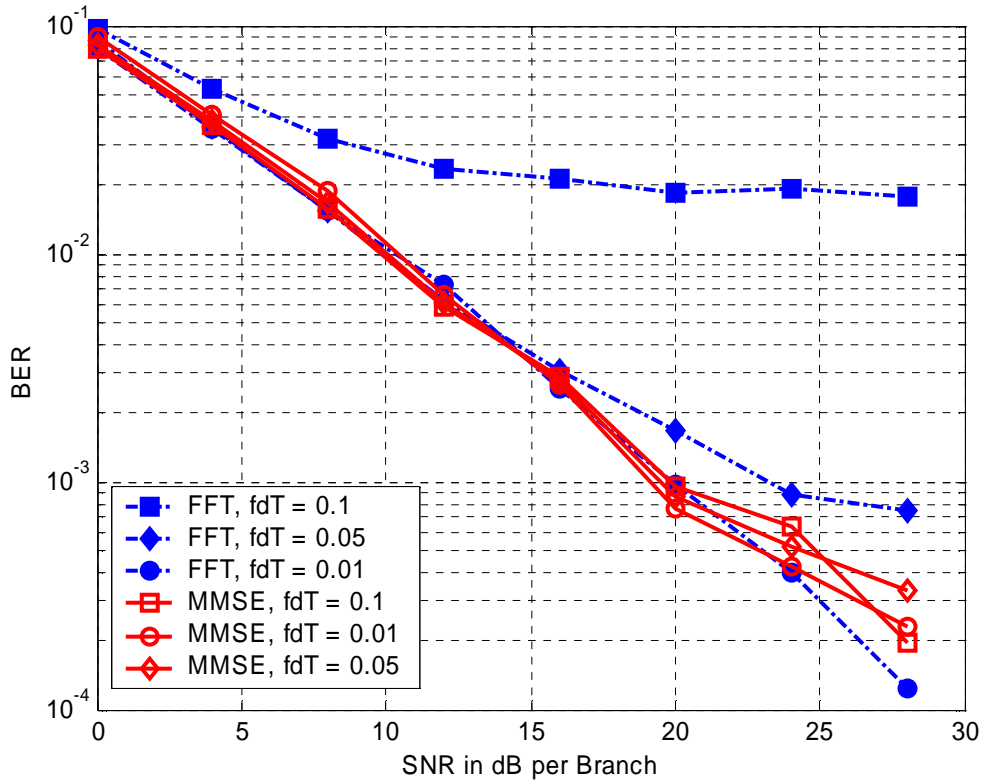


Figure 6.20 Performance comparison of MMSE in space and frequency with FFT in frequency and MMSE in space. SIR = -10dB, N = 128, Spreading Factor = 4. Channel assumed flat Rayleigh fading

The performance of the above technique in frequency selective fading channel is shown in Figure 6.21. We see that the performance of the MMSE detection in frequency does not provide any additional benefit in cases where the angle spread due to the channel is high. Hence at high angle spreads the performance is the same as that of simple FFT detection followed by MMSE beamforming in space. As was the case in the flat fading channel we can see improvement in performance in time varying channels using MMSE in space and frequency. This is evident in Figure 6.22 where FFT detection almost gives an error floor at high Doppler spreads while MMSE detection followed by MMSE beamforming performs better.

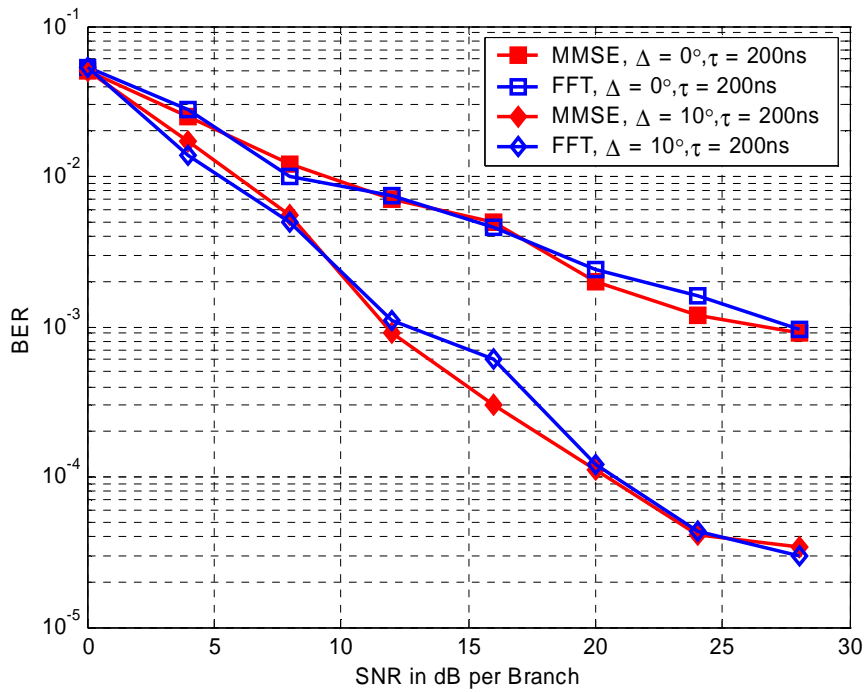


Figure 6.21 Performance of MMSE in space and frequency in frequency selective channel. SIR = -20dB, N=1024, SF = 4, $f_d T = 0.01$.

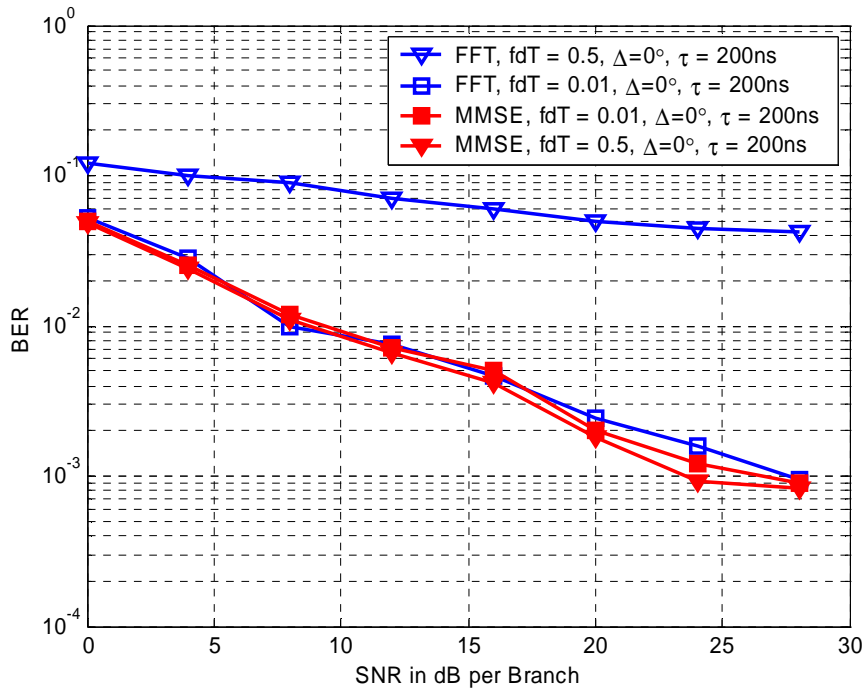


Figure 6.22 Performance of MMSE in space and frequency in frequency selective channel. N = 1024, SIR = -20dB, SF = 4

6.8 Joint weights for MMSE in Space and Frequency for OFDM systems

We studied the performance benefits of some advanced detection techniques for OFDM systems in chapter 4. We also studied the performance of MMSE beamforming and the corresponding benefits associated with it in presence of interferers. In this section we attempt to form a single set of weights that can perform the detection process and combine the signals in all the antenna elements. The set of weights that we attempt to form will minimize the Mean Square Error between the received and the transmitted signal. The following block describes the weight formation.

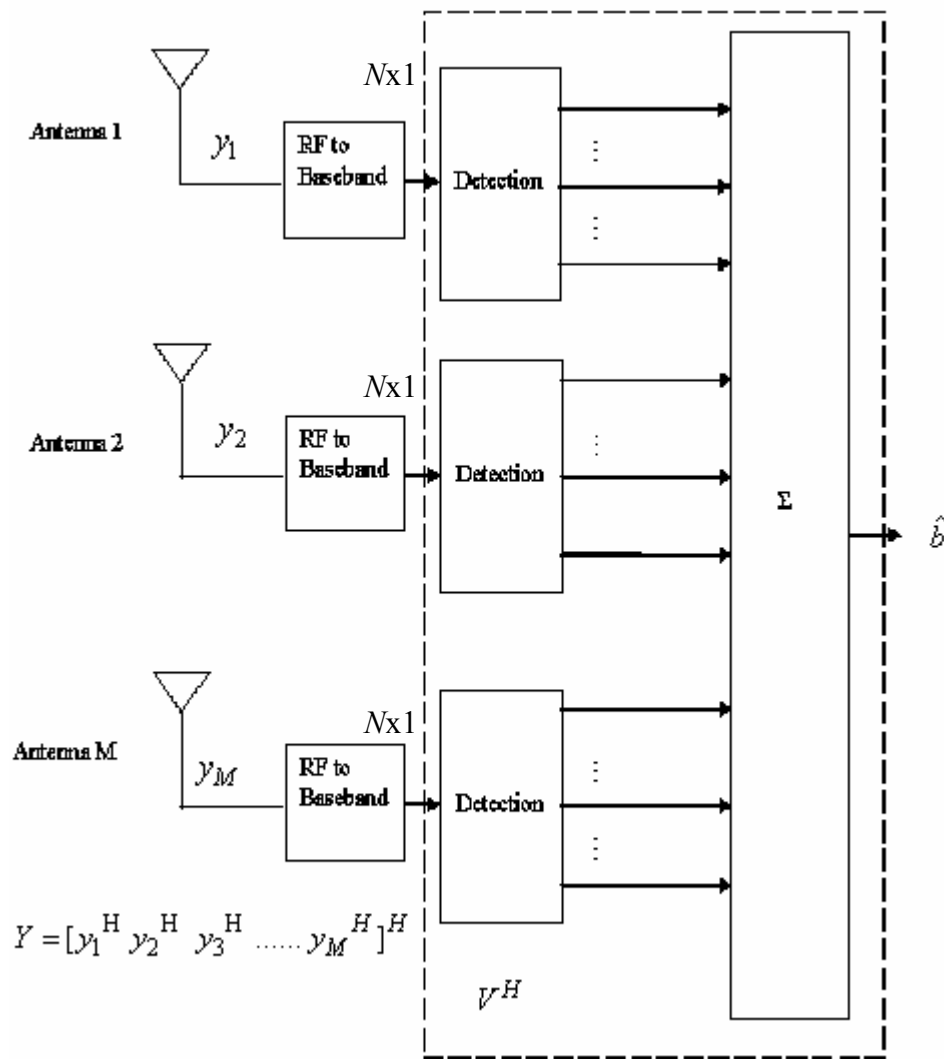


Figure 6.23 Joint weight formation for MMSE in space and frequency

Consistent with the notations before we consider a M element receive array and the received vector at all elements is lumped to get the single vector Y of dimensions $(NM \times 1)$. Thus the vector Y is given as

$$\mathbf{Y} = [\mathbf{y}_1^H \ \mathbf{y}_2^H \ \mathbf{y}_3^H \ \dots \ \mathbf{y}_M^H]^H \quad (6.11)$$

where the y_i 's are the received signal in each of the receive antennas. We have the expression for the received signal at the k th antenna as

$$\mathbf{y}_k = \mathbf{H}_k \bar{b} + n_k \quad (6.12)$$

where H_k is the overall channel between the transmit antenna and the k th antenna at the receive array, b is the individual modulated symbols in each of the subcarriers and n_k is the noise vector. We assume here an N subcarrier MC-CDMA signal.

The received signal at all the elements in the array can be expressed by the following equation.

$$Y = \begin{bmatrix} H_1 & & & & \\ & H_2 & & & \\ & & H_3 & & \\ & & & \ddots & \\ \mathbf{0} & & & & H_M \end{bmatrix} \begin{bmatrix} \bar{b} \\ \bar{b} \\ \bar{b} \\ \vdots \\ \bar{b} \end{bmatrix} + n$$

$$\mathbf{Y} = \tilde{\mathbf{H}}\mathbf{d} + \mathbf{n} \quad (6.13)$$

where \tilde{H} is the super matrix containing all the channel matrices for each of the antenna elements and has dimensions $(NM \times NM)$. The d vector is a stacked version of the transmitted vector \bar{b} and has the dimensions $(NM \times 1)$ and n is the vector of all noise samples in all of the receive antenna elements.

We find a weight matrix such that the estimate \hat{b} of the transmitted vector where \hat{b} is given as

$$\hat{b} = V^H Y \quad (6.14)$$

where the weight matrix V is found in such a way that it minimizes the Mean Square Error and should satisfy the condition

$$V = \arg \min_{V \in \mathbb{C}^{NM \times N}} \left\{ E \left\| V^H Y - \bar{b} \right\|^2 \right\} \quad (6.15)$$

which results in the following standard Weiner solution:

$$V^H = E \left[\bar{b} Y^H \right] \left(E \left[Y Y^H \right] \right)^{-1} \quad (6.16)$$

Now,

$$\begin{aligned} E[YY^H] &= E[(\tilde{H}d + n)(\tilde{H}d + n)^H] \\ &= E \left[(\tilde{H}d + n)(d^H \tilde{H}^H + n^H) \right] \\ &= E \left[\tilde{H}d d^H \tilde{H}^H + \cancel{\tilde{H}d n^H} + \cancel{nd^H \tilde{H}^H} + nn^H \right] \\ &= E \left[\tilde{H}d d^H \tilde{H}^H \right] + E \left[nn^H \right] \\ &= \tilde{H} E \left[dd^H \right] \tilde{H}^H + \sigma^2 I \\ &= \tilde{H} \tilde{H}^H + \sigma^2 I \quad \text{as } E \left[dd^H \right] = \begin{bmatrix} I_{N \times N}^{1,1} & I_{N \times N}^{1,2} & \dots & I_{N \times N}^{1,M} \\ I_{N \times N}^{2,1} & I_{N \times N}^{2,2} & \dots & I_{N \times N}^{2,M} \\ \vdots & & \ddots & \vdots \\ I_{N \times N}^{M,1} & & & I_{N \times N}^{M,M} \end{bmatrix} \end{aligned} \quad (6.17)$$

In the above we have assumed that the noise samples are uncorrelated with the data vector and hence the expected value of the product of the two is zero.

Similarly,

$$\begin{aligned} E \left[\bar{b} Y^H \right] &= E \left[\bar{b} (\tilde{H}d + n)^H \right] \\ &= E \left[\bar{b} (d^H \tilde{H}^H + n^H) \right] \\ &= E \left[\bar{b} d^H \tilde{H}^H + \cancel{\bar{b} n^H} \right] \\ &= E \left[\bar{b} d^H \tilde{H}^H \right] \\ &= E \left[\bar{b} d^H \right] \tilde{H}^H \\ &= \left[I_{N \times N}^{1,1} \ I_{N \times N}^{1,2} \ \dots \ I_{N \times N}^{1,M} \right] \tilde{H}^H \\ &= \left[H_1^H \ H_2^H \ H_3^H \ \dots \ H_M^H \right] \end{aligned} \quad (6.18)$$

We define a vector $\mathbf{H}' = [\mathbf{H}_1^H \mathbf{H}_2^H \mathbf{H}_3^H \dots \mathbf{H}_M^H]$ which is the serial concatenated version of the channels at all receive elements.

Using equations (6.17) and (6.18) we get the expression for the weights as,

$$\mathbf{V}^H = \mathbf{H}' (\tilde{\mathbf{H}} \tilde{\mathbf{H}}^H + \sigma^2 \mathbf{I}_{NM \times NM})^{-1} \quad (6.19)$$

If we assume a single element at the receiver, in the above expression H' and \tilde{H} would break down to the following,

$$H' = H_1^H \quad \text{and} \quad \tilde{H} = H_1 \quad (6.20)$$

Thus the expression for weights would be $V^H = H_1^H (H_1 H_1^H + \sigma^2 I)^{-1}$ which is the simple MMSE solution in frequency.

Thus equation (6.19) can be looked upon as an extension of the MMSE solution in frequency which incorporates the space frequency correlation through \tilde{H} . Semi-analytic results can be derived to determine the BER performance of the Joint Space and Frequency MMSE detector.

The output of the Joint Space and Frequency MMSE detector can be written as

$$\mathbf{z} = \mathbf{V}^H \mathbf{Y} \quad (6.21)$$

Now assuming BPSK as the modulation, the bit estimates are given as $\hat{b}_k = \text{sgn}[\text{Re}(z_k)]$.

The BER is thus given as [Pap01]

$$P_k = Q \left(\frac{E(z/b)_k}{\sqrt{\text{cov}(z)_{k,k}}} \right) \quad (6.22)$$

Now $E(z/b)_k = \text{Re}(\mathbf{V}^H \tilde{H} d)$ for BPSK data, and the covariance of the z is given as,

$$\begin{aligned} \text{cov}(z) &= E[zz^H] - E[z]E[z^H] \\ &= E[V^H Y Y^H V] - E[V^H Y]E[Y^H V] \\ &= E[V^H (\tilde{H}d + n)(\tilde{H}d + n)^H V] - E[V^H (\tilde{H}d + n)]E[(\tilde{H}d + n)^H V] \\ &= E[V^H \tilde{H}d d^H \tilde{H}^H V] + \sigma^2 E[V^H V] - E[V^H \tilde{H}d]E[d^H \tilde{H}^H V] \\ &= V^H \tilde{H}d d^H \tilde{H}^H V + \sigma^2 V^H V - V^H \tilde{H}d d^H \tilde{H}^H V \\ &= \sigma^2 V^H V \end{aligned}$$

(6.23)

Using (6.23) the Probability of Bit Error can thus be written as,

$$P_k = Q\left(\frac{\text{Re}(\mathbf{V}^H \tilde{\mathbf{H}} \mathbf{d})}{\sigma \sqrt{\mathbf{V}^H \mathbf{V}}}\right) \quad (6.24)$$

Simulations were performed to study the performance of the Joint MMSE weights in space and frequency and Figure 6.24 shows the performance of the Joint MMSE weights in space and frequency.

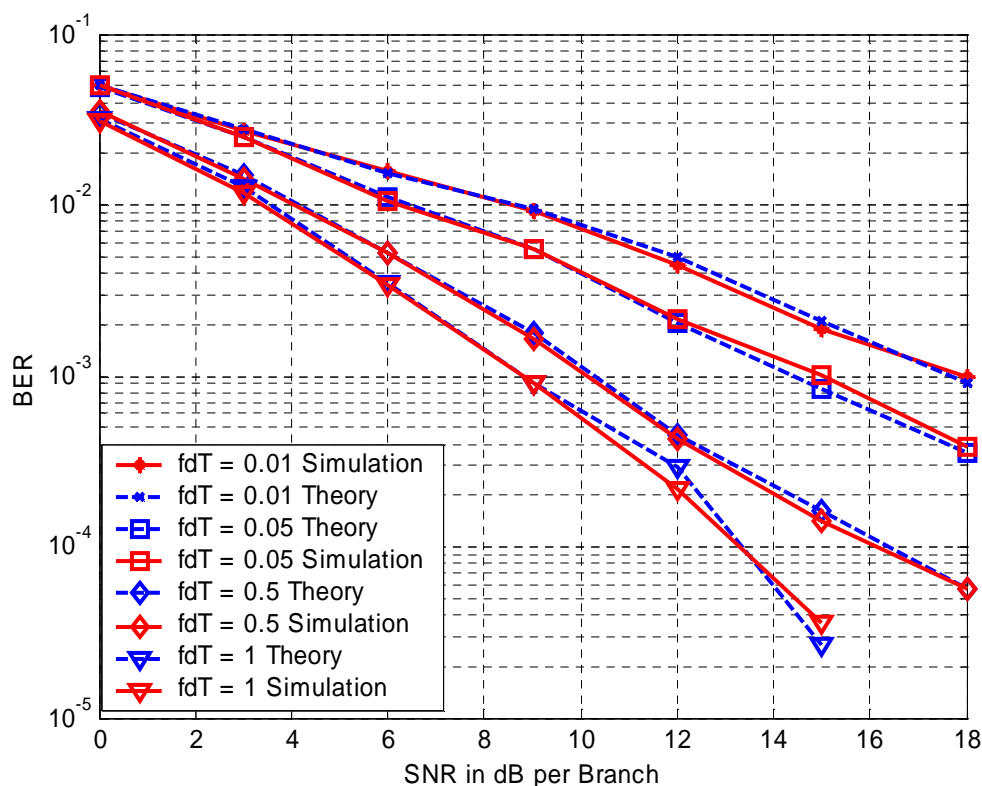


Figure 6.24 Performance of Joint MMSE weights in Space and Frequency through simulations and analysis for BPSK modulation. $N = 16$, Number of receive antennas = 4, $SF = 1$, Flat Rayleigh fading channel, $SIR = \infty$

We observe from Figure 6.24 that the Joint MMSE weights in space and frequency is able to exploit the time diversity offered by the channel. Chapter 4 discussed MMSE detection techniques for OFDM systems and was shown that higher order modulations do

not exploit the time diversity due to the channel very well. In simulations performed with BPSK modulation we could see performance improvement as the normalized Doppler spread is increased and the simulations were found to match with theoretical curves.

6.8.1 Comparison of Joint weights for MMSE in space and frequency with MMSE in space and frequency

MMSE in space and frequency technique as discussed in section 6.7 attempts to bring back orthogonality between subcarriers by MMSE detection in frequency followed by MMSE beamforming in space. Simulation results were shown for various channel conditions in section 6.7. In this section we compare the Joint MMSE weights and that of performing MMSE detection in frequency followed by MMSE beamforming in space (as in section 6.7). The performance of this MMSE detection in frequency followed by MMSE in space combining can be determined through analysis similar to the Joint MMSE case. The received signal at the output of all the receive elements is given as (from Equation 6.13)

$$Y = \begin{bmatrix} H_1 & & & & \\ & H_2 & & & \\ & & H_3 & & \\ & & & \ddots & \\ \mathbf{0} & & & & H_M \end{bmatrix} \begin{bmatrix} \bar{b} \\ \bar{b} \\ \bar{b} \\ \vdots \\ \bar{b} \end{bmatrix} + n$$

$$Y = \tilde{H}d + n \tag{6.25}$$

MMSE detection of the received signals is performed at each of the received elements. Hence the output after MMSE detection at the receive elements is given as,

$$X = G\tilde{H}d + Gn \tag{6.26}$$

where the G matrix is given as

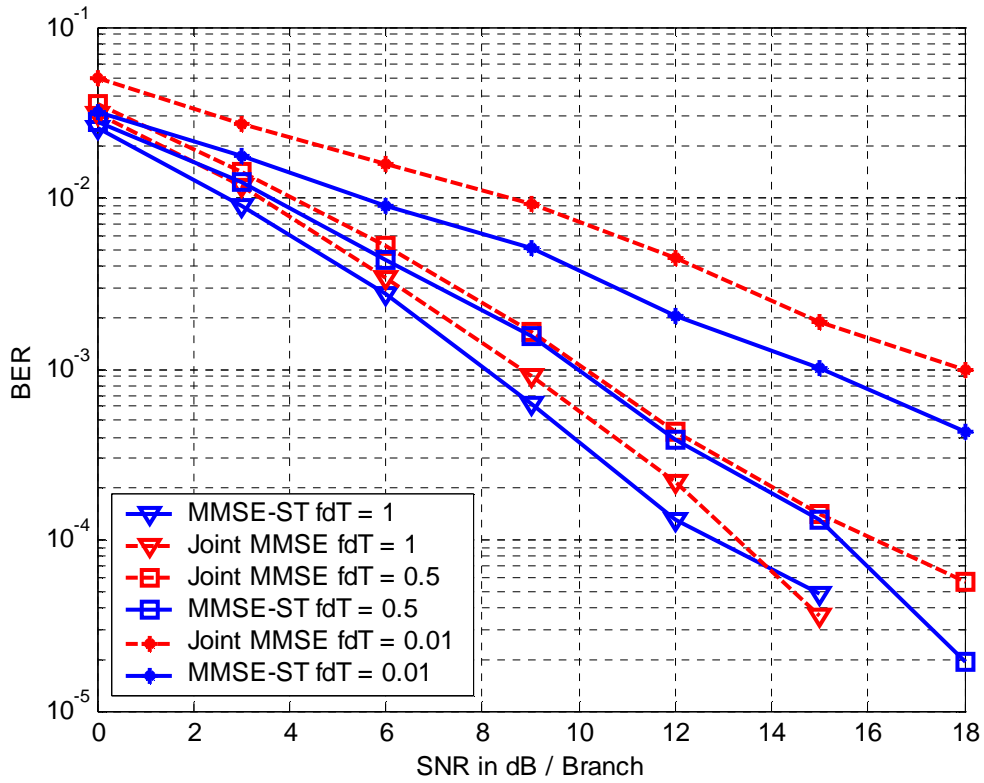


Figure 6.25 Performance comparison of Joint MMSE weights in Space and Frequency with MMSE detection in frequency followed by space for BPSK modulation. $N = 16$, Number of receive antennas = 4, $SF = 1$, Flat Rayleigh fading channel, $SIR = \infty$

The performance comparison curves with varying angle spread values at the receive array is shown in Figure 6.26. As we increase the angle spread there is more decorrelation at the receive antenna elements and hence we see performance improvement in both cases as they are able to exploit spatial diversity.

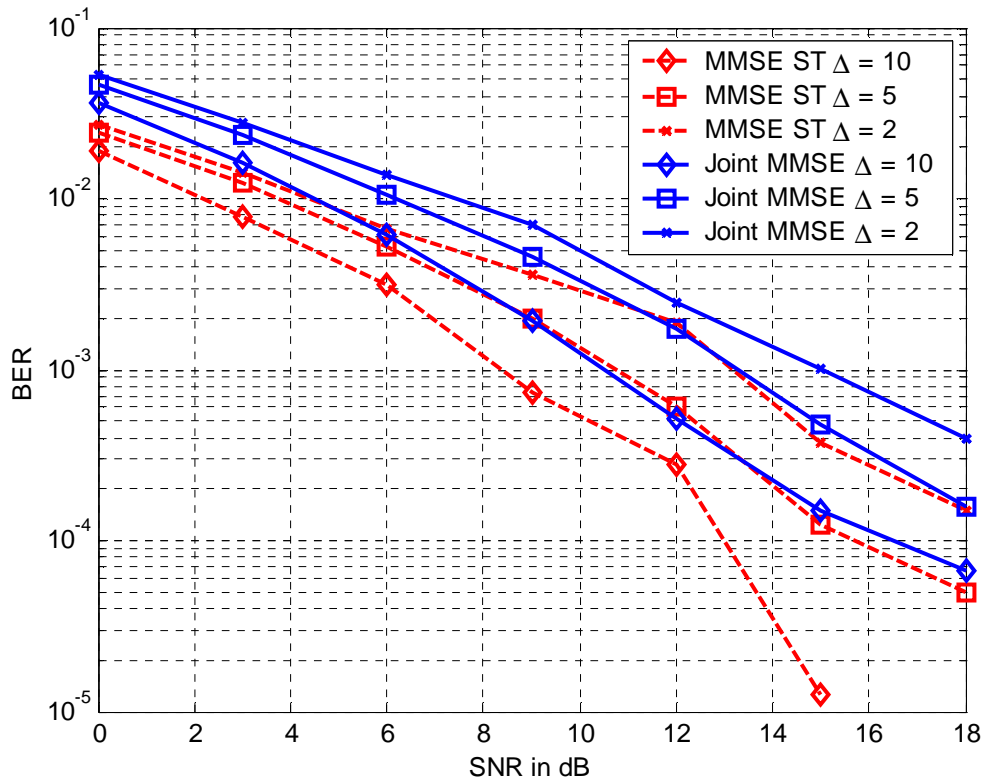


Figure 6.26 Performance comparison of Joint MMSE weights in Space and Frequency with MMSE detection in frequency followed by space for BPSK modulation for varying angle spreads. $N = 16$, Number of receive antennas = 4, $SF = 1$, Flat Rayleigh fading channel, $SIR = \infty$

The performance of these two methods in presence of interference is shown in Figure 6.27 in a flat-Rayleigh fading channel. The Joint MMSE in space and frequency does not provide very good interference suppression and we see error floor. On the other hand MMSE detection followed by MMSE in space provides very good interference suppression.

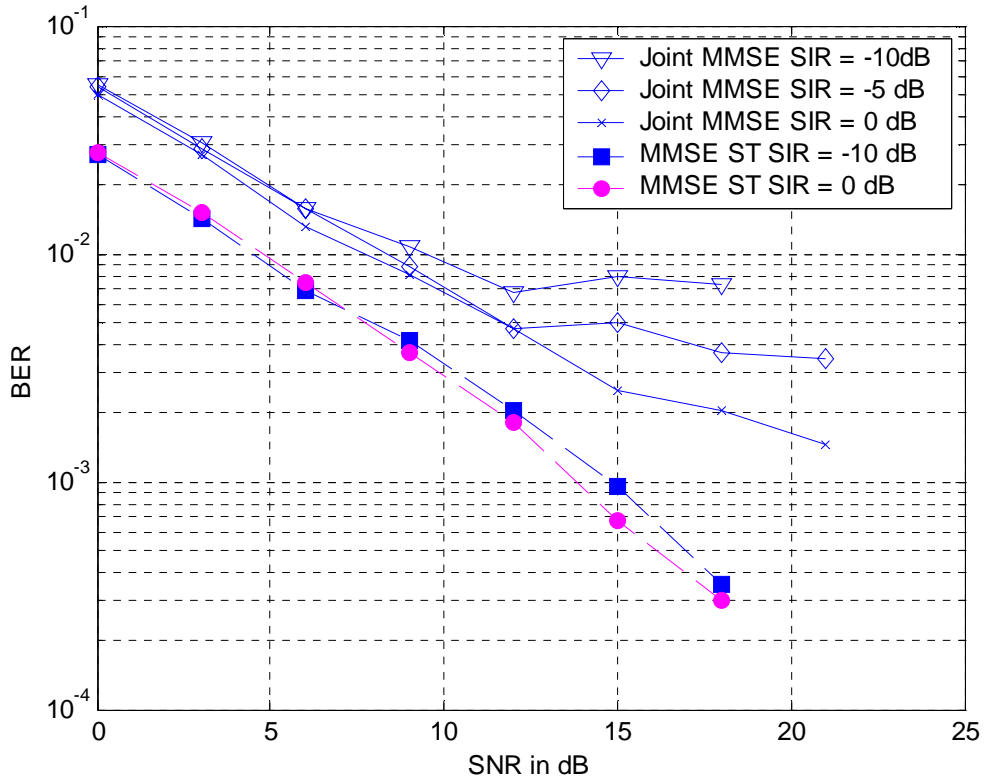


Figure 6.27 Performance comparison of Joint MMSE weights in Space and Frequency with MMSE detection in frequency followed by space for BPSK modulation for varying SIR values. ($N = 16$, Number of receive antennas = 4, SF = 1, Flat Rayleigh fading channel, Angle spread $\Delta = 0$)

6.9 Summary

We presented in this chapter various beamforming techniques for MC-CDMA systems. We first studied the performance of frequency domain beamforming in both flat and frequency selective fading channels. We analyzed the performance of time domain beamforming technique and presented those results also. We see that for low to moderate delay spreads frequency domain beamforming performs well. If the channel delay spread is severe, then sub-band beamforming might be necessary as a single beamformer will not be able to track the changes in the frequency response. Time domain beamforming might be another good alternative. However if the angle spread is large then an error floor results. Hence in such cases time domain beamforming might not be a good scheme. We also studied the performance improvement achieved through MMSE in space and

frequency and showed the results for time varying channels. MMSE technique in space and frequency not only is robust to time variations in the channel but also provides good interference rejection. Joint MMSE in space and frequency is another approach that has been discussed in this chapter. We derived expressions for finding the MMSE weights in both frequency and space and compared the results with that of performing MMSE in frequency followed by that in space. The MMSE in space and frequency method works well in all angle spreads. At high angle spreads it exploits the decorrelation in the receive elements. It performs well in all Doppler spreads. In fact increase in Doppler spread improves temporal diversity and the technique makes use of it. Finally MMSE in space and frequency works reasonably well in time dispersive channels as well. But large delay spread values introduce rapid changes in the frequency response of that channel and the MMSE space and frequency method might not be able to track those rapid changes in frequency. Thus the choice of the beamforming is very much dependent on the channel conditions. For low to moderate delay spreads frequency domain beamforming with a single weight vector for all subcarriers will be sufficient. For large delay spreads sub-band beamforming has to be done. If the angle spread due is large frequency domain beamforming is the solution. For low angle spreads time domain beamforming will be a good alternative. If the channel varies quickly in time then MMSE in space and frequency will be an effective technique. For low order modulations it can utilize the time diversity provided by the channel and can provide interference suppression.

Chapter 7

Conclusions and Future work

7.1 Conclusions

This thesis focuses on multi antenna receivers for OFDM and MC-CDMA systems and more specifically on algorithms that could provide interference and ICI suppression in harsh channel conditions. These algorithms have been discussed in Chapter 6. We have analyzed the performance of frequency domain beamforming for OFDM systems and have also pointed out that having a single weight vector across all subcarriers may not work very well if the channel delay spread is high. Hence sub-band beamforming which uses multiple weight vectors is necessary to track channel variations in frequency.

An alternative solution discussed in this work is to combine antenna signals in time. The performance of this time domain beamforming technique has also been discussed. The algorithm works very well in cases where the angle spread is low. Also it has been shown that the performance of frequency domain and time domain beamforming is the same in a flat Rayleigh fading channel. In terms of complexity, the two beamformers are similar.

The time varying nature of the channel can corrupt the orthogonality between the subcarriers for OFDM systems. Chapter 4 discussed advanced detection techniques for OFDM systems that can utilize the time diversity provided by that channel. We have proposed in this work an MMSE in space and frequency technique that could be very effective in time varying channels. Performance results have shown that this technique provides very good interference suppression while being robust to time variations of the channel. This work also investigated a joint MMSE in frequency and space approach and semi-analytic expressions for the BER performance were derived.

7.2 Future Research Directions

The following are some ideas and potential problems that might be interesting areas to pursue in future.

- All our discussions focused on MC-CDMA although we pointed out the other flavors of OFDM based CDMA such as MT-CDMA and MC-DS CDMA. It will be interesting to study the beamforming algorithms that we have proposed in this thesis for MT-CDMA and MC-DS CDMA.
- The beamforming algorithm that we have chosen in our research is the MMSE Direct matrix inversion algorithm. A nice feature of this MMSE algorithm is that it lends itself to adaptive implementation based on some minimization criterion. Hence the performance of the algorithms can be studied using the common Least Mean Square (LMS) or the Recursive Least Squares (RLS) algorithm instead of DMI.
- Transmit diversity techniques in addition to receive diversity could be another area to explore. Such Multiple Input Multiple Output (MIMO) systems for OFDM are already a very active area of research and promise great benefits for broadband wireless communications.
- Channel estimation algorithms were discussed for OFDM and MC-CDMA in Chapters 3 and 4. A robust time domain channel estimation algorithm was also discussed in Chapter 4. Chapter 6 discussed the impact of cubic- spline interpolation channel estimation along with beamforming. The performance of more robust channel estimation algorithms along with the beamforming algorithms discussed in this work is an interesting area to investigate.
- Frequency and timing synchronization were assumed to be perfectly known at the receiver. Synchronization is another active area of research for OFDM systems from a practical stand point and might be a good problem to explore in future efforts.
- Finally, all simulations in this work are for systems that we believe are analytically tractable. Deriving analytical expressions to determine the performance would help validate the simulation results. Semi-analytic results were presented for the joint MMSE in space and frequency case in Chapter 6. The same could be extended for other cases.

References

- [Bue99] R.M.Buehrer, A.G. Kogiantis, Shang-Chieh Liu, Jiann-an Tsai and Dirck Uptegrove, “Intelligent Antennas for Wireless Communications – Uplink”, *Bell Labs Technical Journal*, vol 4, pp.73-103, July-Sept 1999.
- [Che95] Q.Chen, E.S. Sousa and S.Pasupathy, “Performance of a coded multi- carrier DS-CDMA system in multipath fading channels,” *Wireless Personal Communications*, vol. 2, nos. 1-2, pp. 167-187, 1995.
- [Che02] Bing-Leung Patrick Cheung, “Simulation of Adaptive Array algorithms for OFDM and Adaptive Vector OFDM systems”, M.S. Thesis, Virginia Polytechnic Institute and State University, September 2002.
- [Cho01] Y.S. Choi, P.J.Voltz and F.Cassara, “ On Channel Estimation and Detection for Multicarrier Signals in Fast and Selective Rayleigh Fading Channels,” *IEEE Trans. Commun.*, vol. 49, pp August 2001.
- [Cho93] A.Chouly, A.Brijal and S.Jourdan, “Orthogonal multicarrier techniques applied to direct sequence spread spectrum CDMA systems,” in *Proc. Globecom '93*, Nov 1993, pp.1723-1728.
- [Cim85] Leonard J.Cimini, “Analysis and Simulation of a Digital Mobile Channel Using Orthogonal Frequency Division Multiplexing,” *IEEE Trans. Commun.*, vol. 33 No 4, July 1985, pp. 665-675.
- [Edf98] O.Edfors, M.Sandell, J.J. van de Beek, S.K.Wilson, and P.O.Borjesson, “OFDM channel estimation by singular value decomposition,” *IEEE Trans. Commun.*, vol.46, No 6, pp.931-939, July 1998.

- [**Har97**] S.Hara and S.Prasad, "Overview of multicarrier CDMA", *IEEE Commun. Mag.*, vol. 35, No 3, pp. 126- 133, Dec 1997
- [**How59**] P. W. Howells, "Intermediate frequency side lobe canceller," Technical report, U.S. Patent 3202990, May 1959.
- [**Jak74**] W.C.Jakes,Jr., Ed., *Microwave Mobile Communications*, New York: Wiley, 1974
- [**Kai95**] S.kaiser, "On the performance of different detection techniques for OFDM-CDMA in fading channels," in *IEEE ICC '95*, June 1995, pp.2059 -2063.
- [**Kim00**] C. Y. Kim, K. Lee, and Y. S. Cho, "Adaptive Beamforming Algorithm for OFDM Systems with Antenna Arrays," *IEEE Transactions on Consumer Electronics*, vol. 46, No. 4, November 2000.
- [**Li98**] Y.Li, J.Cimini Jr., N.R.Sollenberger, " Robust Channel estimation for OFDM systems for rapid dispersive fading channels," *IEEE Trans. Commun.*, vol.46, No 5, pp. 902-915, July 1998.
- [**Li99**] Y.Li, N.R.Sollenberger, "Adaptive Antenna Arrays for OFDM systems with co-channel interference," *IEEE Trans. Commun.*, vol.47, No.2 February 1999.
- [**Min00**] Hlaing Minn, V.K.Bhargava, "An Investigation into Time Domain Approach for OFDM Channel estimation," *IEEE Trans. Broadcasting*, vol. 46, Dec2000.
- [**Mor01**] R.Morrison, L.J.Cimini, S.K.Wilson, "On the use of Cyclic Extension in OFDM," *Proc. of 54th IEEE Vehicular Technology Conference*, Sept .2001, vol.2, pp. 664-668
- [**Mor01a**] M.Morelli, U.Mengali, "A Comparison of Pilot-Aided Channel Estimation Methods for OFDM systems," *IEEE Trans. Signal Processing*, vol. 49, Dec 2001.

[Neg98] R.Negi and J.Cioffi, "Pilot tone selection for channel estimation in a mobile OFDM system," *IEEE Trans. Consumer Electronics.*, vol.44, pp.1122-1128, Aug 1998.

[Pap01] C.B.Papadias, H.Huang, "Linear Space-Time Multiuser Detection for Multipath CDMA Channels," *IEEE Journal on Selected Areas in Communications*, vol 19, No 2, Feb 2001.

[Pil89] S. U. Pillai, *Array Signal Processing*, Springer-Verlag, New York, 1989.

[Pra96] R.Prasad and S.Hara, "An overview of multicarrier CDMA," in *Proc. IEEE Int. Symp. Spread Spectrum techniques and Applications*, Sept. 1996, pp. 107-114.

[Pro89] J.Proakis, *Digital Communications*, 2nd Edition, McGraw-Hill, New York.

[Rap95] T. S. Rappaport , *Wireless Communications: Principle and Practice*, Prentice Hall, 1995.

[Rin96] J.Rinne and M.Renfors, "Pilot spacing in orthogonal frequency division multiplexing systems on practical channels," *IEEE Trans. Consumer Electronics.*, vol 42, pp 959-962, Nov 1996

[Rus95] M.Russell, G.L.Stuber, "Interchannel Interference Analysis of OFDM in a mobile Environment," in *Proc of 45th Vehicular Technology Conference 1995*, vol.2, 820-824.

[Sou96] E.A.Sourour and M.Nakagawa, "Performance of orthogonal multicarrier CDMA in a multipath fading channel," *IEEE Trans. Commun.* vol. 44, pp. 356-366, Mar 1996.

[Stu81] W. L. Stutzman and G. A. Thiele, *Antenna Theory and Design*, John Wiley & Sons, New York, 1981.

[Van00] R. Van Nee and Ramjee Prasad, OFDM for Wireless Multimedia Communications, Artech House Publishers, 2000.

[Van88] B. D. Van Veen and K. M. Buckley, "Beamforming: A versatile approach to spatial filtering," *IEEE ASSP Magazine*, pp. 4-24, April 1988.

[Voo98] F.W.Vook and K.L.Baum, "Adaptive Antennas for OFDM," in *Proc. of 48th IEEE Vehicular Technology Conference, 1998*. Vol 1,Page(s): 606 -610

[Wan00] Z.Wang, G.Giannakis, "Wireless Multicarrier Communications," *IEEE Signal Processing Magazine*, vol 17. May 2000, pp. 29-48

[Wol98] P.W.Woliansky, G.J.Foschini, G.D.Golden, and R.A.Valenzuela, "V-BLAST: An architecture for realizing very high data rates over the rich wireless scattering channel," in *Proc. IEEE ISSSE-98*, Sep 1998, pp 295-300.

[Yee93] N.Yee, J.P.Linnartz, and G.Fettweis, "Multi-Carrier CDMA in indoor wireless radio networks," *Proc. IEEE PIMRC '93*, pp. 109-113

Vita

Ramasamy Venkatasubramanian was born in December 27, 1978 in the town of Tirunleveli in southern part of India. He obtained his Bachelor of Engineering (B.E.) from Madurai Kamaraj University with major in Electronics and Communications Engineering in May 2000. He passed with distinction and secured third rank in the ECE department of Madurai Kamaraj University. Following this, he enrolled for M.S. program in Virginia Tech in the fall of 2000. During the summer of 2001 he interned at the Wireless Integration Technology Center (WITC) of Motorola at Boynton Beach, Florida. He joined the Mobile and Portable Radio Research group (MPRG) in the fall of 2001. His interests include multicarrier communications, adaptive antennas and general topics in wireless communications.

He is a student member of IEEE and IEEE Communications Society.